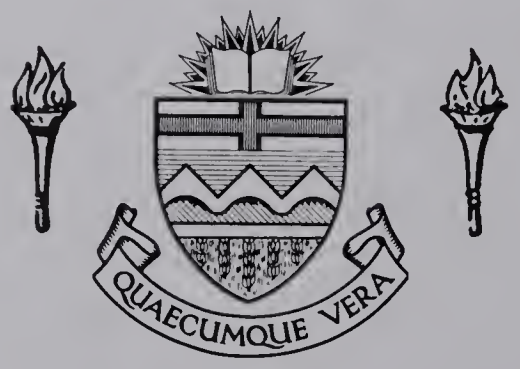

THE UNIVERSITY OF ALBERTA

STUDY OF TURBULENT FREE CONVECTION NEAR A VERTICAL PLATE

by

FRED TROTTER, B.Sc. (Alberta)

A THESIS

SUBMITTED TO THE FACULTY OF GRADUATE STUDIES

IN PARTIAL FULFILMENT OF THE REQUIREMENTS FOR THE DEGREE

OF MASTER OF SCIENCE

DEPARTMENT OF MECHANICAL ENGINEERING

EDMONTON, ALBERTA

October 1967

UNIVERSITY OF ALBERTA

FACULTY OF GRADUATE STUDIES

The undersigned certify that they have read, and recommend to the Faculty of Graduate Studies for acceptance, a thesis entitled "STUDY OF TURBULENT FREE CONVECTION NEAR A VERTICAL PLATE" submitted by FRED TROTTER in partial fulfilment of the requirements for the degree of Master of Science.

ABSTRACT

An experimental investigation into the mechanism of turbulent free convection adjacent to a heated vertical wall is presented. In addition, a similarity analysis is performed in an attempt to describe the system in terms of a suitable physical model. The similarity variables are obtained for negligible dissipation and wall boundary conditions of constant wall temperature and constant heat flux. The experiments give some support to the model and lead to some conclusions about the mechanism of turbulence in the boundary layer. Special attention is given to temperature fluctuations, the intermittency factor, mean velocity and temperature profiles, and the laminar sublayer concept.

ACKNOWLEDGEMENTS

The author wishes to extend his appreciation to

- Dr. G.S.H. Lock for his guidance and supervision of this thesis.
- the members of the Mechanical Engineering Shop, particularly Mr. Bill Kell who built the apparatus and Mr. Ray Marak who aided in the instrumentation.
- Mr. A.J. Weight of N.A.I.T. who helped with the determination of the fibre diameter.
- Mr. R.W. King of the Electrical Engineering Department for his help with several electrical problems and for the use of some equipment.
- Miss Lynne Fiveland for her patience in typing this thesis.
- the National Research Council for financial support under grant no. A-1672.
- my wife, Jane, for her patience and help in the running of tests and the writing of the thesis.

TABLE OF CONTENTS

PAGE

LIST OF ILLUSTRATIONS

FIGURE PAGE

NOMENCLATURE

SYMBOL	QUANTITY
A	the projected area of the fibre
C	constant
C_D	drag coefficient
d	diameter of the fibre
D	coefficient
E	modulus of elasticity
f	stream function
g	acceleration due to gravity
Gr	Grashof number
h	heat transfer coefficient
I	moment of inertia of the fibre
k	thermal conductivity
K	constant
l	length of quartz fibre
L	mixing length
ln	natural logarithm
M	eddy viscosity
N	related to $T_w - T_\infty$ by $T_w - T_\infty = N\ x^S$
Nu	Nusselt number
p	pressure
Pr	Prandtl number
Q	heat flux

SYMBOL	QUANTITY
R	curvature of the fibre beam
Ra	Rayleigh number
Re	Reynolds number
t	time
T	temperature
u	velocity in x direction
v	velocity in y direction
x	vertical distance above the leading edge
y	lateral distance from the plate
w	resistance per unit length

SUBSCRIPTS

x	local values
∞	outside boundary layer
w	wall
m	velocity maximum

SUPERSCRIPTS

-	mean
'	fluctuation, derivative

GREEK LETTERS

β	temperature coefficient of volume expansion
γ	intermittency factor

SYMBOL	QUANTITY
δ	boundary layer thickness defined as 1% of $T_w - T_\infty$
δ	deflection of the quartz fibre
ε	momentum eddy diffusivity
ε_T	thermal eddy diffusivity
κ	thermal diffusivity
ξ	Prandtl number function
η	similarity variable
θ	temperature difference $\Theta = T - T_\infty$
μ	absolute viscosity
ν	kinematic viscosity
ρ	density
τ	shearing stress
ψ	stream function
ϕ	temperature

Other symbols are defined where they appear.

CHAPTER I

INTRODUCTION

When the motion of a fluid is caused solely by density gradients resulting from temperature differences, the resulting phenomenon is termed free or natural convection. Natural convection is often the dominant heat flow mode from pipes, refrigeration equipment and walls. A specific application of such heat transfer is the cooling of hollow gas turbine blades, in which the centrifugal force creates a natural convection flow of the coolant in the blade passages. In order to understand and use such processes, information on free convection heat transfer is needed, especially in the turbulent regime.

In this thesis natural turbulent convection near a hot vertical wall is studied. A brief historical review of the problem now follows.

In 1922 Griffiths and Davis [1]* conducted an experimental investigation into the problem of heat transfer from a hot vertical plate surrounded by air. Although their studies were mainly in the laminar region, they obtained some velocity and temperature profiles in the turbulent region. These profiles, which have recently been supported by the work of Cheesewright [2], were possibly their greatest contribution as they have since served as the basis for several hypotheses.

By means of an optical method, Saunders [3] in 1939 determined that the onset of turbulence occurred at a Rayleigh number of 2×10^9

---

* Numbers indicate references given after Chapter V.

for both air and water. This value is still taken as a criterion today. From data with a Rayleigh number greater than 2×10^9, Saunders concluded that the Nusselt number as a function of the Rayleigh (or Prandtl-Grashof) number could be represented by

$$Nu = K(Ra)^{1/3}$$

where K is 0.17 for water and 0.10 for air.

In 1951, Eckert and Jackson [4] made a semitheoretical analysis of turbulent free convection on a vertical flat plate by introducing simple algebraic approximations of the velocity and temperature profiles of Griffiths and Davis into the von Karman integral equations for the boundary layer. They assumed the wall shearing stress to be the same as in forced convection and utilized the laminar sublayer concept. They concluded that the average Nusselt number varied as the Grashof number to the two-fifths power.

Since 1951, the use of forced convection results in the free convection problem has been commom. This application is questioned here with particular attention given to the hypothesis of the laminar sublayer.

In the investigation that follows, the problem of turbulent flow near a hot vertical wall is studied, considering in particular the mechanism of turbulence in water and the determination of possible similarity variables. The magnitude of fluctuations, the intermittency factor and the temperature distribution are also studied. The fibre anemometer of Schmidt [5] is modified and used to determine velocity profiles in the boundary layer. This use, which met with

limited success, is believed to be the first application of the fibre anemometer to velocity tests conducted in water.

No previous experimental work has been performed dealing with the actual transport mechanism. It is hoped that this work will lead to a greater understanding of the problem.

CHAPTER II

THE TURBULENT FREE CONVECTION MODEL

2.1 THERMAL AND MOMENTUM DIFFUSIVITY MODEL

In analogy with the coefficient of viscosity in Stokes' law for laminar flow, a mixing coefficient M is introduced for the Reynolds stress in turbulent flow by putting

$$\tau = M \frac{d\bar{u}}{dy} .$$

The turbulent mixing coefficient M is often called the "eddy" viscosity, since it corresponds to the viscosity in laminar flow. Unfortunately the eddy viscosity is not a fluid property but depends upon the mean velocity field.

Use is often made of the eddy kinematic viscosity (eddy diffusivity) $\varepsilon = M/\rho$, which is analogous to the kinematic viscosity $\nu = \mu/\rho$. Thus the turbulent shearing stress equation may also be written

$$\tau = \rho\varepsilon \frac{d\bar{u}}{dy} . \qquad 2\text{-}1$$

The above analogy is of little value unless the dependence of ε on velocity is known and therefore it is necessary to find this relationship. In the following discussion two such relationships will be considered. Both rely, in part, on an analogy between the molecular kinetic theory and a hypothetical eddy transfer. In this analogy, lumps of fluid (eddies) move in bulk across the velocity profile, transporting both mass and energy. Prandtl, in formalizing this eddy motion idea,

specifically drew an analogy between the mean free path in molecular transport and a "mixing length" in turbulent flow. In his model the shearing stress in a turbulent boundary layer is given by

$$\tau = \rho L^2 \left|\frac{d\bar{u}}{dy}\right| \frac{d\bar{u}}{dy} \qquad 2\text{-}2$$

where L is the mixing length.

From Prandtl's theory an attempt may be made to predict the distribution of the mixing length and eddy viscosity. Although an exact expression for the velocity in the boundary layer is not available, it is possible to make a sketch on the basis of the work of Griffiths and Davis. Such a sketch is shown in figure 2.1 below.

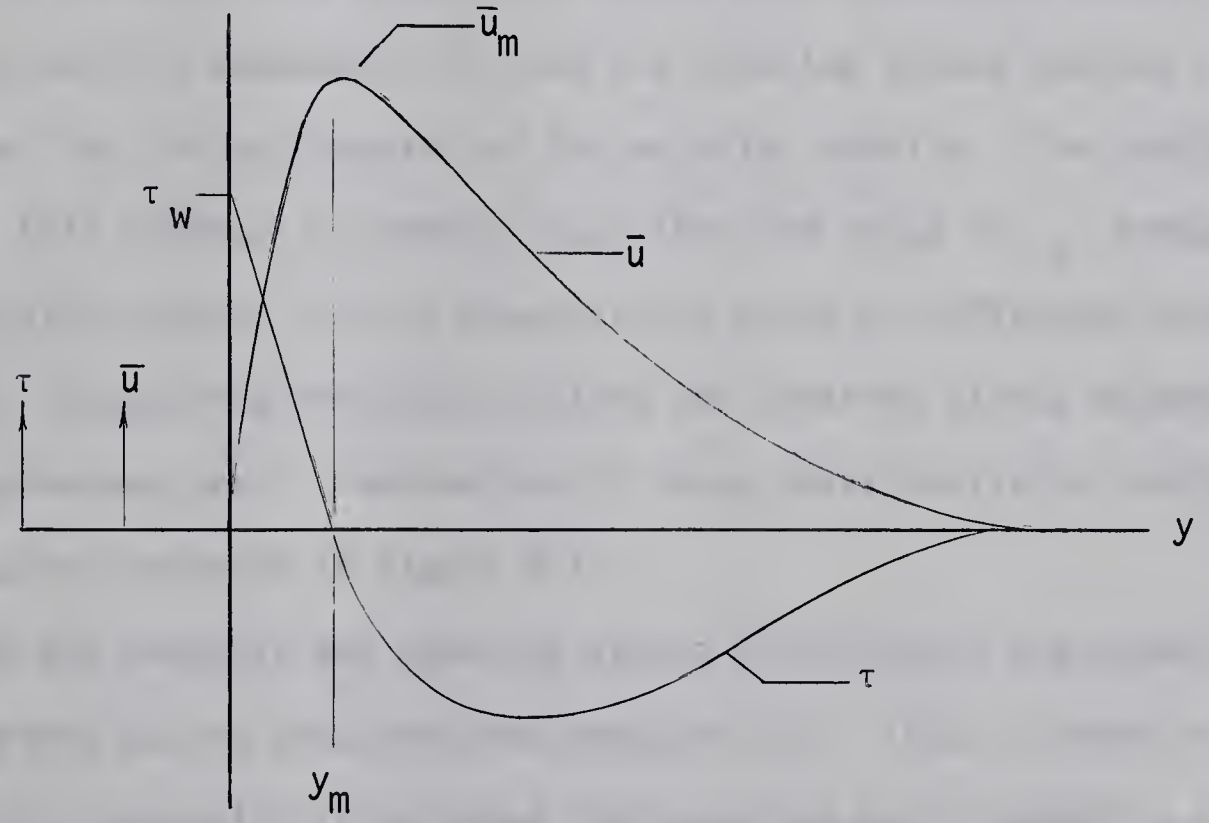

FIG. 2.1 SKETCH OF VELOCITY AND SHEARING STRESS PROFILES

The shearing stress distribution, as well as the velocity, must be known before any relation describing the variation of the mixing length in the boundary layer can be obtained. As no such distribution is known at present, only an approximate representation is possible.

To draw this approximation, it is first noted that the shearing stress has some definite value, τ_w, at the wall and is zero at the position in the boundary layer where the velocity is a maximum. Between this position and the wall, a linear variation in shearing stress could be assumed. It is possible that the variation is actually concave upward, but since this region of the boundary layer is relatively narrow the straight line assumption should give reasonable results. Another plausible assumption is that the shearing stress reaches a minimum at the inflection point of the velocity profile. The absolute value of this minimum is probably less than the value of τ_w, because the velocity gradient is less steep at the point of inflection than at the wall. Beyond the inflection point, the shearing stress asymptotically approaches zero. Combination of these characteristics results in the curve presented in figure 2.1.

Once the velocity and shearing stress distribution are known, the mixing length may be obtained from equation 2-2. This is shown in figure 2.2, from which it is noted that near the wall, Prandtl's original hypothesis that L = Ky seems reasonable. Past the point of maximum velocity this relation is not defensible, since the effect of a rigid wall is not felt. Near the velocity maximum, mixing lengths

appear to be much longer than those away from the influence of the wall. This relatively sharp peak may be the result of the form of the original profile sketched, but likely reflects the existence of a maximum of similar shape.

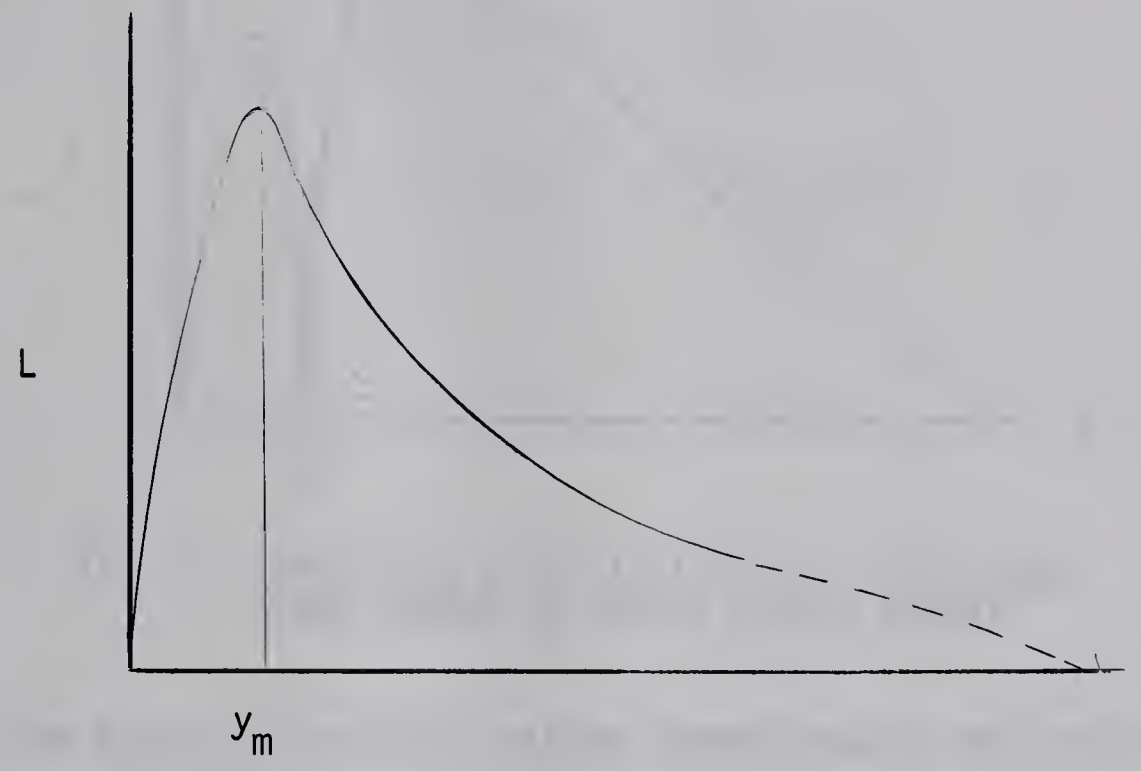

FIG. 2.2 SKETCH OF MIXING LENGTH PROFILE

It is now possible to determine the variation of the eddy viscosity as a function of position using

$$\varepsilon = L^2 \left|\frac{d\bar{u}}{dy}\right|. \qquad 2\text{-}3$$

This variation is illustrated in figure 2.3. In this illustration, the eddy viscosity increases almost linearly from the plate until it reaches a maximum about two-thirds of the way towards the point of maximum velocity. It then decreases sharply until it is zero again when $d\bar{u}/dy$ is zero. From this point the viscosity rises to a maximum and slowly decays toward the boundary layer edge.

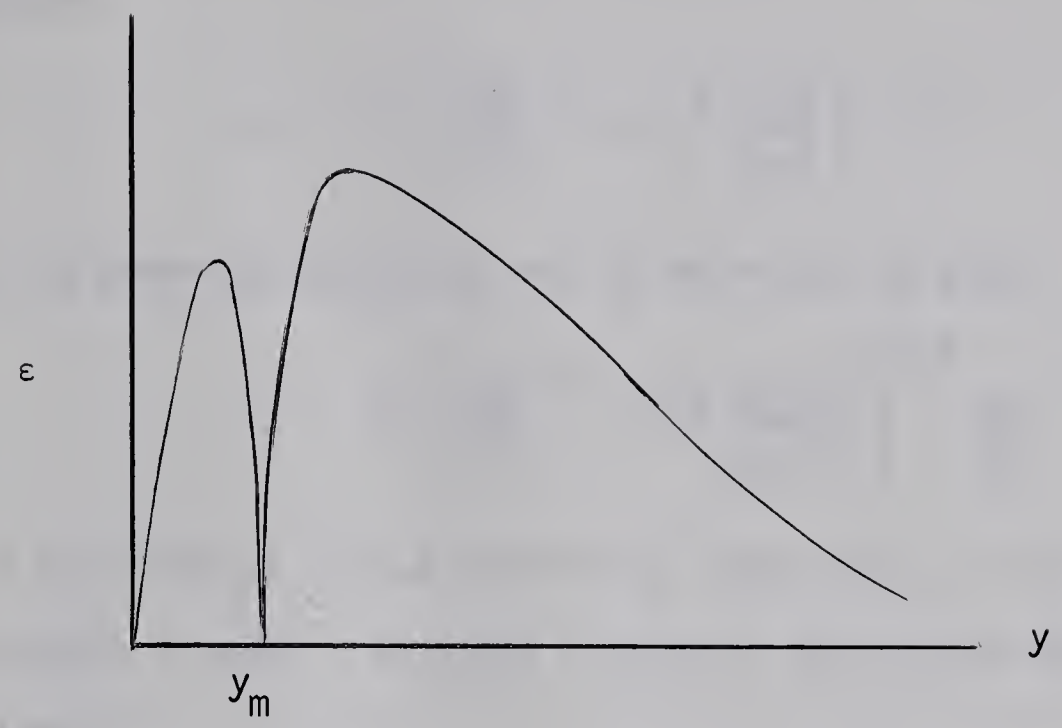

FIG. 2.3 VARIATION OF EDDY DIFFUSIVITY OBTAINED FROM PRANDTL'S MIXING LENGTH THEORY

From Prandtl's original mixing length theory, any velocity profile which exhibits a maximum must have a zero eddy viscosity at that point as this is an inherent characteristic of the early theory. However, there is no apparent physical explanation why the eddy viscosity should be zero at the points of maximum velocity, since turbulent mixing does not vanish there. In fact, Schlichting [6] quotes Reichardt as showing that in the centre of a channel the fluctuations in both directions (u' and v') differ from zero. Thus Prandtl's original theory is not wholly compatible with other physical considerations and is not recommended as a model for the turbulent boundary layer in free convection.

Now consider a second possible relation between eddy viscosity and velocity. Prandtl, who was himself aware of the above objection

to his theory, proposed a modification replacing equation 2-3 with the relation

$$\varepsilon = L^2 \left[\left[\frac{d\bar{u}}{dy} \right]^2 + L_1^2 \left[\frac{d^2\bar{u}}{dy^2} \right]^2 \right]^{1/2} \qquad 2\text{-}4$$

so that the shearing stress may now be rewritten to give

$$\tau = L^2 \left[\left[\frac{d\bar{u}}{dy} \right]^2 + L_1^2 \left[\frac{d^2\bar{u}}{dy^2} \right]^2 \right]^{1/2} \frac{d\bar{u}}{dy} . \qquad 2\text{-}5$$

In these equations, L is the new mixing length and L_1 is a value used to modify Prandtl's original hypothesis and called the "extended mixing length".

Since the velocity and shearing stress distributions are given in figure 2.1, it is now possible to determine the mixing length from equation 2-5 if the variation of L_1 is known. In general, L_1 would probably be a function of the distance from the plate, but for purposes of this discussion it will be considered constant. Two arbitrary values, $L_1 = 1$ and $L_1 = 2$, will be considered as examples.

With these two values, figure 2.1, and equation 2-5, the variation of the new mixing length L across the boundary layer can be estimated. Figure 2.4 illustrates such variations for both values of L_1. It can be seen that the main effect of the extended mixing length is to decrease the sharp peak which appears when using Prandtl's original theory (figure 2.2). That is, in the region of maximum velocity, where $d\bar{u}/dy$ is small, the effect of the term $d^2\bar{u}/dy^2$ is most significant. As well as decreasing the peak, increasing L_1 tends to shift the maximum slightly outward from the plate. Thus, if the exact

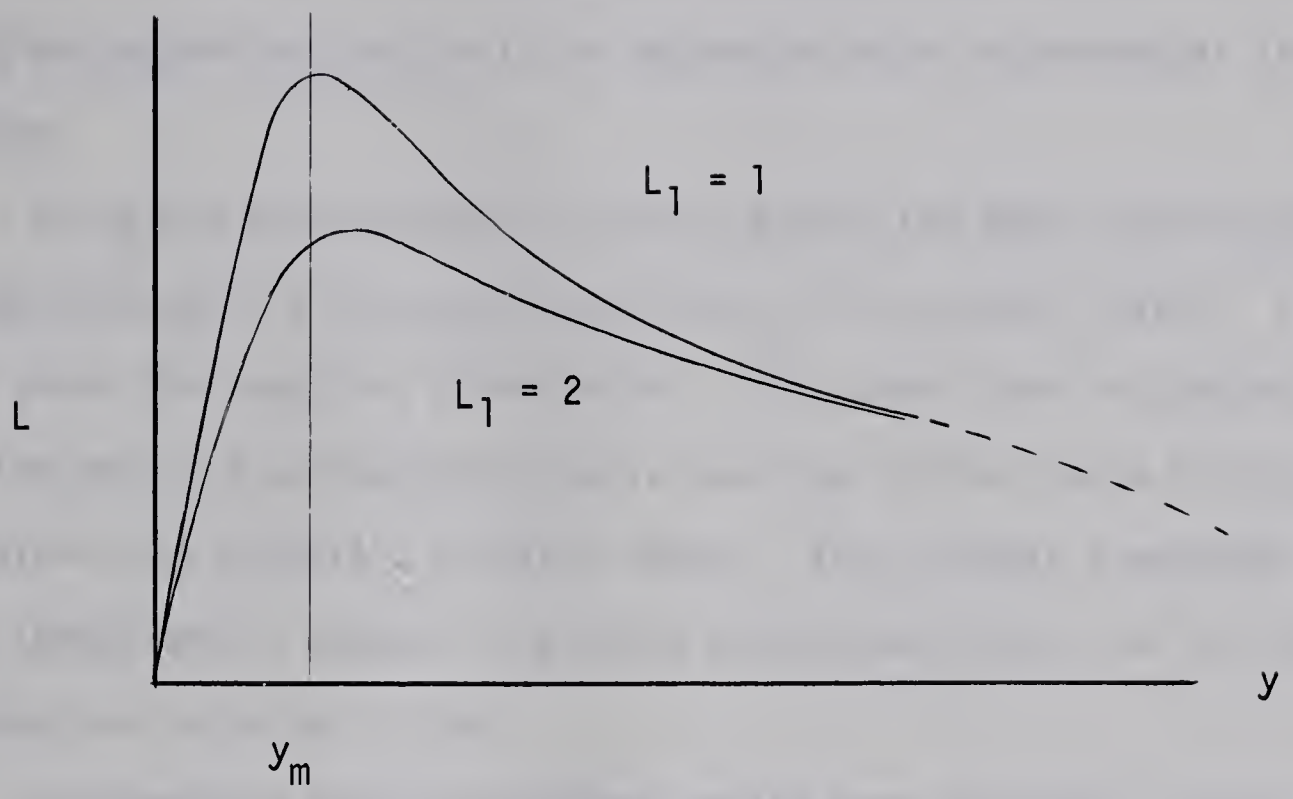

FIG. 2.4 SKETCH OF THE MIXING LENGTH IN THE BOUNDARY LAYER

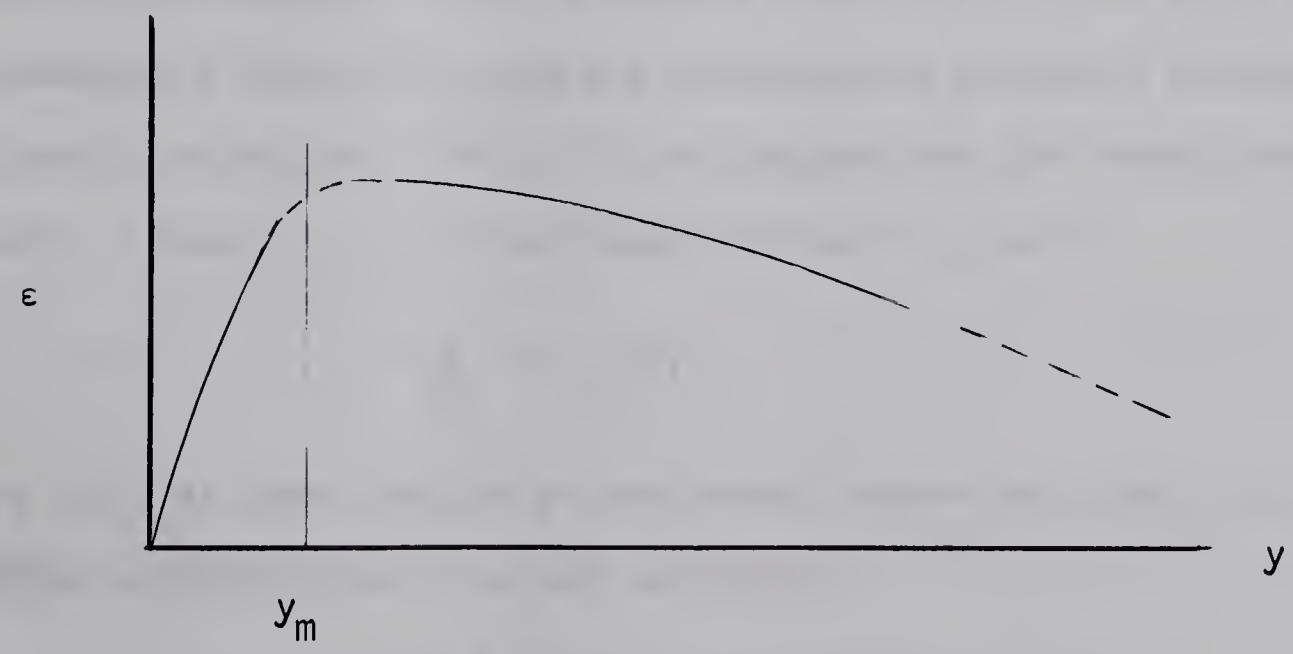

FIG. 2.5 SKETCH OF EDDY DIFFUSIVITY
USING PRANDTL'S EXTENDED MIXING LENGTH THEORY

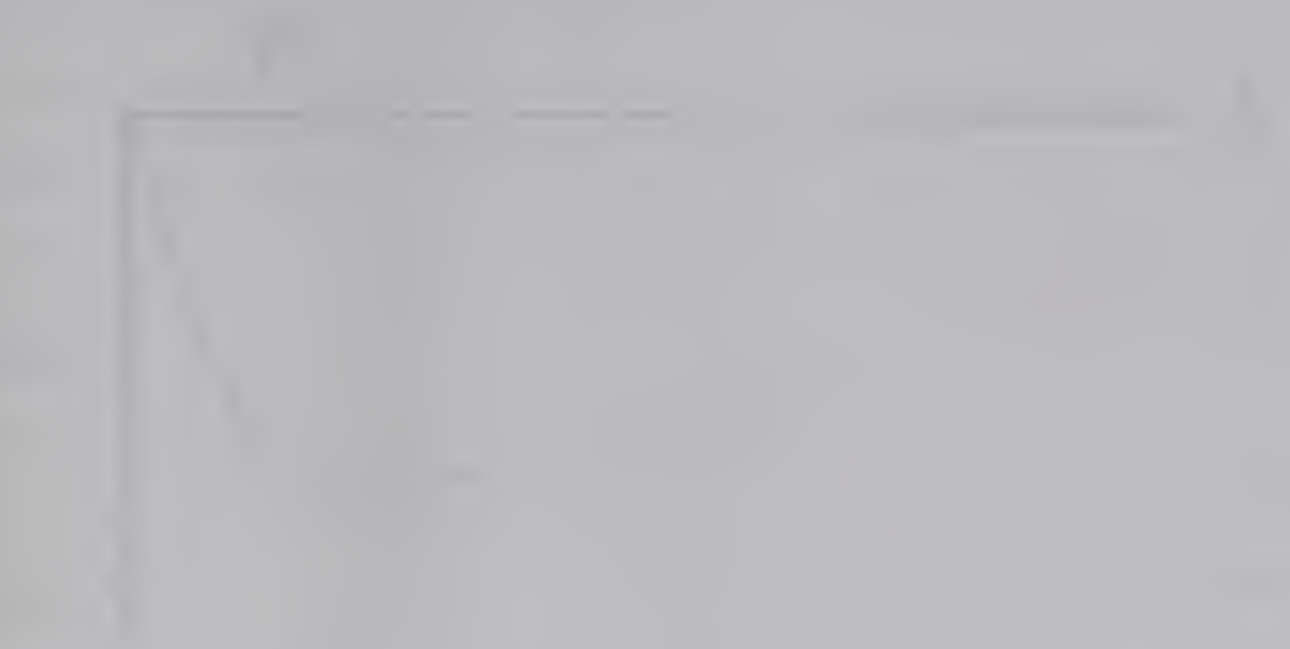

variation of a mixing length L was known, equation 2-5 could probably be made to fit the curve by choosing an appropriate expression for L_1. Such an expression could only be determined by an experimental investigation.

Using the distribution of L given above, the eddy viscosity can be determined as a function of position in the boundary layer. Figure 2.5 shows the resulting distribution. This curve does not become zero at the point of maximum velocity as does the similar curve (figure 2.3) obtained with Prandtl's original theory. Thus Prandtl's extended mixing length theory appears to provide a reasonable model for the free convection turbulent system.

The momentum diffusivity model having been discussed, consider now the model for thermal diffusivity. In the mixing length analogy, lumps of fluid are considered to move in bulk. Thus the mixing length for the transport of "heat" is identical to the mixing length for the transport of momentum. But the thermal diffusivity is not equal to the momentum diffusivity unless the corresponding molecular processes are equally effective. This will only happen when the Prandtl number is unity. Thus, if ε_T is the thermal diffusivity, with

$$\frac{\varepsilon}{\varepsilon_T} = \xi(Pr) ,$$

where $\xi(Pr)$ is some function of the Prandtl number such that $\xi(1) = 1$, then the turbulent heat flux may be written

$$q = -\frac{\rho C_p L^2}{\xi(Pr)} \left[\left[\frac{d\bar{u}}{dy} \right]^2 + L_1^2 \left[\frac{d^2\bar{u}}{dy^2} \right]^2 \right]^{1/2} \frac{d\bar{T}}{dy}$$

where $\bar{T}$ is the mean temperature.

2.2 SIMILARITY ANALYSIS

The governing equations in a free turbulent flow in an incompressible fluid, ignoring dissipation are:

CONTINUITY: $$\frac{\partial V_j}{\partial x_j} = 0^* \qquad 2\text{-}6$$

MOMENTUM: $$\frac{DV_i}{Dt} = G_i - \frac{1}{\rho}\frac{\partial p}{\partial x_i} + \nu \frac{\partial^2 V_i}{\partial x_j^2} \qquad 2\text{-}7$$

ENERGY: $$\frac{DT}{Dt} = \kappa \frac{\partial^2 T}{\partial x_j^2} \qquad 2\text{-}8$$

where V_i, V_j, p and t are instantaneous values.

The momentum equation will now be studied in greater detail. From the continuity equation it follows that

$$v_i \frac{\partial V_j}{\partial x_j} = 0$$

---

* In general, the steady state continuity equation is given by

$$\rho \nabla \cdot \underset{\sim}{V} + \underset{\sim}{V} \cdot \nabla \rho = 0$$

where ρ is temperature dependent. This equation may be written as

$$\nabla \cdot \underset{\sim}{V} - \left[\frac{\beta \theta_w}{1+\beta\theta}\right] \underset{\sim}{V} \cdot \nabla \frac{\theta}{\theta_w} = 0$$

where $\theta = T - T_\infty$ and $\theta_w = T_w - T_\infty$. If $\theta_w \beta$ is much less than unity, then the above equation reduces to equation 2-6. Small fluctuations will not change this result.

Adding this term to the momentum equation and rearranging slightly, equation 2-7 becomes

$$\frac{\partial V_i}{\partial t} + \frac{\partial V_i V_j}{\partial x_j} = G_i - \frac{1}{\rho}\frac{\partial p}{\partial x_i} + \nu \frac{\partial^2 V_i}{\partial x_j^2} \quad .$$

Now let $V_i = \overline{V}_i + V_i'$, $V_j = \overline{V}_j + V_j'$ and $p = \overline{p} + p'$. If the result is averaged over a sufficiently long period during steady state boundary conditions, the momentum equation will become

$$\frac{\partial \overline{V}_i \overline{V}_j}{\partial x_j} + \frac{\partial \overline{V_i' V_j'}}{\partial x_j} = G_i - \frac{1}{\rho}\frac{\partial \overline{p}}{\partial x_i} + \nu \frac{\partial^2 \overline{V}_i}{\partial x_j^2}$$

or

$$\overline{V}_j \frac{\partial \overline{V}_i}{\partial x_j} = G_i - \frac{1}{\rho}\frac{\partial \overline{p}}{\partial x_i} + \frac{\partial}{\partial x_j}\left[\nu \frac{\partial \overline{V}_i}{\partial x_j} - \overline{V_i' V_j'}\right] .$$

In the discussion of the momentum diffusivity model, the Reynolds stress, $-\overline{\rho u' v'}$ was represented by

$$\tau = -\overline{\rho u' v'} = \rho \varepsilon \frac{d\overline{u}}{dy} .$$

Extending this model to

$$\rho \overline{V_i' V_j'} = \rho \varepsilon_{ij} \frac{\partial \overline{V}_i}{\partial x_j}$$

where ε_{ij} is the diffusivity tensor, the momentum equation may be written

$$\overline{V}_j \frac{\partial \overline{V}_i}{\partial x_j} = G_i - \frac{1}{\rho}\frac{\partial \overline{p}}{\partial x_i} + \frac{\partial}{\partial x_j}\left[\nu + \varepsilon_{ij}\right]\frac{\partial \overline{V}_i}{\partial x_j} .$$

The energy equation may be treated similarly. Using

$$\overline{V_j' T'} = -\varepsilon_{ijT} \frac{\partial \overline{T}}{\partial x_j}$$

i.e.,

$$\overline{V_j'T'} = -\frac{\varepsilon_{ij}}{\xi(Pr)} \frac{\partial \overline{T}}{\partial x_j} ,$$

the energy equation 2-8 becomes

$$\overline{V}_j \frac{\partial \overline{T}}{\partial x_j} = \frac{\partial}{\partial x_j} \left[\kappa + \frac{\varepsilon_{ij}}{\xi(Pr)} \right] \frac{\partial \overline{T}}{\partial x_j} . \qquad 2\text{-}9$$

In the fully turbulent boundary layer, ε_{ij} is usually very much greater than ν, and $\varepsilon_{ij}/\xi(Pr)$ is usually very much greater than κ. Therefore the kinematic viscosity ν and the thermal diffusivity κ will be neglected and the momentum and energy equations become

$$\overline{V}_j \frac{\partial \overline{V}_i}{\partial x_j} = G_i - \frac{1}{\rho} \frac{\partial \overline{p}}{\partial x_i} + \frac{\partial}{\partial x_j} (\varepsilon_{ij}) \frac{\partial \overline{V}_i}{\partial x_j}$$

and

$$\overline{V}_j \frac{\partial \overline{T}}{\partial x_j} = \frac{\partial}{\partial x_j} \left[\frac{\varepsilon_{ij}}{\xi(Pr)} \right] \frac{\partial \overline{T}}{\partial x_j} ,$$

respectively.

In general, the momentum and energy equations are three dimensional. In a boundary layer along a flat plate, however, it is reasonable to assume that the flow is two dimensional. Any rate of change in a boundary layer is usually much less in the direction of the flow than perpendicular to it. Thus it is reasonable to expect that

$$\frac{\partial}{\partial x} \left[\varepsilon \frac{\partial \overline{u}}{\partial x} \right] << \frac{\partial}{\partial y} \left[\varepsilon \frac{\partial \overline{u}}{\partial y} \right]$$

and

$$\frac{\partial}{\partial x}\left[\frac{\varepsilon}{\xi(Pr)}\frac{\partial \overline{T}}{\partial x}\right] << \frac{\partial}{\partial y}\left[\frac{\varepsilon}{\xi(Pr)}\frac{\partial \overline{T}}{\partial y}\right]$$

and thus the terms

$$\frac{\partial}{\partial x}\left[\varepsilon\frac{\partial \overline{u}}{\partial x}\right] \quad \text{and} \quad \frac{\partial}{\partial x}\left[\frac{\varepsilon}{\xi(Pr)}\frac{\partial \overline{T}}{\partial x}\right]$$

will be ignored. The governing equations applied to a vertical flat plate then reduce to:*

CONTINUITY: $$\frac{\partial u}{\partial x} + \frac{\partial v}{\partial y} = 0$$

MOMENTUM: $$u\frac{\partial u}{\partial x} + v\frac{\partial u}{\partial y} = -g - \frac{1}{\rho}\frac{\partial p}{\partial x} + \frac{\partial}{\partial y}\varepsilon\frac{\partial u}{\partial y}$$

ENERGY: $$u\frac{\partial T}{\partial x} + v\frac{\partial T}{\partial y} = \frac{\partial}{\partial y}\frac{\varepsilon}{\xi(Pr)}\frac{\partial T}{\partial y}$$

Applying thermodynamic principles,

$$-g - \frac{1}{\rho}\frac{\partial p}{\partial x} \text{ becomes } g(T - T_\infty) - \frac{1}{\rho}\frac{\partial p_l}{\partial x},$$

where p_l is the incremental increase in pressure due to the boundary layer system. Outside the boundary layer $\partial p_l/\partial x = 0$. Thus, since it is also small at the plate (and $\partial p/\partial y \simeq 0$) it may be neglected. The momentum equation then becomes

$$u\frac{\partial u}{\partial x} + v\frac{\partial u}{\partial y} = g\beta(T - T_\infty) + \frac{\partial}{\partial y}\varepsilon\frac{\partial u}{\partial y}.$$

The continuity equation implies the existence of a stream function $\psi = \psi(x,y)$ such that

$$u = \frac{\partial \psi}{\partial y} \quad \text{and} \quad v = -\frac{\partial \psi}{\partial x}.$$

The mean velocity components in the momentum and energy equations

---

* From this point onward the bar above the symbol used to denote time averages will be omitted as confusion with time-dependent quantities is no longer possible. In the interest of simplicity ε_{ij} has been replaced by ε, a scalar.

may be replaced in favour of the stream function. From this substitution come the following pair of partial differential equations with ψ and T as functions of x and y:

$$\frac{\partial\psi}{\partial y}\frac{\partial^2\psi}{\partial x\partial y} - \frac{\partial\psi}{\partial x}\frac{\partial^2\psi}{\partial y^2} = \beta g(T - T_\infty) + \varepsilon\frac{\partial^3\psi}{\partial y^3} + \frac{\partial^2\psi}{\partial y^2}\frac{\partial\varepsilon}{\partial y} \qquad 2\text{-}10$$

$$\frac{\partial\psi}{\partial y}\frac{\partial T}{\partial x} - \frac{\partial\psi}{\partial x}\frac{\partial T}{\partial y} = \frac{\varepsilon}{\xi(Pr)}\frac{\partial^2 T}{\partial y^2} + \frac{\partial T}{\partial y}\frac{\partial}{\partial y}\left[\frac{\varepsilon}{\xi(Pr)}\right].$$

Now a single independent variable, η, is sought in order to transform the above partial differential equations into ordinary differential equations. In general $\eta = \eta(x,y)$, so let

$$\eta = \frac{C_1 y}{x^n}.$$

In addition, let the stream function $\psi(x,y)$ be "similar" to another stream function $f(\eta)$ such that

$$\psi(x,y) = C_2 x^m f(\eta).$$

Also, the eddy diffusivity ε is in general a function of x and y. A simple expression admitting such a dependency is

$$\varepsilon = D x^p y^q .$$

This will be adopted for future use.

Up to this point nothing has been said about the wall temperature variation. A useful extension of the isothermal wall condition is achieved by letting the wall temperature vary as x to the power s. That is,

$$T_w - T_\infty = N x^s.$$

It is now possible to determine C_1, C_2, D, m, n, and s and then justify "a posteriori" these forms.

If the momentum equation (2-10) is to be transformed to an

ordinary equation then it must be independent of x and y. The above substitutions thus yield

$$m = \frac{s + 2p + 3 - (s + 1)q}{2(2 - q)} \qquad 2\text{-}11$$

and

$$n = \frac{1 + 2p - s}{2(2 - q)} \, . \qquad 2\text{-}12$$

The similarity variable η is then given by

$$\eta = C_1 \, y \, x^{(s-2p-1)/(4-2q)} \qquad 2\text{-}13$$

where

$$C_1 = \left[\frac{g\beta N}{4D^2}\right]^{1/(4-2q)}$$

and the independent variables $f(\eta)$ and $\phi(\eta)$ are given by

$$f(\eta) = \frac{\psi}{4 \, D \, C_1^{1-q} \, x^m} \quad \text{and} \quad \phi(\eta) = \frac{T - T_\infty}{T_w - T_\infty} \, . \qquad 2\text{-}14$$

Under the transformation equations 2-13 and 2-14, the partial differential equations become

$$\eta^q f''' + 4mf''f + q\,\eta^{q-1} f'' - 2(s+1)(f')^2 + \phi = 0 \qquad 2\text{-}15$$

$$\frac{\eta^q \phi''}{\xi(Pr)} + 4m\phi' f + \frac{q\eta^{q-1}}{\xi(Pr)}\phi' - 4s\phi f' = 0. \qquad 2\text{-}16$$

2.3 LOCAL HEAT TRANSFER

The local heat transfer from the plate to the fluid may be calculated using a modification of Fourier's law. That is,

$$Q = - \left[k + \frac{\rho \varepsilon C_p}{\xi(Pr)}\right]\left[\frac{\partial T}{\partial y}\right]_{y=o} .$$

In section 2.2 the assumption that $\varepsilon_T >> \kappa$ was made. This is defen-

sible across the boundary layer except very near the plate. Although turbulent fluctuations are believed to exist at the plate (see section 4.3-4) they are not as dominant as in the main boundary layer stream and it is assumed that at the plate the local heat transfer is given exactly by Fourier's law. That is

$$Q = - k \left[\frac{\partial T}{\partial y}\right]_{y=0}.$$

Introducing the dimensionless variables from equations 2-11 and 2-12, the expression for the heat transfer becomes

$$Q = - k N C_1 x^{s-n} \phi'(0).$$

Thus the local heat transfer coefficients h_x is

$$h_x = \frac{Q}{T_w - T_\infty} = - k C_1 x^{-n} \phi'(0) \qquad 2\text{-}17$$

and the local Nusselt number Nu_x is

$$Nu_x = \frac{h_x x}{k} = - C_1 x^{1-n} \phi'(0). \qquad 2\text{-}18$$

Considering figure 2.5, it is reasonable to divide the boundary layer into two regions:

a) the region from the wall to the point of maximum velocity ($q = 1$),

b) the region from the maximum velocity to the edge of the boundary layer ($q = 0$).

If the wall is at a constant temperature, the exponent s is zero. For turbulent flow it is estimated [3] that a constant wall temperature gives rise to a constant heat flux. That is, since

$$- k N C_1 x^{s-n} \phi'(0) = \text{constant}$$

the exponent n must be zero also. Throughout the region close to the

wall, conditions of constant heat flux and constant temperature would most likely prevail to a good approximation because this layer is quite thin.

If both s and n are equal to zero in both regions, equation 2-12 fixes the power p at a value of -1/2. Therefore the eddy diffusivity becomes

$$\varepsilon = Dy^{q}x^{-1/2} .$$

With this value of p, equation 2-11 fixes the value of m at 1/2. Thus the similarity variable may be written as

$$\eta = C_1 y ,$$

with the dependent variables $f(\eta)$ and $\phi(\eta)$ given by

$$f(\eta) = \frac{x}{4DC_1^{1-q}x^{1/2}} \qquad \text{and} \qquad \phi(\eta) = \frac{T - T_\infty}{T_w - T_\infty}$$

In these equations

$$C_1 = \left[\frac{g\beta(T_w - T_\infty)}{4D^2}\right]^{\frac{1}{4-2q}}$$

Equations 2-15 and 2-16 now become

$$\eta^{q} f''' + 2f''f + q\,\eta^{q-1} f'' - 2(f')^2 + \phi = 0 \qquad 2\text{-}19$$

and $$\eta^{q}\phi'' + 2\phi' f\xi(Pr) + q\eta^{q-1}\phi' = 0. \qquad 2\text{-}20$$

Also, the local heat transfer coefficient reduces to

$$h_x = -kC_1\phi'(0)$$

and the local Nusselt number becomes

$$Nu_x = C_1 x\phi'(0).$$

In the inner region of the boundary layer $q \simeq 1$. That is

$$\varepsilon = D\, y\, x^{-1/2}$$

and the governing equations become

$$\eta f''' + 2f''f + f'' - 2(f')^2 + \phi = 0$$

and

$$\eta\phi'' + 2\phi' f\xi(Pr) + \phi' = 0.$$

In the outer region the dependency of the eddy diffusivity on the distance from the plate is not strong, i.e. $q \simeq 0$. That is,

$$\varepsilon = D\, x^{-1/2}$$

and the corresponding forms of the governing equations are

$$f''' + 2f''f - 2(f')^2 + \phi = 0$$

and

$$\phi'' + 2\phi' f\xi(Pr) = 0.$$

It is interesting to note that this turbulent free convection system cannot be described by a single set of differential equations. A unique set of equations exists for each of the inner and outer regions of the boundary layer.

CHAPTER III

EXPERIMENTAL WORK

3.1 APPARATUS

To gain a greater insight into the mechanism of turbulence, certain experiments were executed. These were performed inside an 8" x 18" x 75" steel tank. As the tests were run in water it was necessary to paint the tank to prevent rusting. A zinc cathodic protection paint, Devcon Z, was found most satisfactory. The tank was open at the top, with an access port (6" x 6") on its right side, a plexiglass observation window (2" x 10") at the front and a one-half inch drain pipe in the rear. A sketch of the testing tank and accompanying equipment is presented in figure 3.1.

The vertical plate and the probe positioning equipment, housed in the bottom half of the tank, are shown in figure 3.2. The plate, 14" high by 6" wide, was cut from 0.010 inch stainless steel shimstock and held under tension by adjustable brass jaws. The leading edge attachment, which formed the bottom jaw, was proven satisfactory in air by the Schlieren investigation discussed in Appendix A. Four leveling screws on the bottom of the vessel could be adjusted to make the plate vertical.

Positioning equipment had to be designed to enable the operator to adjust the probe (a thermocouple or fibre anemometer) from outside the tank once the access port was closed. The probe was thus mounted

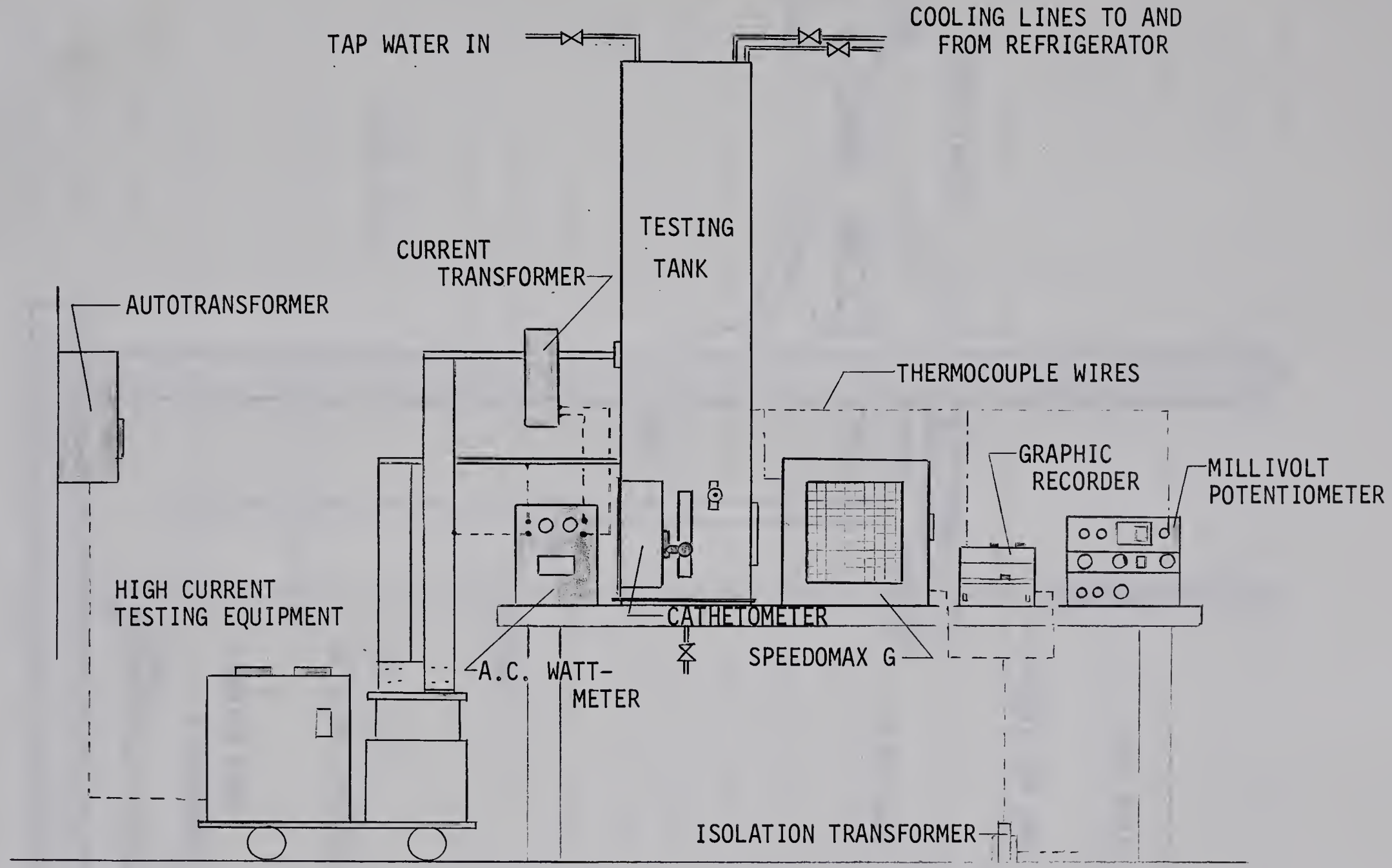

FIG. 3.1 GENERAL VIEW OF EQUIPMENT

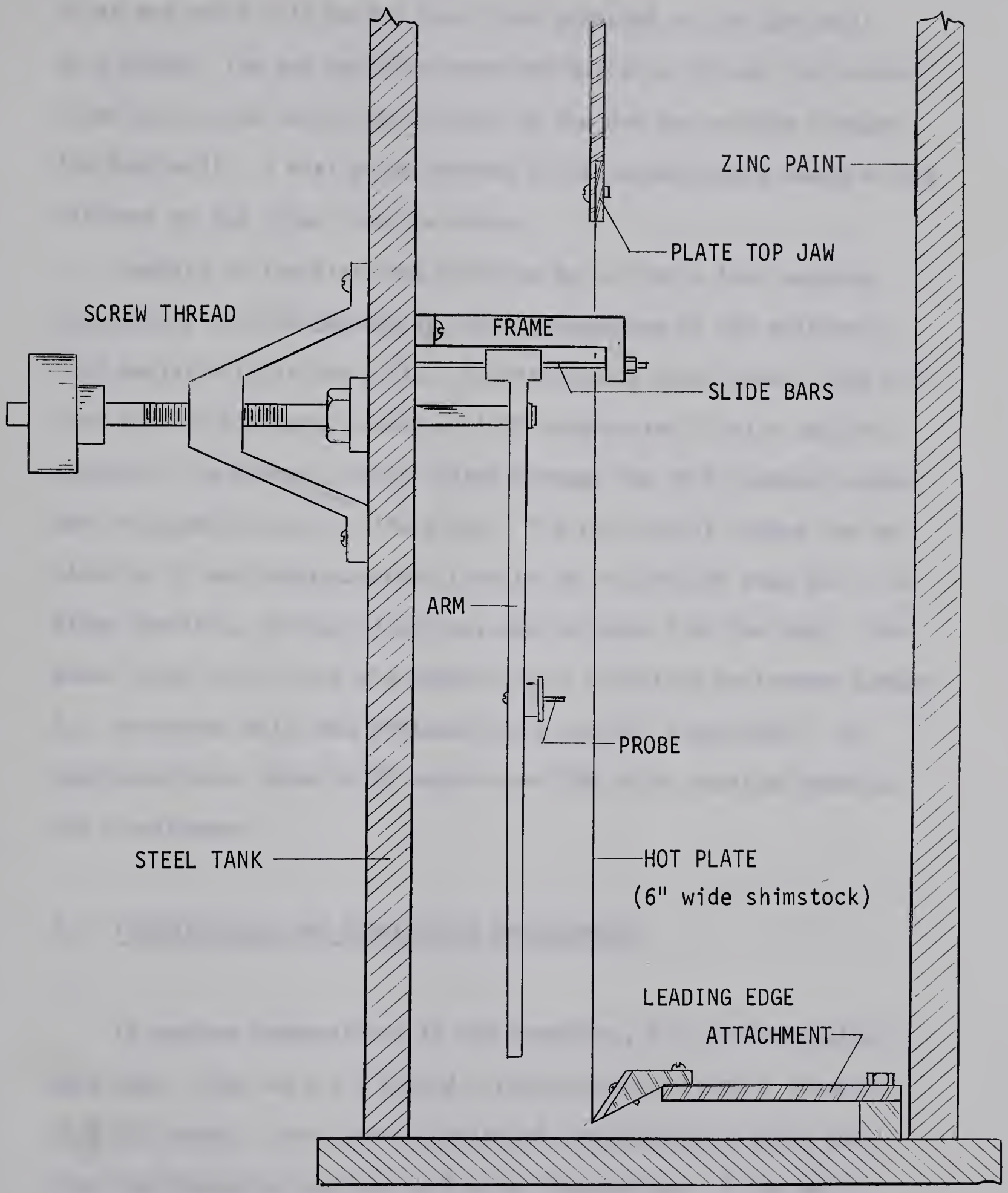

FIG. 3.2 DETAILED VIEW OF HOT PLATE AND PROBE POSITIONING EQUIPMENT

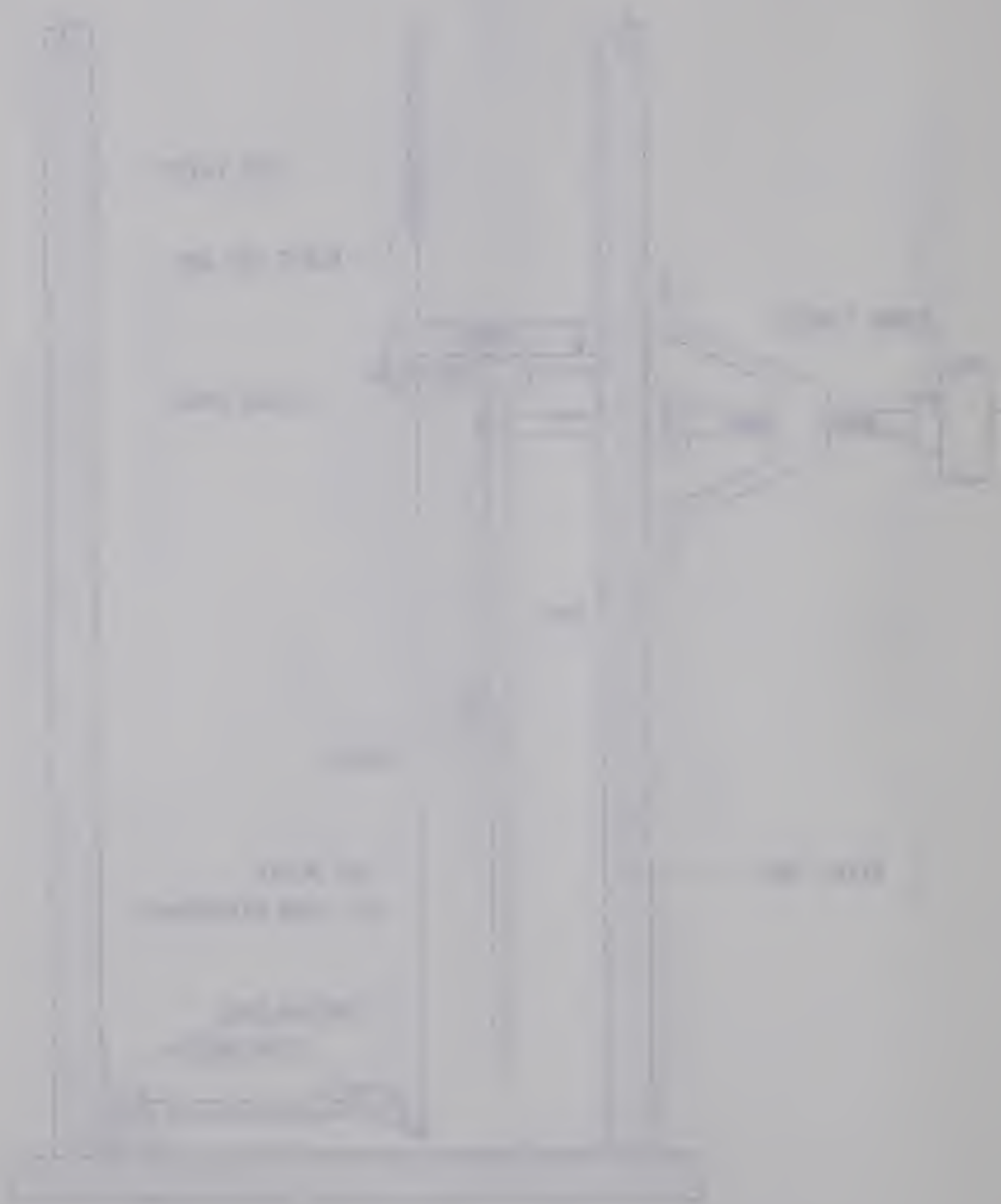

on an arm which slid on two steel rods attached to the tank wall by a frame. The arm could be moved horizontally through the boundary layer by a screw mechanism attached to the arm and passing through the tank wall. A dial gauge mounted on the screw handle measured the distance of the probe from the plate.

Heating of the plate was achieved by passing a high amperage alternating current through it, taking advantage of the relatively high resistivity of the plate. A Westinghouse transformer (High Current Testing Equipment) rated at 1000 amperes and 8 volts was the source of the current, which passed through one inch diameter copper bars to opposite jaws of the plate. The tank itself formed one terminal as it was connected electrically to the leading edge jaw. The other terminal, the top plate jaw, was isolated from the tank. The power input to the tank was measured on a Cambridge Instrument Company A.C. wattmeter which was protected by a current transformer. An autotransformer rated at 20 amperes and 280 volts supplied power to the transformer.

3.2 THERMOCOUPLES AND TEMPERATURE MEASUREMENTS

To measure temperatures in the apparatus, five thermocouples were used. They were all Type-J (iron-constantan) with a diameter of 0.010 inches. Four were distributed throughout the tank, away from the plate, to read the bulk water temperature. A lap weld formed the joint in each case. The fifth, referred to here as the

"probe" thermocouple, was joined by a butt weld and attached to a support which in turn was fastened to the arm shown in figure 3.2. This thermocouple was used for measuring the boundary layer temperature profiles and the nominal bulk and plate temperatures.

The signals from the four thermocouples measuring bulk water temperatures were fed into four channels of a Leeds and Northrup Speedomax G strip chart recorder. This recorder has twenty-four channels and executes one complete cycle in about fifty-five seconds. The signal from the probe thermocouple was sent to one of three instruments: the above mentioned Leeds and Northrup Speedomax G strip chart recorder, a Leeds and Northrup millivolt potentiometer, or a Varian continuous output graphic recorder. Each unit is shown in figure 3.1 and had specific applications which will now be discussed.

For most laminar results the readings were taken from the millivolt potentiometer, with the advantage that the temperatures could be measured to $\pm$ 0.1 Fahrenheit degrees. It had the disadvantage that the values obtained could not be checked later. For this reason, some of the laminar results were obtained with the Speedomax G, which makes a permanent record of each test. However, this unit can be read only to $\pm$ 0.3 Fahrenheit degrees.

For transitional and turbulent mean velocity profiles the Speedomax G was used. The output signal from the boundary layer thermocouple was fed into twenty of the twenty-four channels so that at any given distance from the plate an average temperature could be calculated by averaging the twenty values punched out.

In fluctuating temperature investigations for transitional and turbulent flow, the signal was fed into the Varian continuous output recorder. A typical output from this recorder is shown in figure 4.9. A chart speed of sixteen inches per minute, with a full scale deflection of 10 millivolts in 0.5 seconds, permitted temperature fluctuations to be recorded with a response rate of 480 Fahrenheit degrees per second. Before the probe thermocouple was placed inside the tank its response rate was estimated at 1760 Fahrenheit degrees per second. (See Appendix B). Experiments later revealed that the turbulent system demands a maximum response rate of 200 Fahrenheit degrees per second. Thus the thermocouple and Varian recorder were able to pick up and record, with ample accuracy, any temperature fluctuations produced within the boundary layer.

During test preparations, a certain amount of drift appeared in the readings. This was overcome by passing the power supplied to the recorders through the isolation transformer shown in figure 3.1.

The plan, initially, was to run the tests in distilled water, but equipment complications led to the substitution of tap water. To remove the dissolved air it was necessary to bring the water in the tank to a full boil. This proved most satisfactory and air bubbles were never observed in the water or on the equipment inside the tank.

In an attempt to achieve steady conditions during each test, cooling coils were placed near the top of the tank. A baffle directed the rising heated water through the coils and another baffle directed the cooled water downward near the back of the tank. (See Appendix C for a sketch of this arrangement). The cooling coils were connected

to a one-half ton (3.52 kilowatts) refrigerator. As the heat input during a turbulent test was about seven kilowatts, steady conditions were never completely achieved.

3.3 TEMPERATURE TEST PROCEDURES

When a transition or turbulent temperature test was run, the probe thermocouple was connected to either the Speedomax G or the Varian recorder. (An initial arrangement, feeding the same signal to both recorders simultaneously, proved unsatisfactory.) After the thermocouple was positioned somewhere in the outer region of the boundary layer and the dial gauge reading noted, the power was turned on and adjusted to the required input. The Varian was run continuously for one to two minutes with the thermocouple fixed at some given distance from the plate, but had to be turned off while the probe position was being changed. When this recorder was used, a datum had to be established on the chart by taking the initial tank temperature with the millivolt reading on the potentiometer at the start of the run. The Speedomax G did not require this, as its chart gives temperature directly. Also, the latter could be run continuously when probe position adjustments were made during the recording of signals from the four tank thermocouples.

When the thermocouple was just touching the plate, it was assumed to be recording the temporal mean temperature at a distance equal to the thermocouple radius from the plate. The maximum temperature recorded was taken as the plate temperature. Although changes in the

probe thermocouple's position could be read to ± 0.0002 inches, using the dial gauge, the position relative to the plate could be judged only to ± 0.0025 inches.

For laminar temperature tests the procedure was identical to that for the turbulent runs if the Speedomax G recorder was used.

3.4 THE FIBRE ANEMOMETER

In 1934, Schmidt [5] determined experimental velocity profiles across a laminar air boundary layer near a hot vertical plate by using a fibre anemometer. This anemometer was simply a small quartz rod, fixed at one end with the free end deflecting when placed in a moving fluid. The amount of deflection was an indication of the fluid velocity. The fibre had previously been calibrated in a forced air stream, the velocity of which was known. The results Schmidt obtained were excellent.

In view of the success of Schmidt, an attempt was made to construct a similar anemometer suitable for measuring mean turbulent velocities. It would be very difficult to calibrate the fibre by placement in a stream of water at a known velocity because the properties of that fluid are very temperature dependent. As an alternative, an attempt was made to obtain an expression relating fluid velocity to the deflection of the fibre.

To develop this formula, the fibre may be treated as a cantilever beam, uniformly loaded by virtue of a velocity-induced drag force. If simple beam theory is assumed it can be shown (see Appendix D) that the

deflection of the fibre is given by

$$\delta = \frac{4\rho_\infty l^4 U^2 C_D}{\pi E d^3} \qquad 3\text{-}1$$

where U is the "free stream" velocity, l is the fibre length, d is the fibre diameter, E is the modulus of elasticity, and C_D is the drag coefficient. Now this expression represents the deflection of an unyawed circular cylinder in a forced flow, but it is assumed to be valid in a free flow also if ρ_∞ and U are replaced by their local values and the deflections are small.

If the Reynolds number is between 0.5 and 6, the drag coefficient may be represented by

$$C_D = -0.2Re + 3.6 + 6.6/Re$$

where $Re = Ud/\nu$. This expression is obtained by curve fitting the graph presented by Schlichting [7] for the drag coefficient of a circular cylinder in a forced flow.

The fibre anemometer used in this study consisted of a fibre, probe, and support. The fibre was mounted on the probe and held by CIL Household Cement. The probe was fixed to the support by a screw and the support was clamped to the arm illustrated in figure 3.2. A sketch of the anemometer is given in figure 3.3.

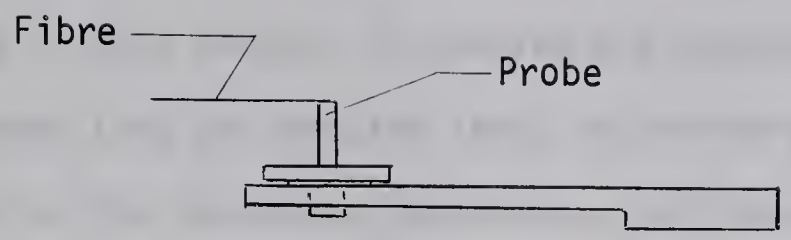

FIG. 3.3 FIBRE ANEMOMETER

The fibre was made of fused quartz with a nominal diameter of 50 microns. As 50 microns was only the approximate diameter, an attempt was made to measure it more accurately. Because of the very small diameters involved, a micrometer was useless. A toolmaker's microscope and shadowgraph were also of little value because of the cylindrical shape of the probe and its small dimension. The most precise dimensions obtained were measured by interferometric techniques, as discussed in Appendix D. Although the precision of this method was good ($\pm$ 2 x 10^{-6} inches) the accuracy was unreliable. The most reliable measurements were obtained with the Pitter Gauge and Tool Company Limited Diameter Measuring Machine represented in figure D.2, and discussed in Appendix D. This machine found the diameter of one fibre, 10 centimetres in length, to vary between 0.00190 and 0.00200 inches, with the average of eight readings being 0.00197 inches, or 50.04 microns. This fibre was the one used in the velocity measurement tests.

As well as finding the diameter, it is necessary to know the modulus of elasticity of quartz before equation 3-1 can be applied. As the temperature of the water is changing through the boundary layer from about 5 degrees centigrade to about 90 degrees centigrade, it is

important to anticipate possible changes in the modulus. Eitel [8] has demonstrated graphically that elasticity changes little with temperature in this range. His curves are reproduced in figure 3.4a. Boys [9] found that the modulus tends to increase as diameter decreases. This is due to the increased importance, for the smaller fibres, of the surface layer, which has a different elastic constant from the bulk material. For fibres between fifty and one hundred microns, Boys found that $E = 5.2 \times 10^{11}$ dynes/cm.^{2}.

To determine its modulus of elasticity, the 50 micron fibre was treated as a simply supported beam with a load applied at midspan. A series of weights was placed on the fibre and the resultant deflections read with a cathetometer. This procedure gave the modulus of elasticity as 5.61×10^{11} dynes/cm.^{2}. The results of this test are indicated in figure 3.4b.

With equation 3-1 it is now possible to find the velocity of a fluid if its properties and the deflection of the fibre are known. For most fluids, the properties are functions of temperature and it is thus convenient to plot the fluid velocity against the fibre deflection for a constant temperature. A set of such curves appears in figure 3.5. In this case the fluid is water and the curves are those subsequently used to determine the mean turbulent velocity profile. The fibre involved had an average diameter of 50 microns, a length of 1.44 centimetres and a modulus of elasticity of 5.61×10^{11} dynes/cm.^{2}.

If another fibre of length l_N is tried, the same curves are still applicable, since the velocity for any given deflection is $(1/l_N)^4$ times the velocity obtained from figure 3.5. It should be noted,

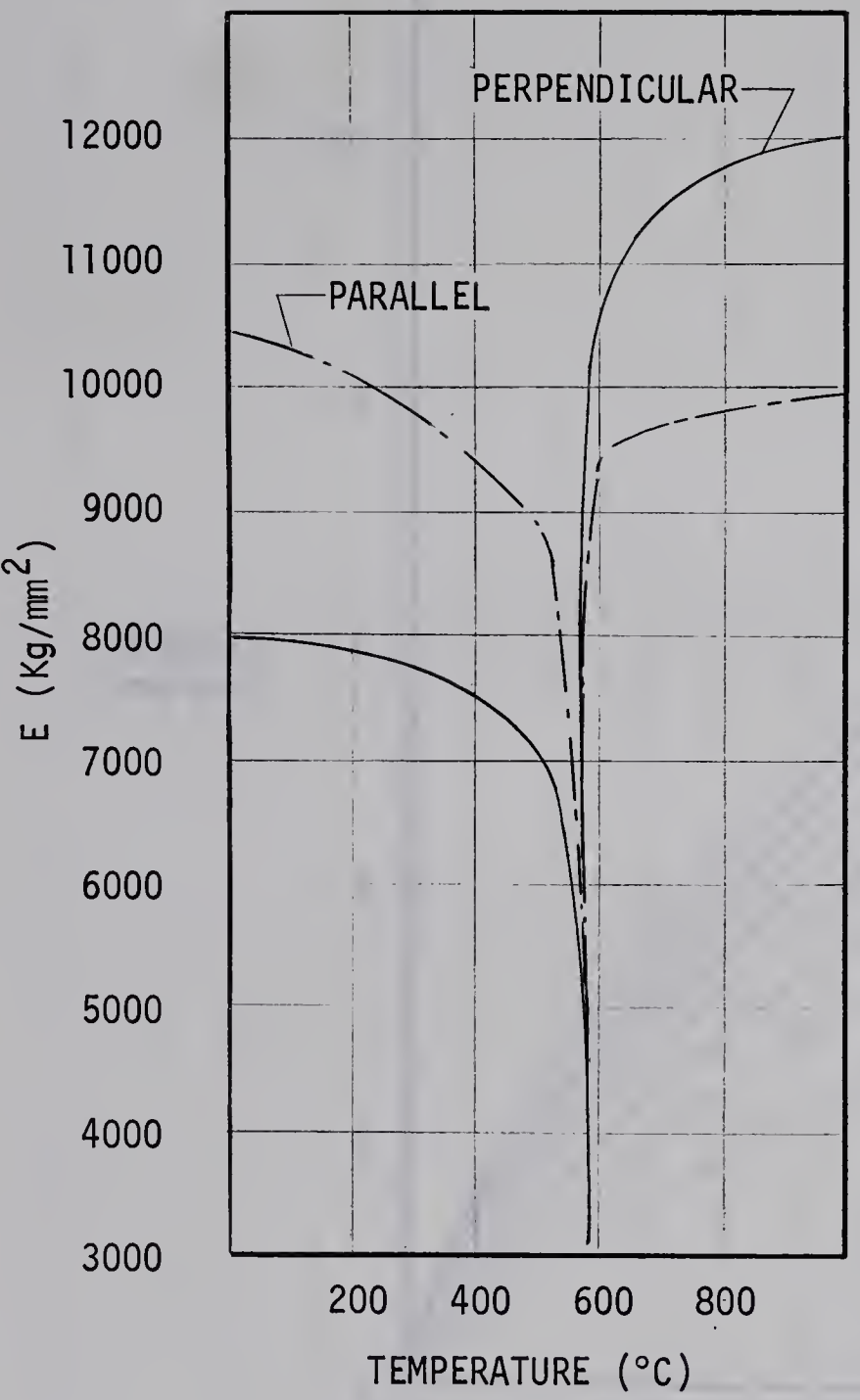

(a) MODULUS OF ELASTICITY OF QUARTZ

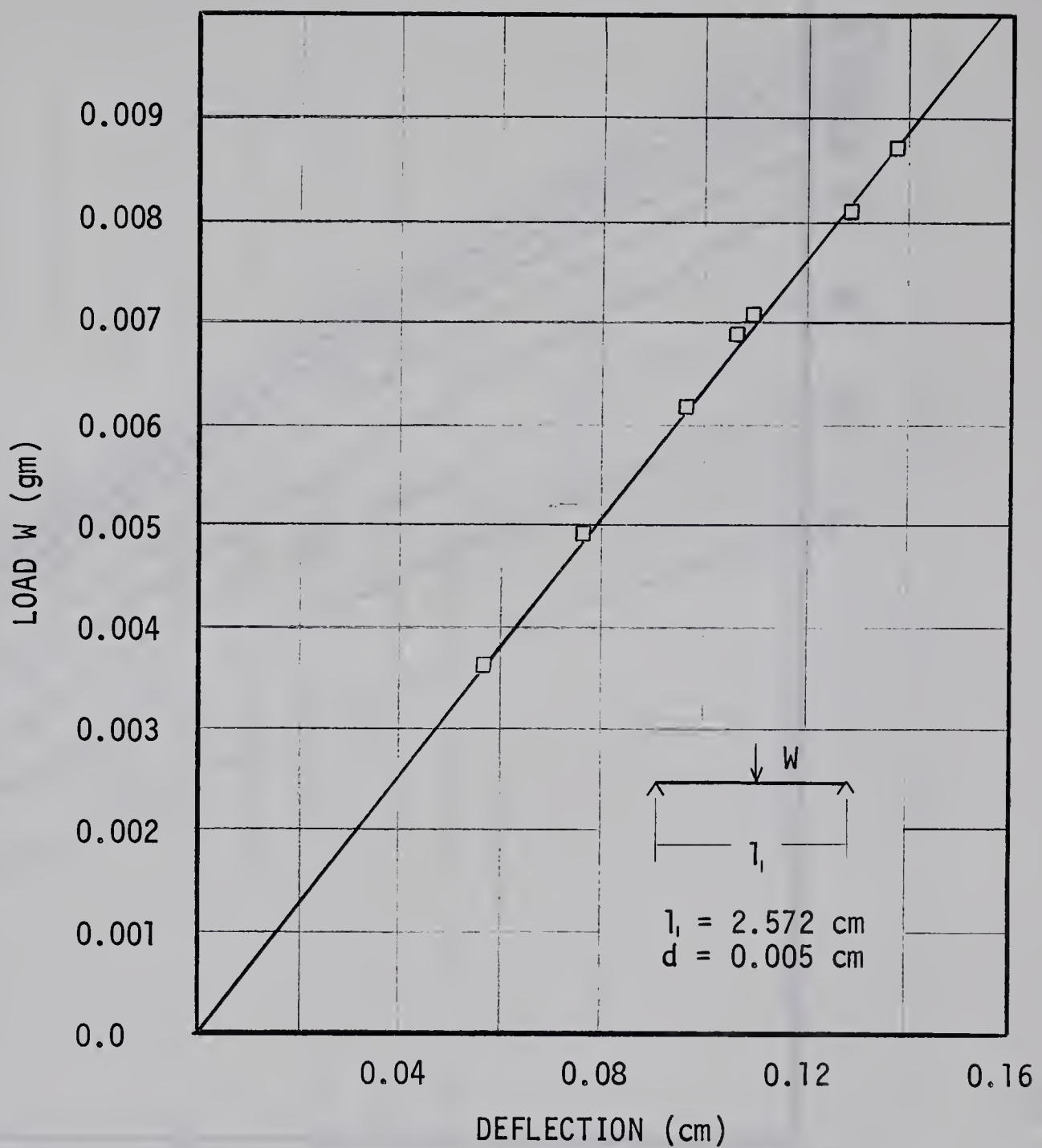

(b) LOAD DEFLECTION CURVE FOR QUARTZ FIBRE

FIG. 3.4

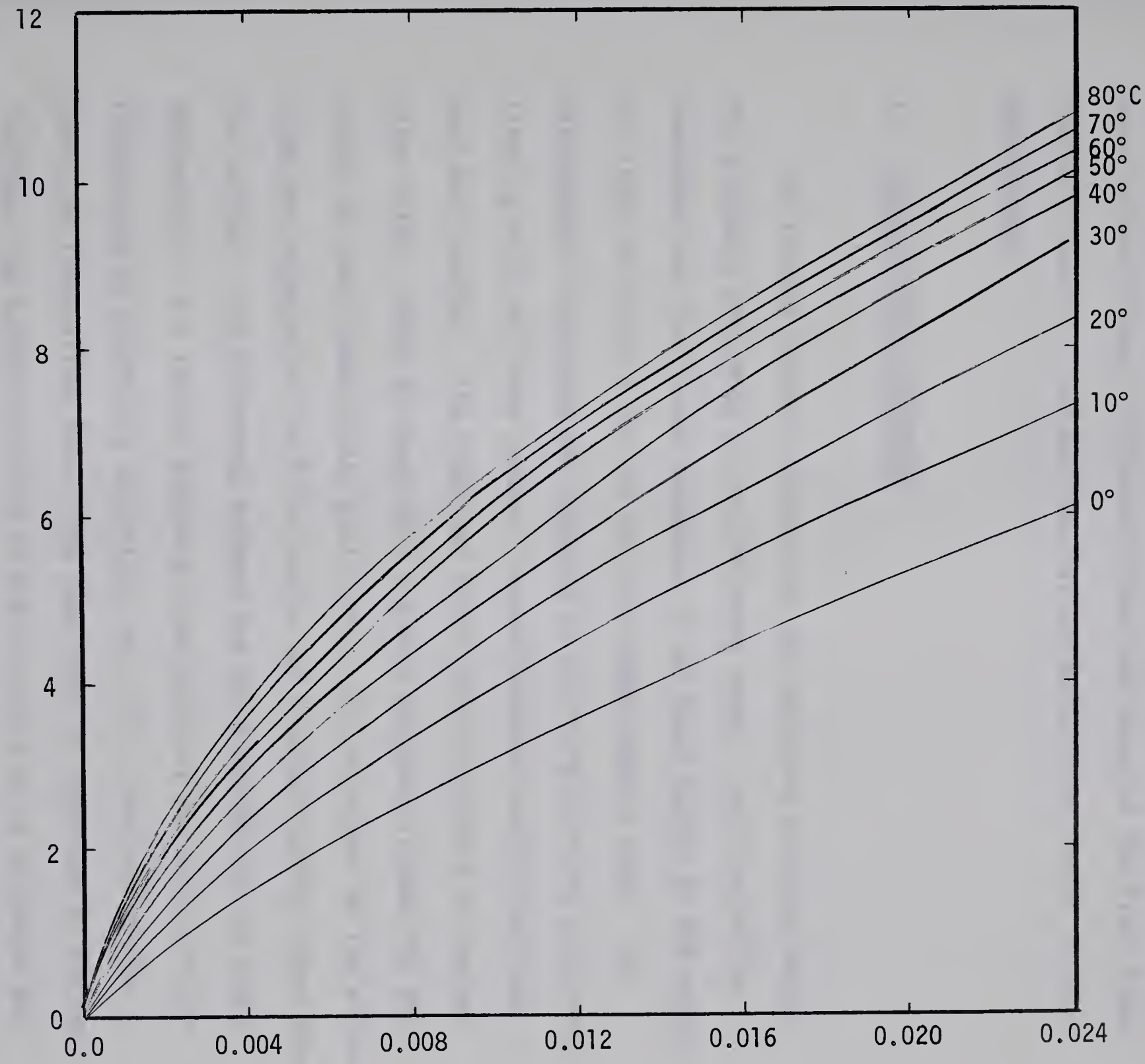

FIG. 3.5 VELOCITY FOR A PARTICULAR DEFLECTION

however, that the diameter and modulus of elasticity must be the same for both fibres. If these differ from those of the first fibre, figure 3.5 can still be applied, but the multiplying factor is more complicated.

3.5 VELOCITY TEST PROCEDURE

For running laminar, transition, and turbulent velocity tests, the procedure consisted of the following steps. The fibre of the anemometer was positioned somewhere in the outer region of the boundary layer (0.75δ to 1.5δ) and the dial gauge reading noted. The cathetometer microscope was focussed on the fibre with the cross hair lined up with the fibre centre. The cathetometer vernier was then read and recorded. The power was turned on and adjusted to the desired value. After at least half a minute had been allowed for the system to reach steady state equilibrium, the cross hair on the microscope was adjusted to the fibre centre and a second reading taken from the vernier. The difference between the two readings was the fibre deflection. If a laminar boundary layer existed, the centre of the fibre could be determined accurately, but for a turbulent system, where the fluctuations are of the same order of magnitude as the deflection, the average position of the fibre had to be estimated and this introduced larger errors. Once the fibre centre had been determined as accurately as possible the power was turned off and the anemometer moved closer to the plate. Here the dial gauge was again

read and the procedure repeated. The deflection observed when the fibre eventually touched the plate was taken as that at a distance equal to the fibre radius away from the plate.

CHAPTER IV

RESULTS AND DISCUSSIONS

4.1 MEAN TEMPERATURE PROFILES

A boundary layer developed near a hot vertical plate is classically divided into laminar, transition, and turbulent flow regions. Near the leading edge, the flow is said to be laminar and any disturbance felt by the boundary layer will be damped out, as the flow is stable. Further downstream, slight fluctuations occur in what is known as the transition region. This region is past the point of neutral stability beyond which any disturbance will continue to grow. In free convection near a plate, the instability due to the outer critical layer appears to be predominant and sets in first [10, 11, 12]. In fact, the outer layer so dominates the flow that the wavelength of an outside wave is impressed on the wave disturbance in the inner layer. Szewczyk [11], who studied the stability of the free convection layer along a vertical flat plate, concluded that the critical Grashof number was about 8.15×10^8. As the fluid moves still farther away from the leading edge, the fluctuations lose any degree of order they possessed in the transition region and become more violent. A free convection boundary layer is normally considered turbulent when the Rayleigh number is 2×10^9. It should be remembered, however, that this is an approximate value experimentally obtained by Saunders and there is nothing fundamental about it.

4.1-1 Laminar, Transition, and Turbulent Temperature Profiles

As the buoyant force is the driving mechanism in any free convection problem, the point at which a "fully developed" turbulent boundary layer exists may be moved closer to the leading edge by increasing the plate temperature. Thus, as the wall temperature rises, the flow may change from laminar to transition to turbulent at a given distance from the leading edge. Figure 4.1 shows laminar, transition, and turbulent mean temperature profiles under such conditions. In this case, the power supplied was increased from 40 to 7040 watts with a resulting increase in $T_w - T_\infty$ from 6 to 150 Fahrenheit degrees.

Laminar flow, represented by the curve with the least slope (□), resulted from a power input of 40 watts. When the power was increased to 600 watts (△) the plate temperature rose but the boundary layer remained laminar. In this case the flow was approaching the limit of stability and the few disturbances which did appear died out. At a power input of 2000 watts (0) the flow was in the transition region, with fluctuations present. These fluctuations grew in magnitude when the power was increased to 7040 watts (⊞), at which point the boundary layer appeared to be fully turbulent.

4.1-2 Variable Property Effects on Laminar Profiles

To test the apparatus, several laminar temperature experiments were carried out, the results of which were to be compared with

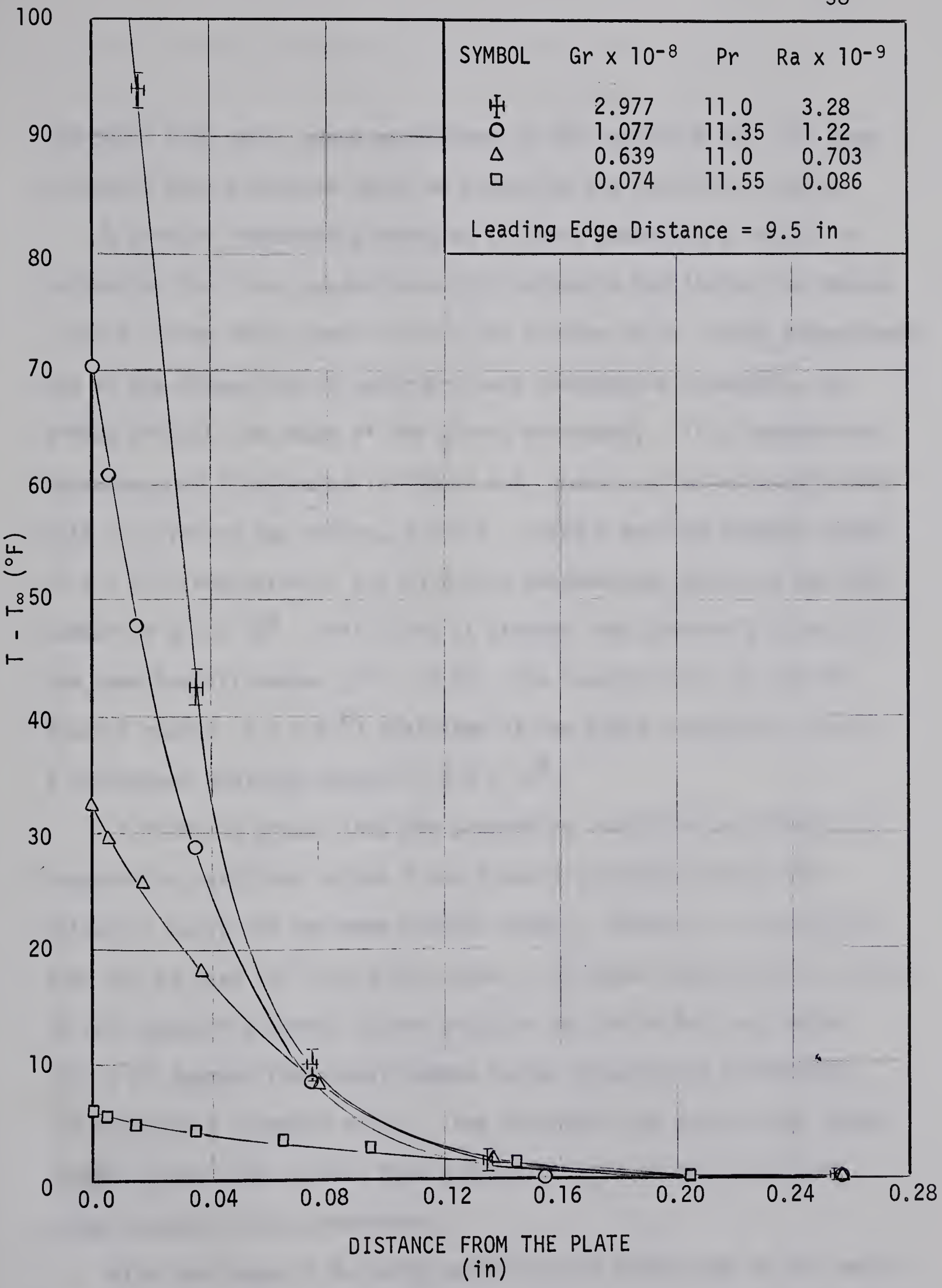

FIG. 4.1 LAMINAR, TRANSITION, AND TURBULENT TEMPERATURE PROFILES

Ostrach's [18] work. Once confidence in the apparatus had thus been achieved, more assurance could be placed on the turbulent results.

A problem immediately arose as to which temperature to use in evaluating the fluid properties which determine the laminar variables ν and β. When doing tests in air, the problem is of little consequence, but as the properties of water are very temperature dependent, the choice affects the shape of the curves noticeably. This temperature dependency is illustrated in figure 4.2, where one set of experimental data is given on two curves, A and B. Curve A has the Grashof number (4.8×10^7) evaluated at the bulk tank temperature, giving a Rayleigh number of 4.8×10^8. This curve is steeper than Ostrach's curve of the same Prandtl number (Pr = 10.0). The second curve, B, has the Grashof number (2.1×10^8) evaluated at the plate temperature, with a consequent Rayleigh number of 6.9×10^8.

It might be argued that the properties should be evaluated at a temperature such that curves A and B would coincide exactly with Ostrach's curve for the same Prandtl number. However, no justification can be seen for such action when it is noted that Ostrach's curve is for constant property fluids and thus not valid for cool water (30 to 60 degrees Fahrenheit) where larger temperature differences (60 Fahrenheit degrees) exist. Thus to obtain the appropriate theoretical curves, the laminar free convection problem must be solved using variable fluid properties.

With the range of Rayleigh numbers which exists due to the variation of fluid temperature, it is apparent that prediction of the point

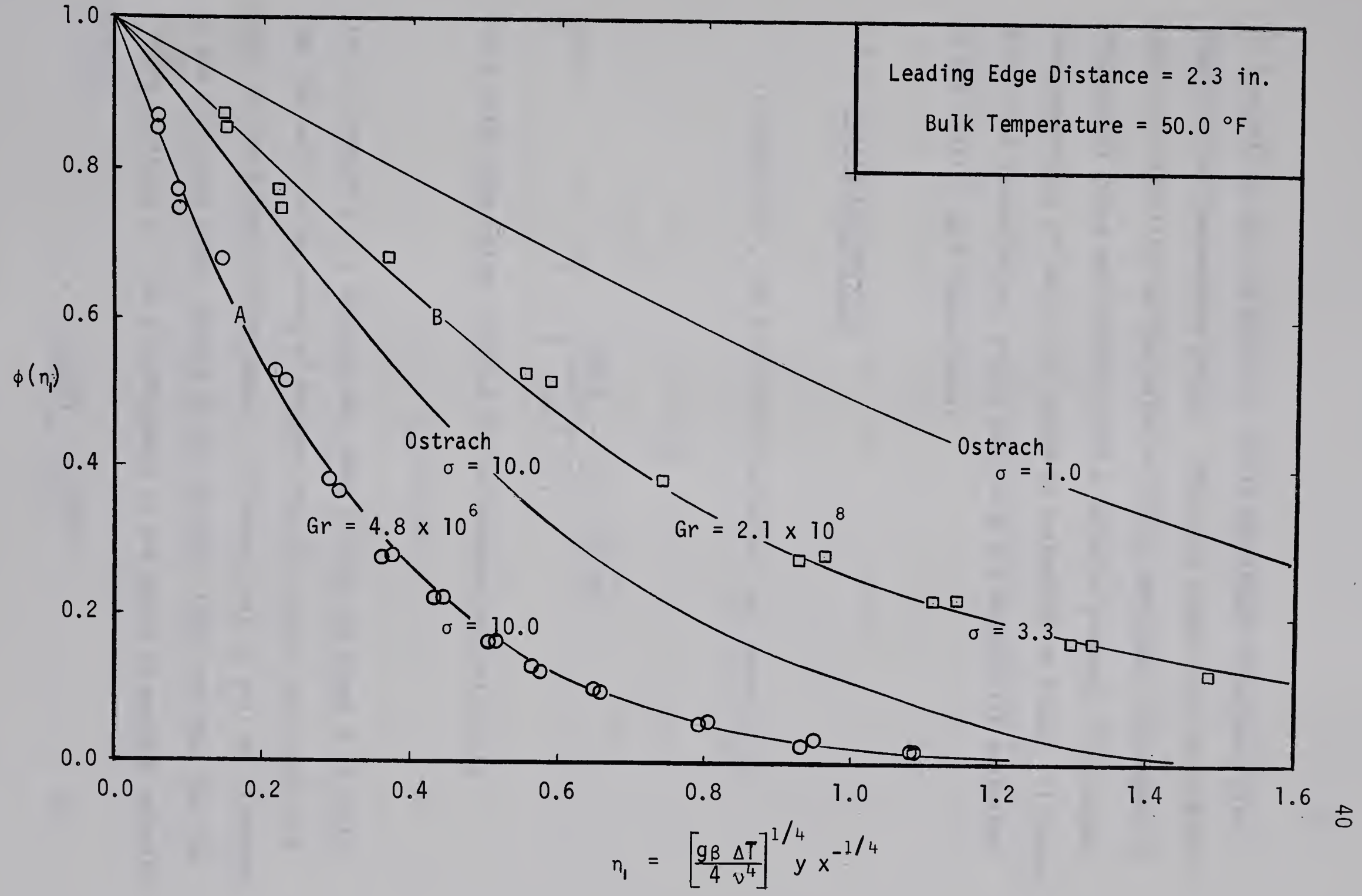

FIG. 4.2 VARIABLE PROPERTY EFFECT ON LAMINAR PROFILES

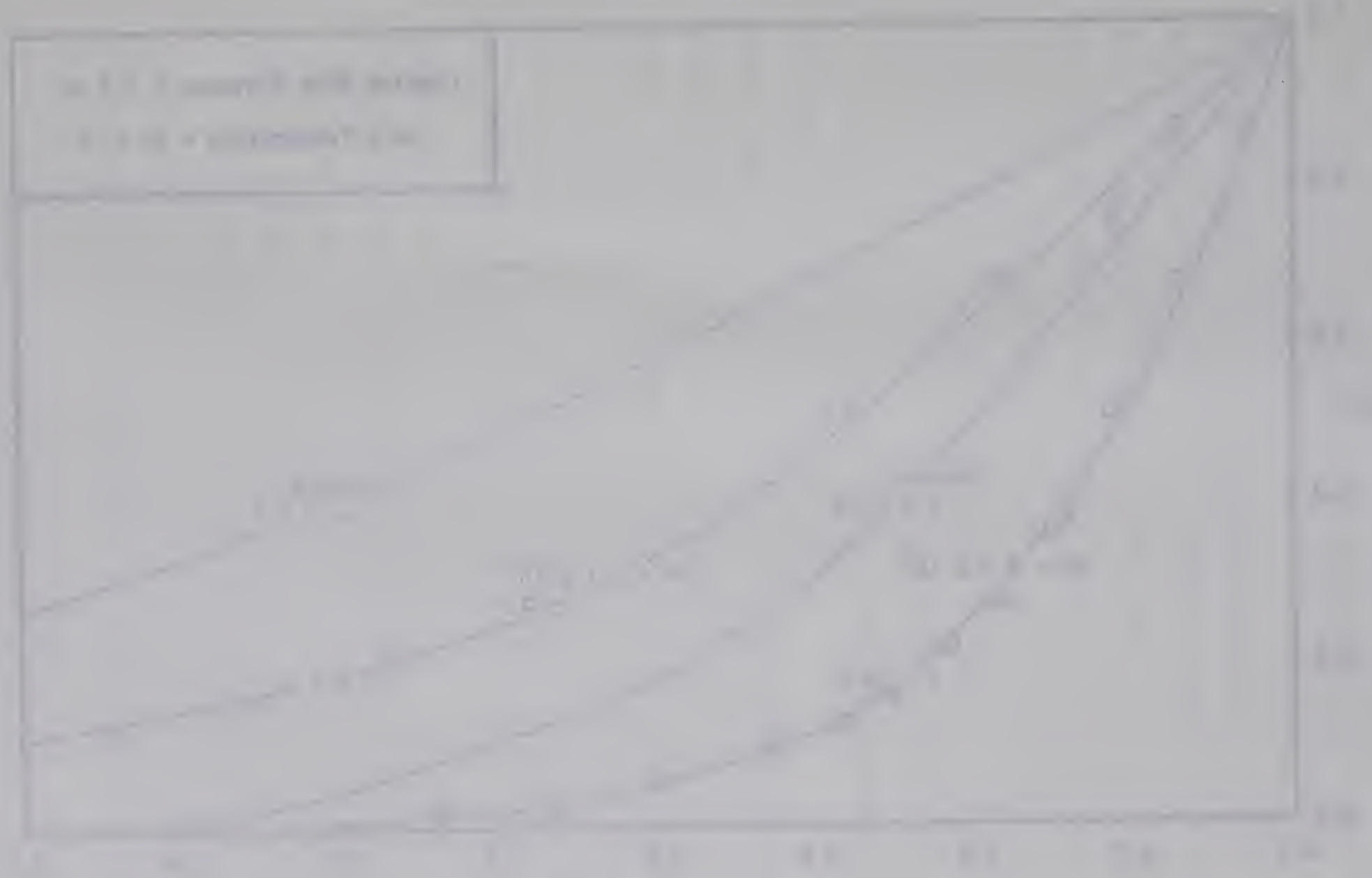

of instability and the point of "fully developed" turbulence also depend on the temperature choice. Thus, any number used to mark the point of instability or the point of "fully developed" turbulence is of doubtful value when working with a variable property fluid unless the temperature criterion for property evaluation is known. All properties and dimensionless groups used here are arbitrarily evaluated at the initial bulk temperature.

4.1-3 Similarity Profile

In Chapter II, the similarity variable η was shown to be

$$\eta = C_1 y$$

with $$C_1 = \left[\frac{g\beta(T_w - T_\infty)}{4D^2}\right]^{1/(4-2q)}$$

and D being some value related to the momentum diffusivity by

$$\varepsilon = Dx^{-1/2} y^q .$$

Also in Chapter II, a decision was made to take the power q as unity from the wall to the point of maximum velocity and as zero from this point to the boundary layer edge. This means that C_1 will be different in the inner and outer regions of the boundary layer and that the similarity variable will be discontinuous at the point of maximum velocity unless

$$D = 1/2[g\beta(T_w - T_\infty)]^{1/2} . \qquad 4\text{-}1$$

If D has this value then C_1 will be identical to unity and the discontinuity will no longer exist. For convenience in this chapter, D will take the value given by equation 4-1. The similarity variable then becomes

$$\eta = y.$$

Note, however, that η is dimensionless, whereas y has the dimension of length, thus implying the existence of a constant equal to unity but with the dimensions of length taken to the power minus one.

It should now be possible to plot the dependent variable ϕ as a function of η. Figure 4.3 shows such a graph, composed of data from fourteen turbulent runs. Each point on the graph is the average of twenty consecutive readings punched by the Speedomax G recorder. The constant C is simply a convenient multiplying constant equal to 10.0 inches^{-1}. The distance from the plate is measured in inches. A discussion of figure 4.3 is presented in section 4.1-4, while pertinent data on each symbol is given in Appendix E.

All properties listed in Appendix E were evaluated at the initial bulk temperature. If they had been evaluated at some other datum, such as the average of the bulk and plate temperatures, the values for the Prandtl, Grashof, and Rayleigh numbers would be different from those shown in the appendix. However, the choice of reference temperature has no effect on the ϕ versus η plot of figure 4.3 because the similarity variable is not temperature dependent when D takes the value given in equation 4-1. That is, figure 4.3 would simply be reproduced regardless of the choice of reference temperature.

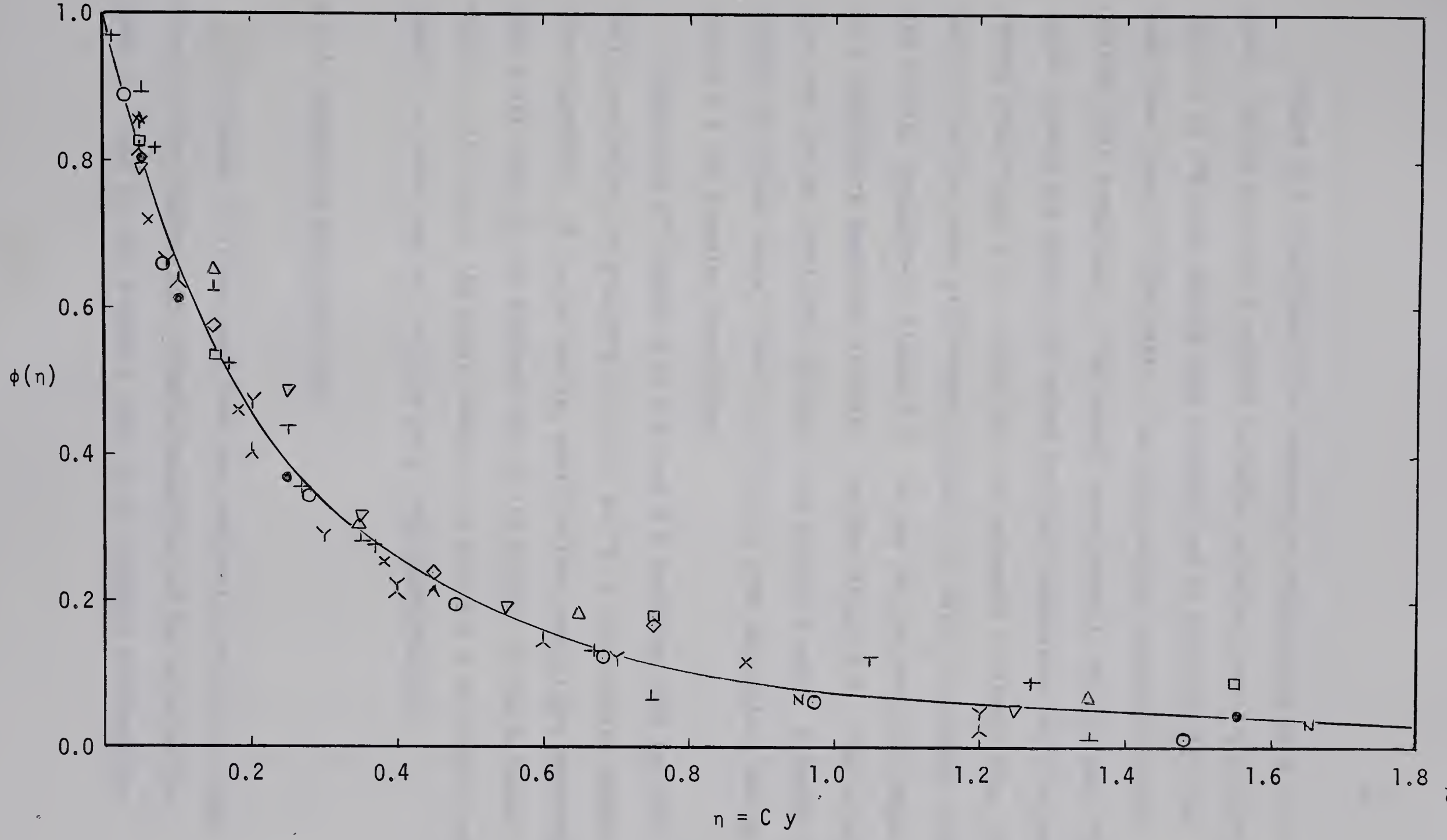

FIG. 4.3 TEMPERATURE DISTRIBUTION IN TURBULENT BOUNDARY LAYER USING SIMILARITY VARIABLE η

Figure 4.4 illustrates this temperature independence even further. On the graph of ϕ against η, three turbulent runs are plotted. Each is at the same leading edge distance and is supplied with the same power input of 6000 watts. The only varying condition is the initial bulk temperature. The smooth curve shown is not the best fit curve through the points but rather the mean temperature profile transferred from figure 4.3. Notice that the agreement is fairly good, especially for the curve with Prandtl number 5.0, which is furthest from the results presented in figure 4.3. To see how the same runs appear on a temperature dependent variable, consider figure 4.5. The variable η_l is the laminar similarity variable from Ostrach's work. Although the scatter is rather large, there is definitely some separation, making figure 4.4 the superior correlation.

Comparison of figures 4.3, 4.4, and 4.5 indicates that the similarity variable η is accurate in so far as it is not strongly temperature dependent. It is, of course, possible that some slight dependency does exist which is not apparent due to the scatter in the turbulent results. If this is the case, however, the variable η as given is not greatly in error and will suffice as a first approximation.

4.1-4 Comparison with Other Work

In Chapter II it was seen that the similarity variable is independent of the leading edge distance regardless of the value of the power q. That is, the boundary layer is of constant thickness for

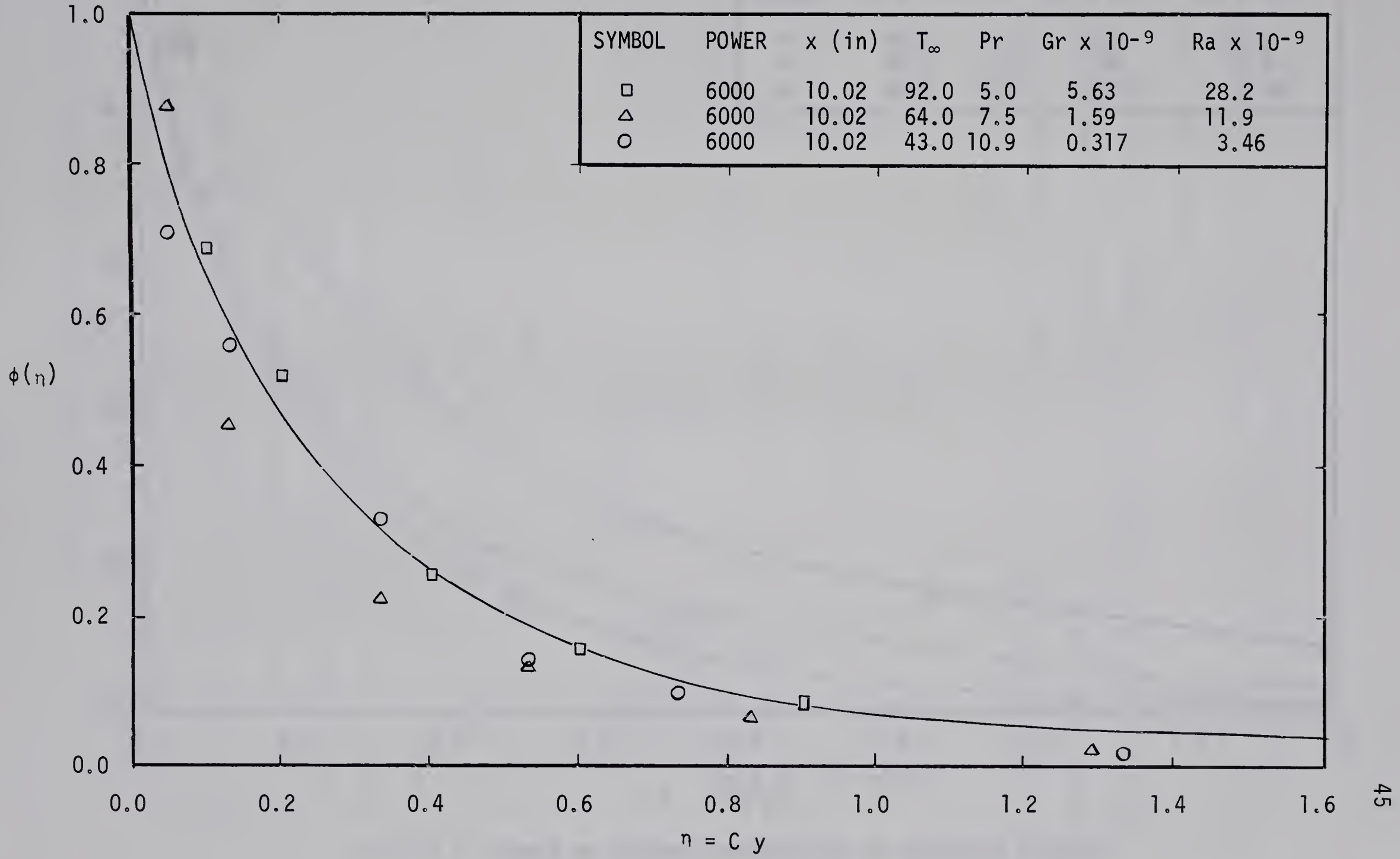

FIG. 4.4 TEMPERATURE DISTRIBUTION IN TURBULENT BOUNDARY LAYER USING SIMILARITY VARIABLE η

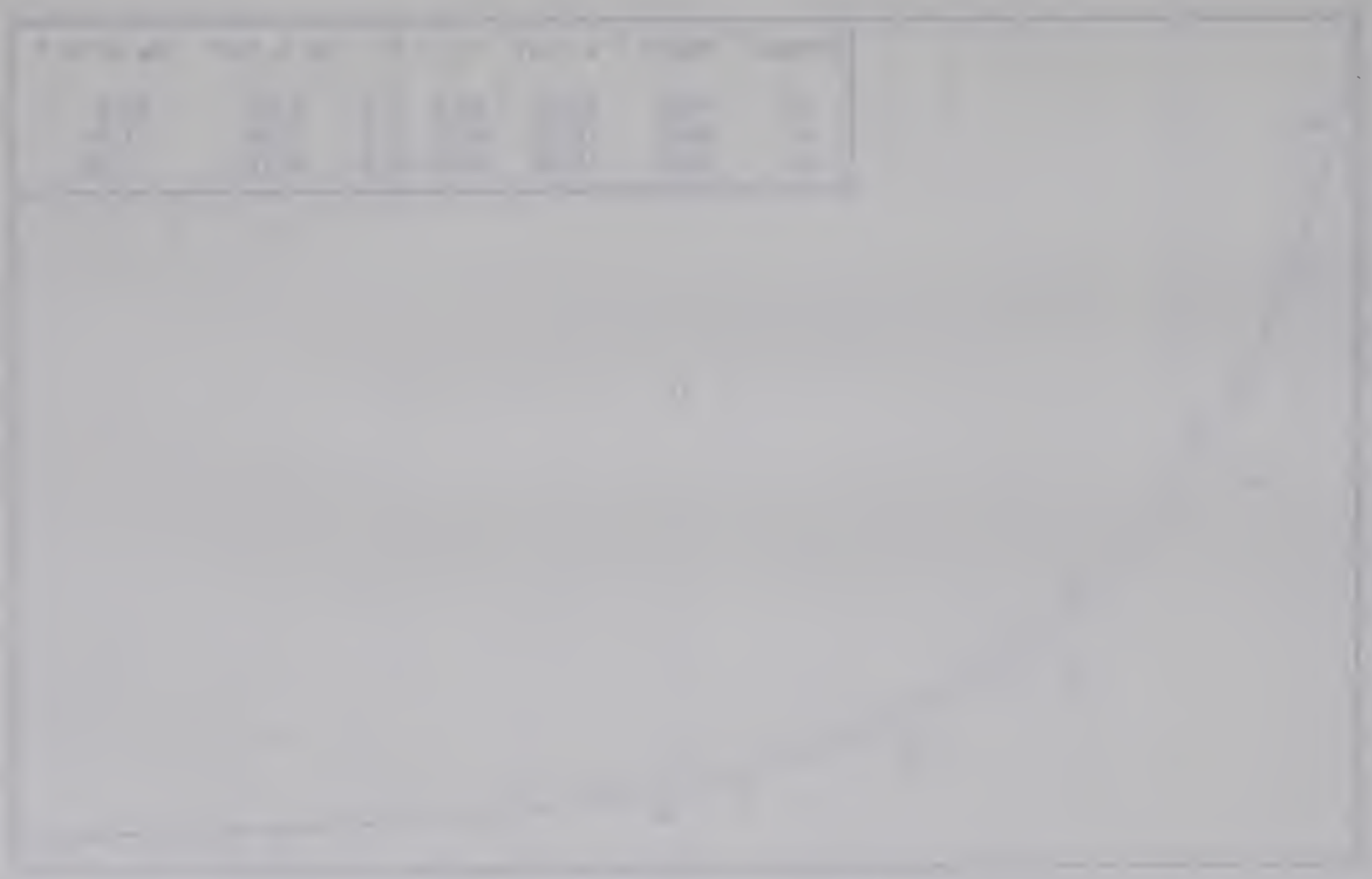

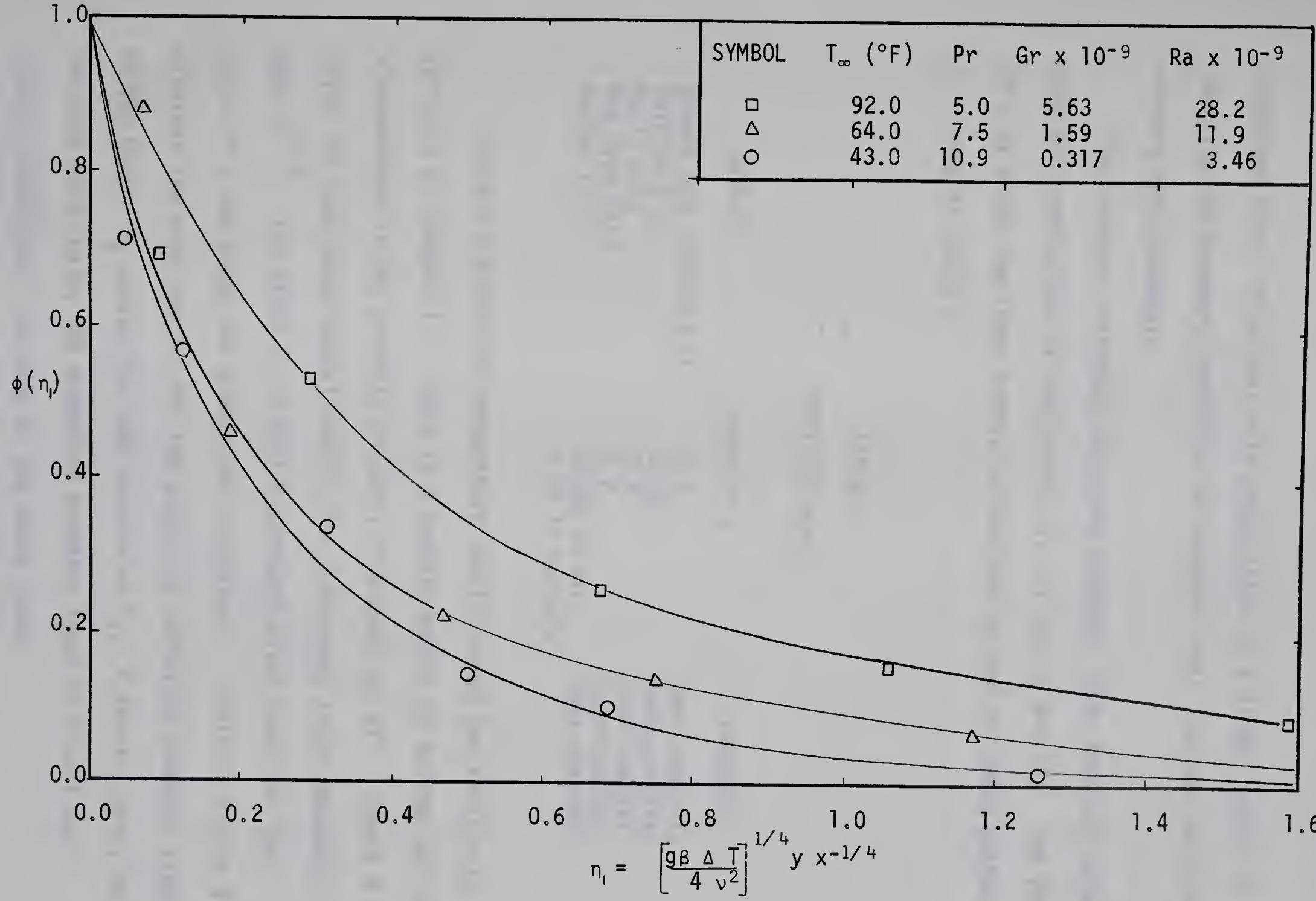

FIG. 4.5 EFFECT OF VARIABLE PROPERTIES ON TURBULENT RESULTS

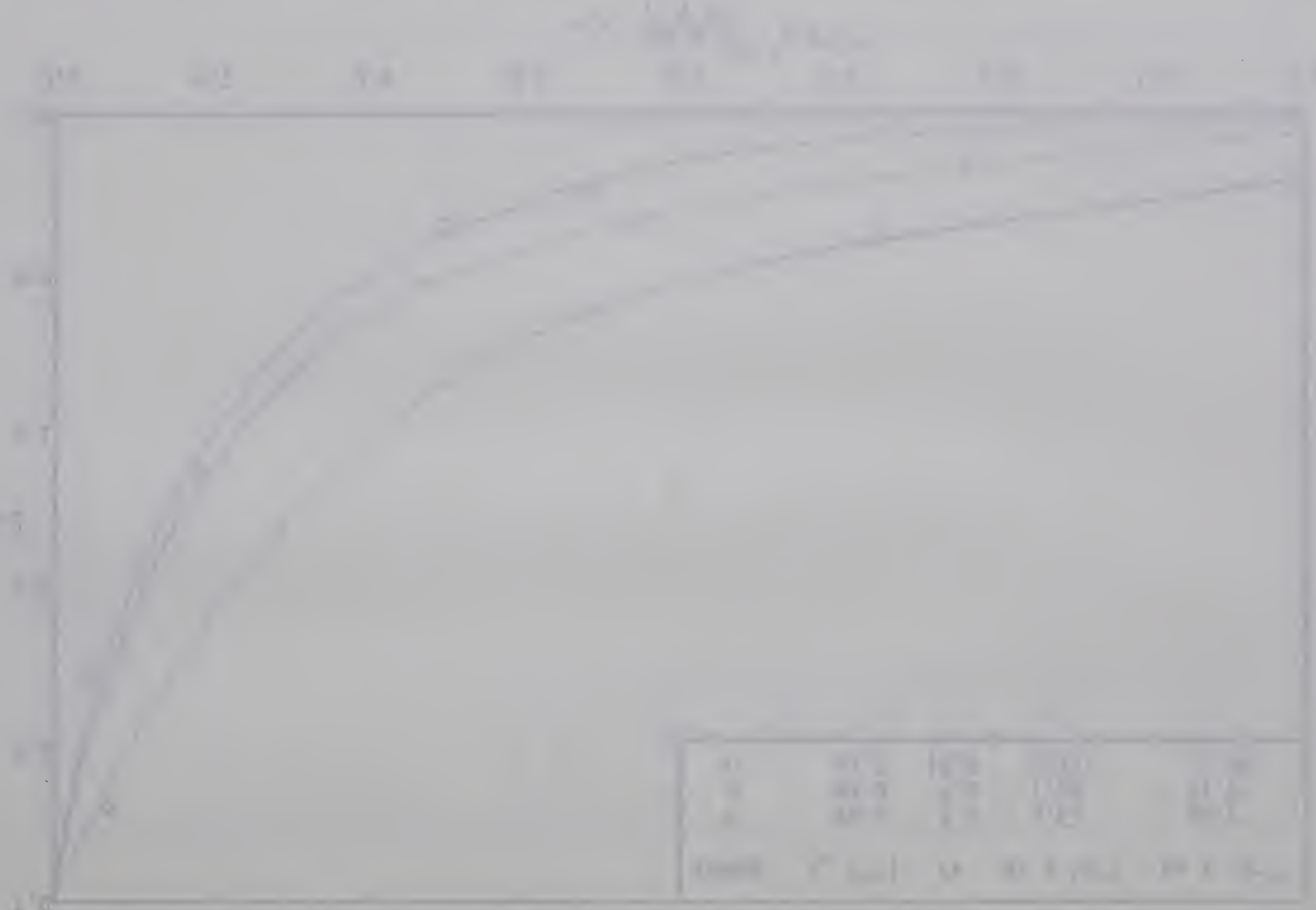

turbulent flow. Note that this proposition is a direct result of imposing the boundary conditions of constant heat flux and wall temperature simultaneously.

The constant thickness turbulent boundary layer does not agree with the conclusions of past works (4, 13, 14, 15 and 16). The power of x by which the layer grows, as obtained by each of these authors, is listed in Table I.

TABLE I

PREVIOUS WORK

Author	Power of x	Treatment
Eckert and Jackson [4]	0.7	Semi-analytic
Waibler [13]	0.667	Semi-analytic
Fujii [14]	0.7	Semi-analytic
Van Dyke [15]	$\simeq$ 0.2	Experimental
Bayley [16]	0.348 in air 0.25 in mercury	Semi-analytic

Figure 4.3 presented temperature results using the similarity variable of Chapter II. There is a certain amount of scatter but an x dependency is not strongly evident, if present at all. Figure 4.6 gives the same experimental results for a boundary layer dependent upon $x^{-0.2}$. The value K_1 is just a constant which regulates the scale of η and keeps the dimensions consistent. Similarly figure 4.7 displays the same results for the expanding turbulent boundary layer of Van Dyke. K_2 serves the same purpose as K_1. A fourth curve, not included here, using the expanding boundary layer of Eckert and Jackson looked much the same as the above three.

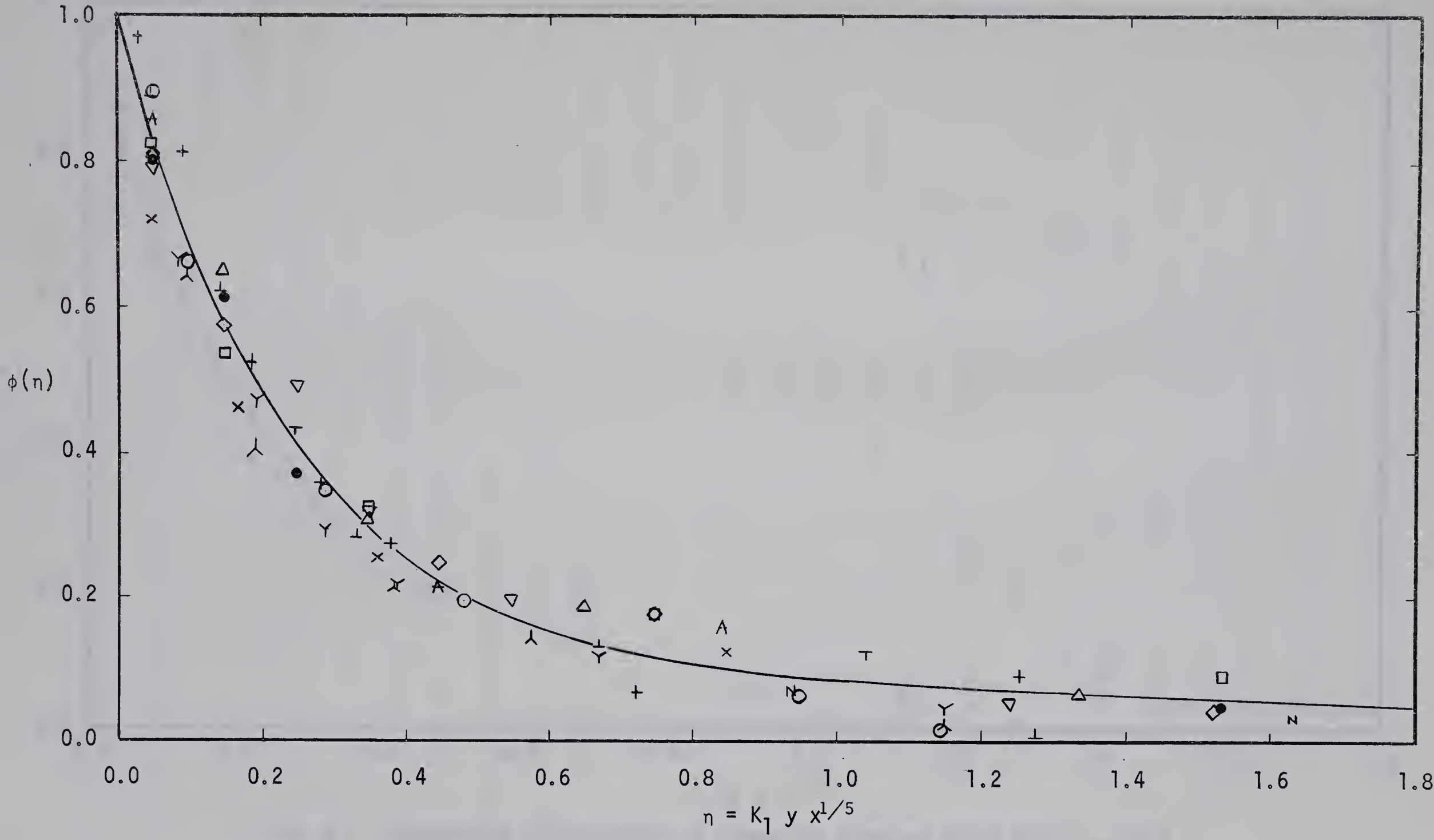

FIG. 4.6 TEMPERATURE DISTRIBUTION IN TURBULENT BOUNDARY LAYER WITH $\delta \sim x^{-1/5}$

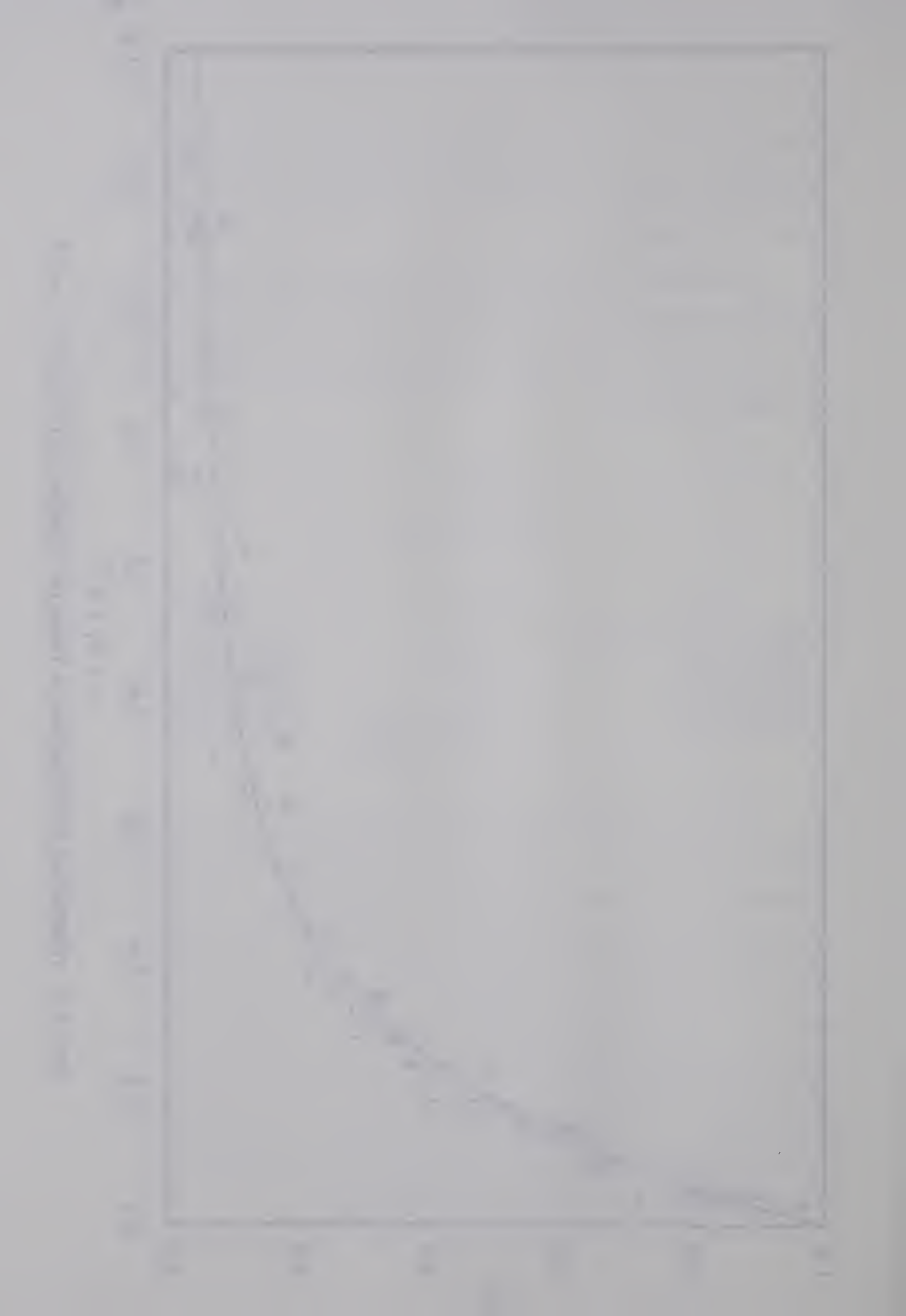

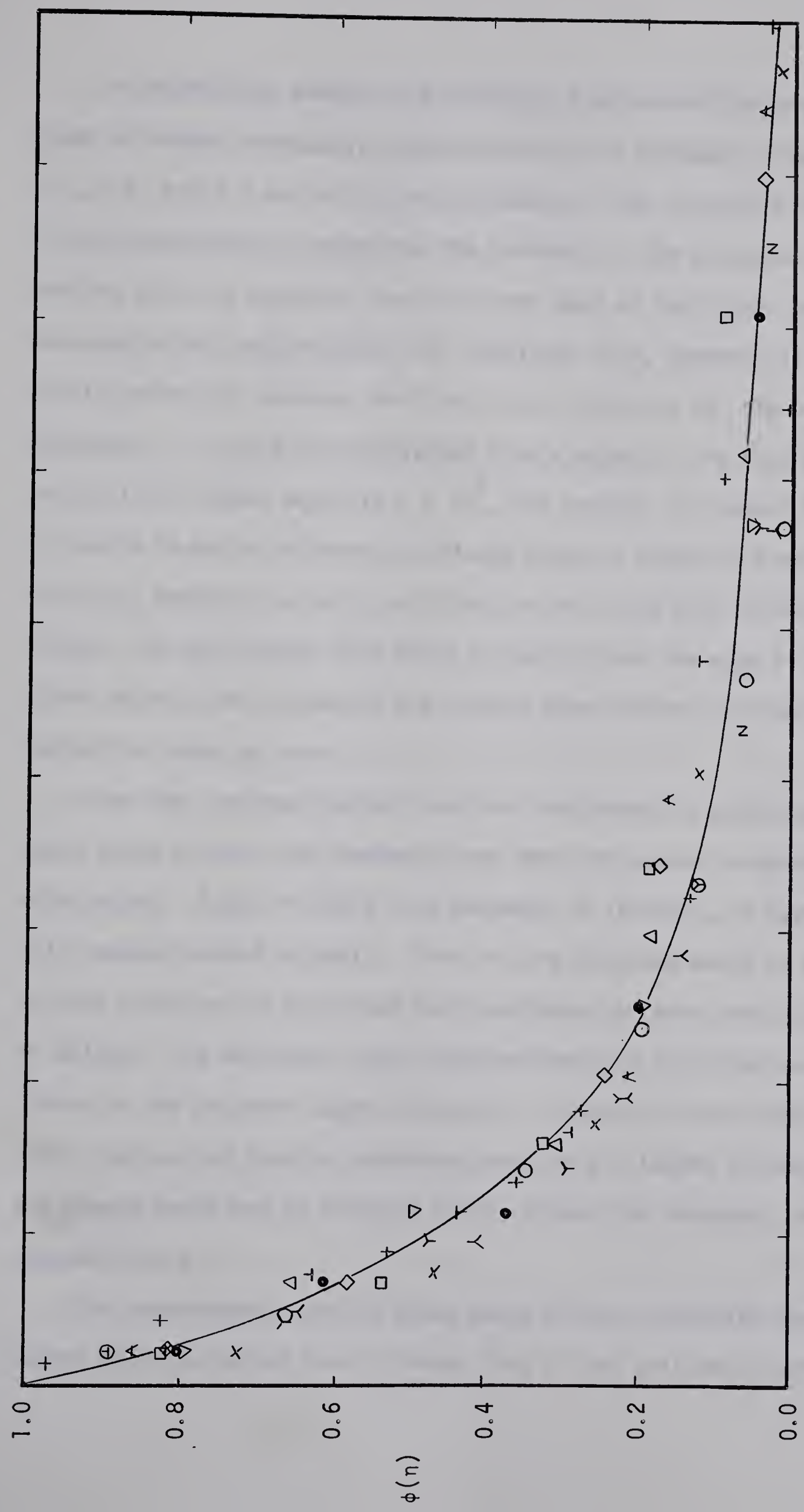

FIG. 4.7 TEMPERATURE DISTRIBUTION IN TURBULENT BOUNDARY LAYER WITH $\delta \sim x^{1/5}$

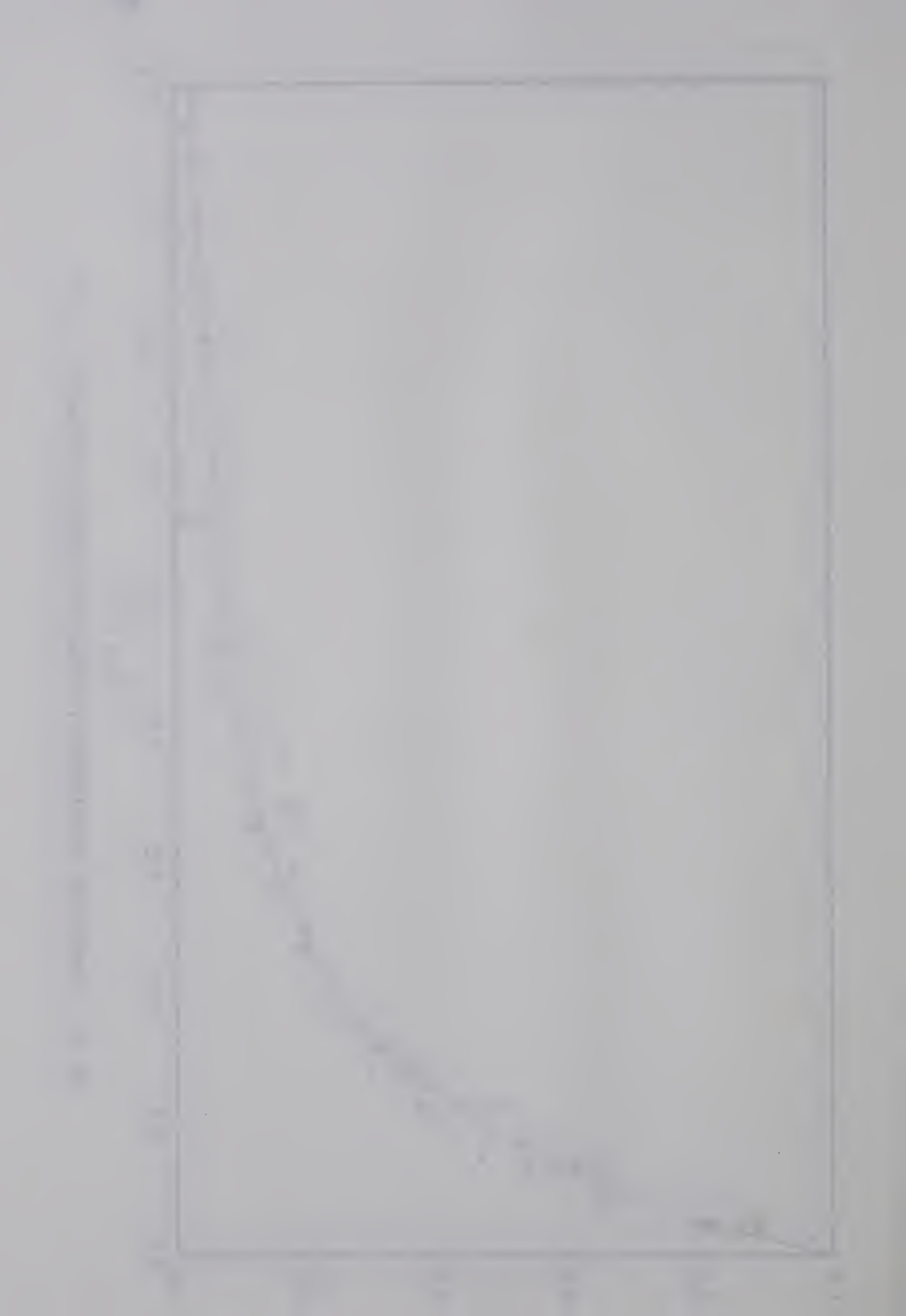

In determining whether the turbulent free convection boundary layer thickness decreases, remains constant or increases, figures 4.3, 4.6, and 4.7 are of little assistance. This is partly because of the uncertainty in obtaining the correct x. The distance from the leading edge was measured from the lower edge of the plate, which is reasonable for laminar flow. For turbulent flow, however, it is not really defensible because the flow is not turbulent for the entire distance. If x were to be measured from a point in the flow where the Rayleigh number equalled 2×10^9, the results in figures 4.6 and 4.7 would be quite different, although those in figure 4.3 would not. There is, however, no real justification for using this criterion either. If the laminar flow field is small, then the edge of the plate can be used to measure the leading edge distance without introducing too large an error.

When the raw experimental data are considered in addition to the above three curves, the boundary layer does not appear to decrease with height. Also, if there is a tendency to increase, it appears that this tendency would be small. That is, any increase would be closer to that found by Van Dyke than that predicted by Eckert and Jackson or Waibler. In addition, visual observations did not detect any increase in the boundary layer thickness. It should be mentioned, however, that as the lengths considered vary only 4 inches in one foot, any change would not be detected easily unless the thickness was strongly dependent on x.

The experimental results given above do not invalidate the turbulent model presented here although they do not positively confirm it.

There is some support for the condition that the similarity variable does not depend on fluid properties but little evidence to prove or disprove that the thickness is constant. Further tests are required to study the variation of thickness of the boundary layer.

4.2 TEMPERATURE FLUCTUATIONS

4.2-1 Comparison of Mean and Fluctuating Readings

A continuous graphic record representing the temperature fluctuations at various distances y from the plate was obtained with the Varian strip chart recorder described in Chapter III. From this record, the mean temperature for each y was calculated and the maximum and minimum temperatures reached at this position were recorded. These results were then plotted against distance from the plate to form curves 1, 2, and 3 (representing the maximum, mean and minimum temperatures respectively) in figure 4.8.

Notice that at distances greater than about 0.025 inches from the plate, the magnitude of the deviation from curve 2 is greater for curve 1 than for curve 3. At y less than 0.025 inches, the reverse is true. Thus, if the ratio of the deviation of curve 3 to that of curve 1 was plotted against y, the resulting graph would be roughly hyperbolic in form and less than unity across 93 per cent of the boundary layer. (The mean edge of the boundary layer, $\overline{\delta}$, is arbitrarily defined as the point where the average temperature becomes one per cent of $T_w - T_\infty$.)

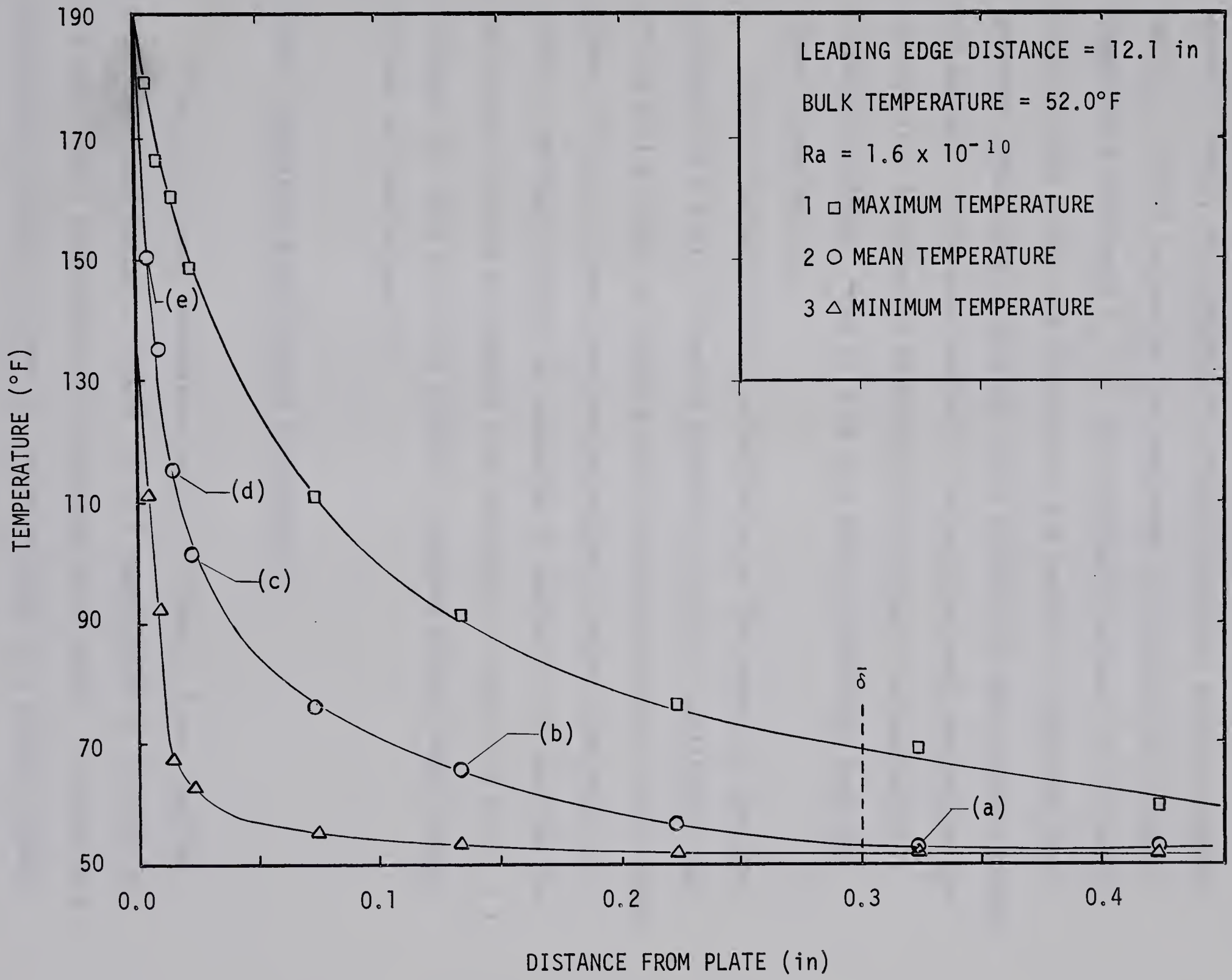

FIG. 4.8 COMPARISON OF MEAN AND FLUCTUATING TEMPERATURE READINGS

Of the fluctuations represented here by the distance between curves 1 and 3, the largest (90 Fahrenheit degrees) occur at approximately y = 0.025 and are of the same order of magnitude as the mean temperature difference $T_w - T_\infty$ (80 Fahrenheit degrees) at this point. Closer to the plate, the fluctuations are smaller in magnitude than the mean temperature difference, while farther out they are much larger. For example, at the mean boundary layer edge the mean temperature difference is 1.8 Fahrenheit degrees and the largest fluctuation is 17 Fahrenheit degrees. More will be said about fluctuations near the plate in section 4.3-4.

As the fluctuations are an indication of the amount of turbulent transport in a fluid, it may be possible to obtain a qualitative idea of the mixing length by studying the relative magnitudes of the fluctuations. If this is done, the peak magnitude is found to be near the point of maximum velocity (as suggested in section 4.3-2) and the mixing length is found to resemble that presented in figure 2.4 for $L_1 = 1$. Although this does not prove Prandtl's extended mixing length theory, it does at least support it.

4.2-2 Transition and Turbulent Fluctuations

Five of the mean temperature points in figure 4.8 are labelled with lower case letters. Figure 4.9 is a reproduction of portions of the strip chart recording used to evaluate these points. Fluctuations were drawn from right to left as the chart moved at a constant speed

NOT SIMULTANEOUS TRACES $Ra = 1.6 \times 10^{10}$ TIME ——— 16 in. PER MIN.

FIG. 4.9 STRIP CHART RECORDINGS OF TEMPERATURE FLUCTUATIONS IN TURBULENT BOUNDARY LAYER

a) $y = 1.08\ \bar{\delta}$ d) $y = 0.050\ \bar{\delta}$

b) $y = 0.444\ \bar{\delta}$ e) $y = 0.017\ \bar{\delta}$

c) $y = 0.077\ \bar{\delta}$

ONE SMALL DIVISION ABOUT MEAN ≈ 3 FAHRENHEIT DEGREES

of 16 inches per minute. One inch in the vertical direction is equivalent to two millivolts, with temperature increasing toward the top of the page. The maximum temperature was obtained by recording the value closest to the top of the page and the minimum, by recording the value closest to the bottom.

Figure 4.9 represents the fluctuations in a fully turbulent boundary layer ($Ra = 1.6 \times 10^{10}$). This chart can be better understood by comparing it with figure 4.10, which is a set of strip chart recordings from a boundary layer flow with Rayleigh number of 1.38×10^{8}; that is, a transition flow. Figure 4.10 was made at the same chart speed as the previous figure was, but at a sensitivity ten times as great (1 inch = 0.2 millivolts).

Comparison of these two sets of recordings reveals that the magnitude of the turbulent fluctuations is about ten times as great as that of the transitional fluctuations. Also, for transitional flow the frequency of waves, about one Hertz, is independent of the position in the boundary layer. On the other hand, for "fully developed" turbulent flow there is no dominant frequency.

Notice that the transitional fluctuations have a tendency to die out with time. This tendency can even be observed occasionally in some of the turbulent curves. The importance of this observation is that, because the flow is classified as "unstable" past the point of neutral stability, any disturbance is expected to increase. This is the reverse of what was observed. Further studies into this phenomenon

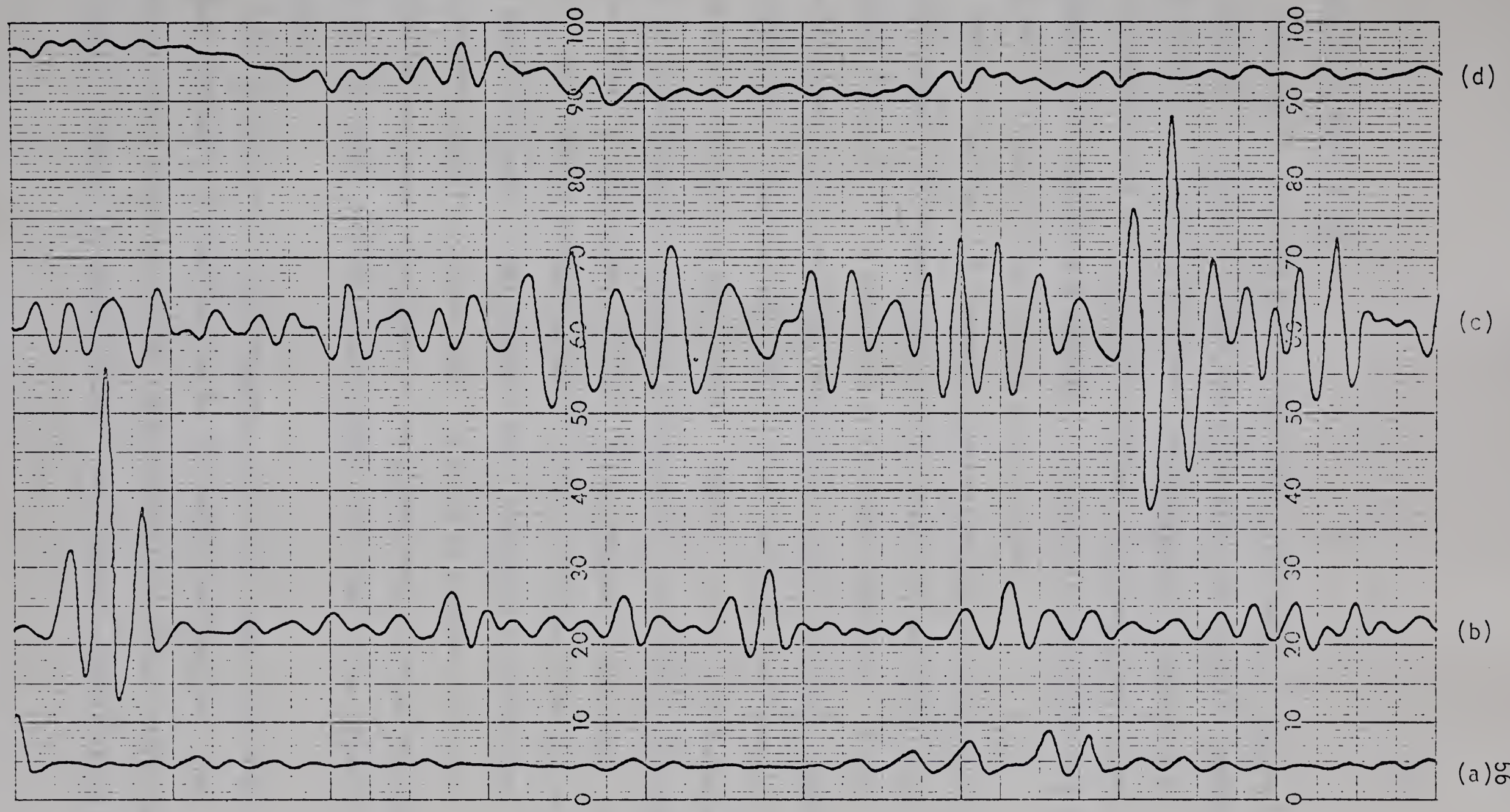

FIG. 4.10 STRIP CHART RECORDINGS OF TEMPERATURE FLUCTUATIONS IN TRANSITION BOUNDARY LAYER

a) $y = 0.715\ \delta$ c) $y = 0.320\ \delta$

b) $y = 0.535\ \delta$ d) $y = 0.038\ \delta$

might be in order [10].

Now consider any one of the five curves reproduced in figure 4.9. By counting the number of times the curve cuts each constant temperature line, it is possible to obtain the frequency of occurrence of each temperature at that particular distance from the plate. Such frequency distributions are plotted in figure 4.11 for curves 4.9a and 4.9b and in figure 4.12 for curves 4.9c and 4.9d.

Notice that near the boundary layer outer edge the distribution is very skewed. This stems from the fact that only hot eddies surge into the fluid, as it is nominally at the tank temperature. Figure 4.9a illustrates this one-sided fluctuating, while its effect appears in figure 4.8. Closer to the plate, as for curve (b) in figure 4.9, there are still only hot eddy effects. However, as the mean temperature is increasing, the frequency distribution is noticeably less skewed. As the plate is approached, the distribution becomes increasingly symmetric, until almost perfect symmetry occurs at the position of curve (c), about one-tenth of the boundary layer thickness from the plate. This symmetry appears to occur near the point of maximum velocity. Fluctuations recorded any closer to the plate, such as those in figure 4.9d, are no longer symmetric, but skewed, this time in the opposite direction.

Not included here is the frequency curve for figure 4.9e, which has been omitted since nothing can be concluded from its form. The frequency curves obtained for the transitional fluctuations reproduced in figure 4.10 have also been omitted. These curves resemble those for

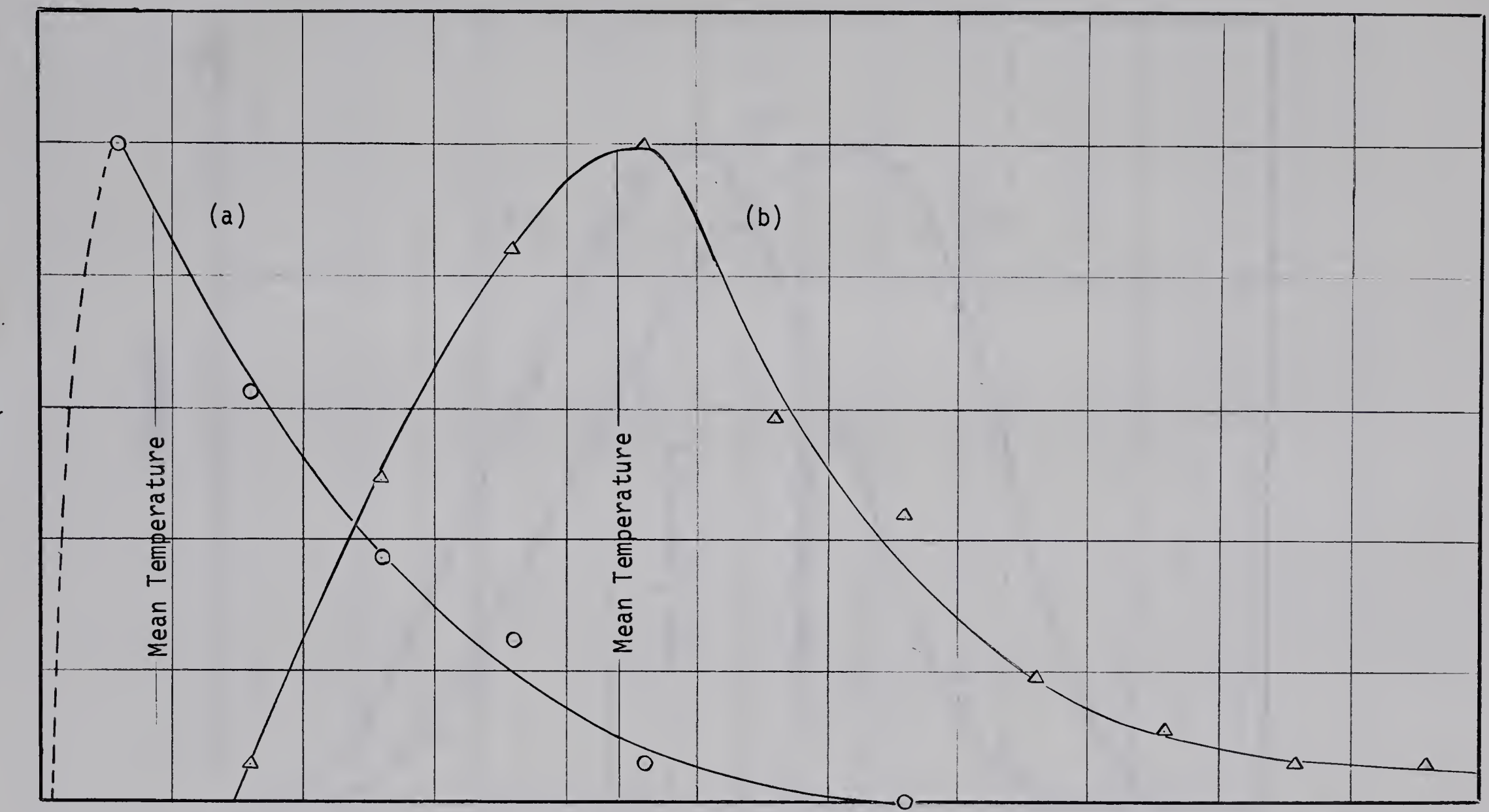

FIG. 4.11 TEMPERATURE DISTRIBUTION AT FIXED POINTS IN THE BOUNDARY LAYER
(a) $y = 1.08\delta$ (0.323 in)
(b) $y = o.444\delta$ (0.133 in)

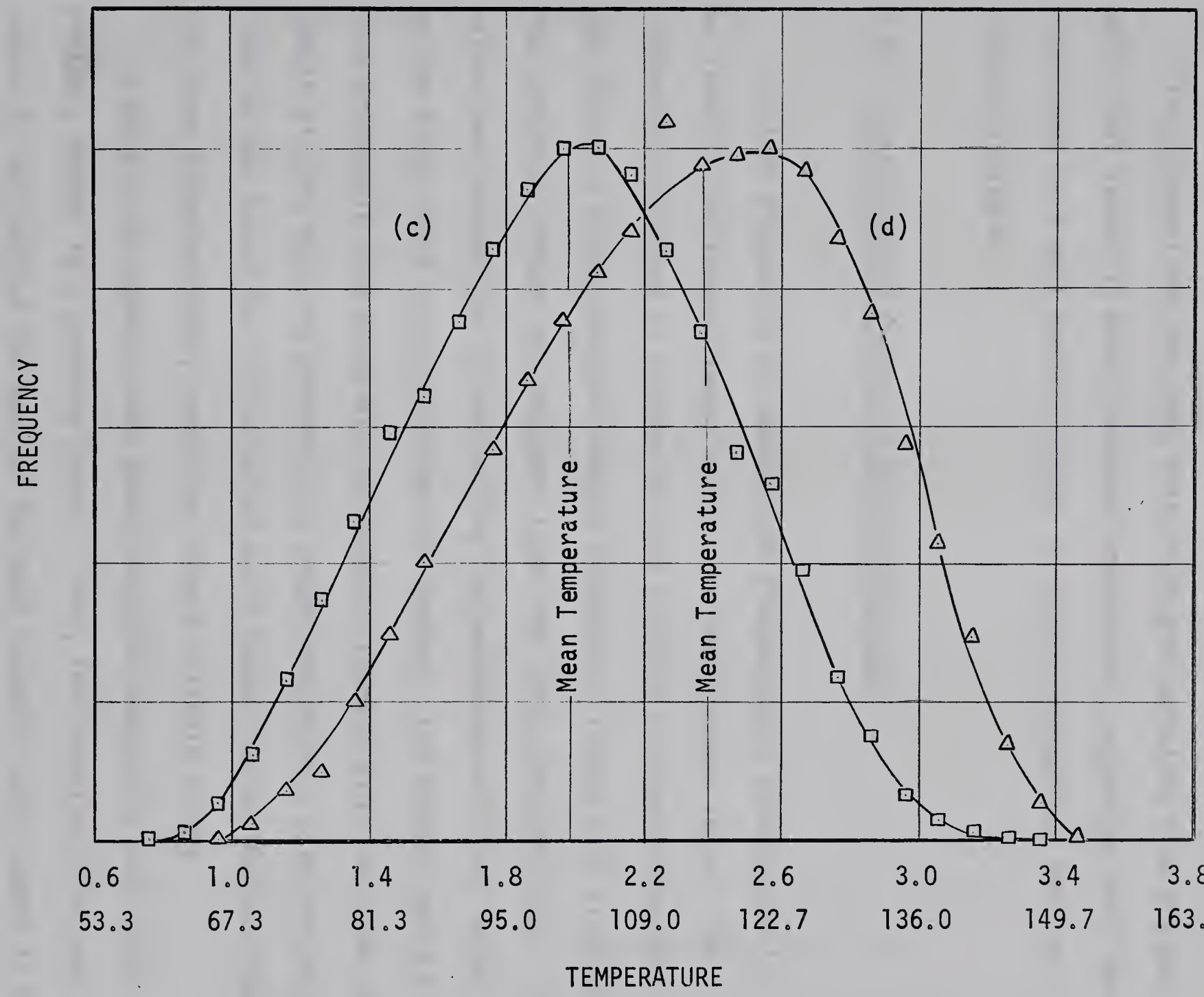

FIG. 4.12 TEMPERATURE DISTRIBUTION AT FIXED POINTS IN THE BOUNDARY LAYER
(c) $y = 0.0766\delta$ (0.023 in)
(d) $y = 0.0050\delta$ (0.015 in)

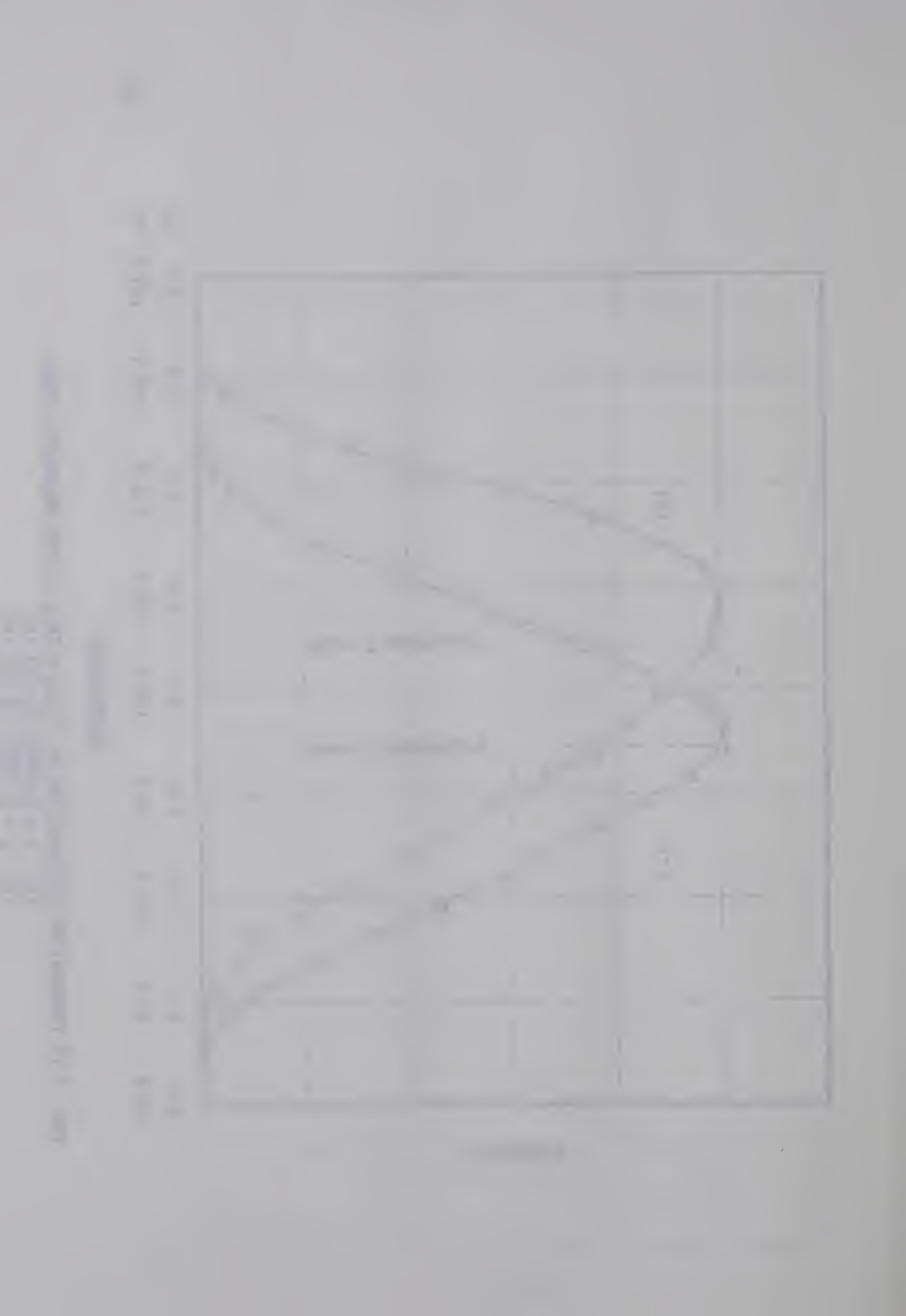

the turbulent flow region, with the one exception that they are noticeably narrower.

The fluctuations for both transition and turbulent flow are generally not symmetric about the mean temperature, suggesting that the turbulence in a wall boundary layer is neither homogeneous nor isotropic in nature.

4.2-3 Intermittency Factor in the Boundary Layer

In this discussion on temperature fluctuations, attention will be given to the intermittency factor γ in the boundary layer. The intermittency factor is defined as that fraction of time during which the flow at a given position remains turbulent. Figure 4.13 illustrates its variation through the boundary layer for three turbulent runs. The values were determined by subtracting the percentage of "flat" areas on the strip chart recordings from one hundred. The factors could be more accurately determined with an electric counter which recorded the length of time that the thermocouple output was below a selected value close to the base line. This method would remove the estimating from the curve interpretation, resulting in more reliable points.

Figure 4.13 suggests some generalizations concerning the intermittency factor in a boundary layer. First, for turbulent flow the factor is not zero at the edge of the mean boundary layer, where it can, in fact, be as high as $\gamma = 0.4$ and may be higher. For transitional flow it is very close to zero at this point. Secondly, near the plate

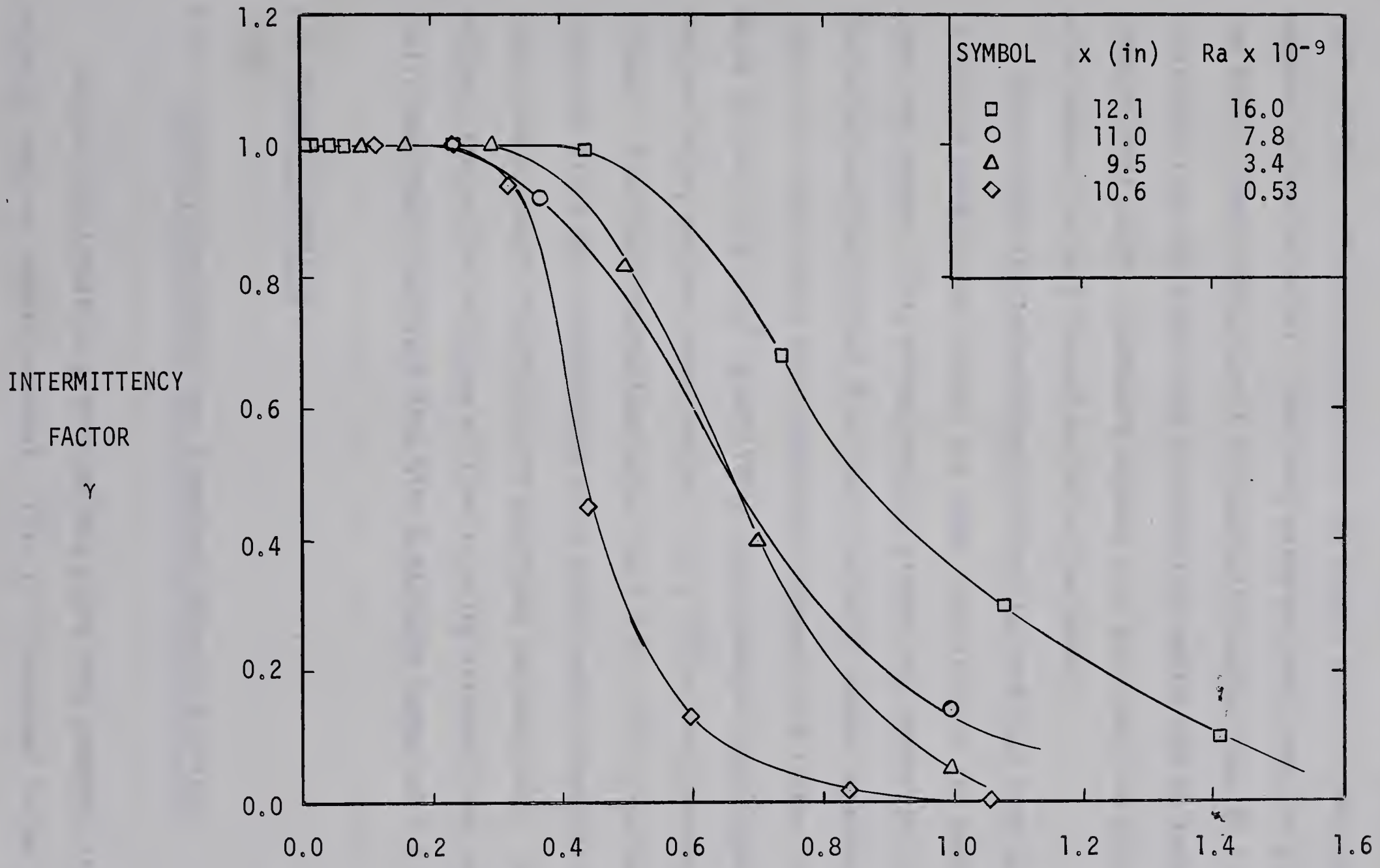

FIG. 4.13 INTERMITTENCY DISTRIBUTION ACROSS A BOUNDARY LAYER

the factor is unity, remaining so for about one-third of the boundary layer width. Further discussion of the region close to the plate appears in section 4.3-3. From this value of unity near the plate, the factor slowly decays until it eventually reaches zero at a point so distant from the plate that the turbulent eddies can no longer penetrate to that depth. Somewhere between this point and the plate, the curve appears to pass through an inflection point.

Notice that the intermittency factors for the four runs do not follow the same curves through the outer two-thirds of the boundary layer and beyond. This effect results either from errors in estimating the factor and the correct $\overline{\delta}$ or from a Rayleigh number dependency. A study of all four strip chart recordings suggests the latter. The curve for Ra = 7.8×10^9 is of little value because insufficient points are available, but the curve for Ra = 5.3×10^8 is most certainly transitional. Even the intermediate curve (Ra = 3.4×10^9) is not completely turbulent since the corresponding strip chart record resembles the transition curves of figure 4.10 in magnitude and wave form. The intermittency factor for this type of flow is quite distinct from that of "fully developed" turbulent flow with a Rayleigh number of 1.6×10^{10}.

4.3 VELOCITY PROFILES

4.3-1 Laminar, Transition, and Turbulent Velocity Profiles

As the fluid next to a vertical hot plate flow upwards, its velocity does not remain constant. This is illustrated in the lower

two curves of figure 4.14, where the flow changes from laminar to transition at a constant power input to the plate. Here the maximum velocity is approximately doubled as the fluid moves six inches up the wall. Varying the power input also changes the velocity. The upper three curves of figure 4.14 demonstrate this effect on the mean velocities at a fixed distance from the leading edge. The power varied from 2000 to 7120 watts with a resultant velocity change of from 4 centimetres per second to over 8 centimetres per second at the point of maximum velocity.

The laminar curve of figure 4.14 is reproduced in figure 4.15 using Ostrach's nondimensional variables, $f'(\eta_1)$ and η_1, with the properties evaluated at both the bulk and the plate temperature. This graph also reproduces Ostrach's velocity distributions for Prandtl numbers of one and ten. It is once again evident from the experimental curves that water cannot be treated as a constant property fluid.

Whether or not the effect of variable properties is considered, it is apparent that the laminar velocity results obtained in this study are not reliable close to the plate. This is evident in figure 4.14 where the velocity gradient for laminar flow at the wall appears greater than that for transitional flow. Both curves presented in figure 4.15 exhibit this high wall velocity gradient and are much steeper than those of Ostrach's curves for similar Prandtl numbers. This is not defensible. It can only be concluded that near the wall the experimentally determined points are in error, either as a result of incorrect observation or as a result of an invalid assumption.

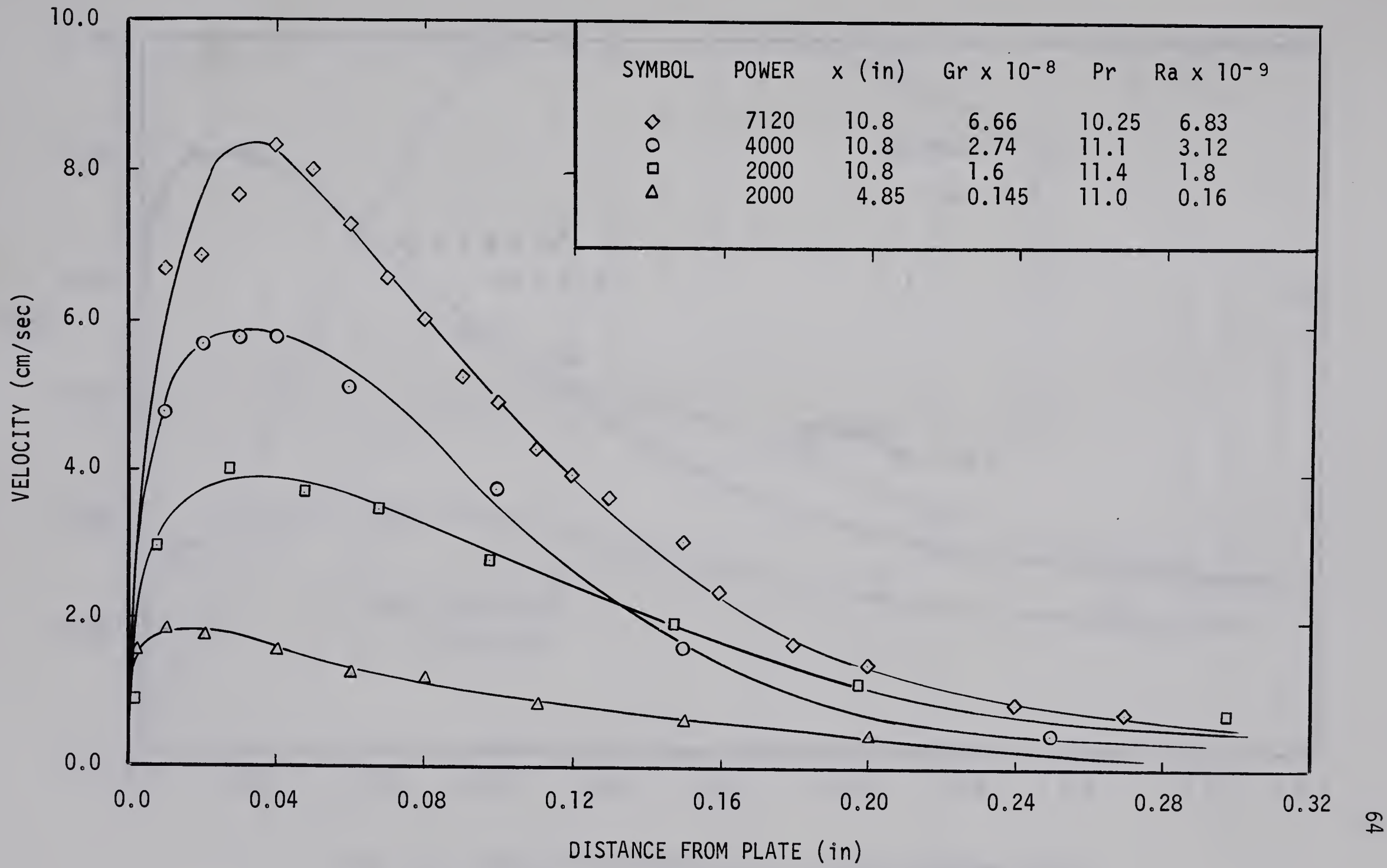

FIG. 4.14 LAMINAR, TRANSITION, AND TURBULENT VELOCITY PROFILES

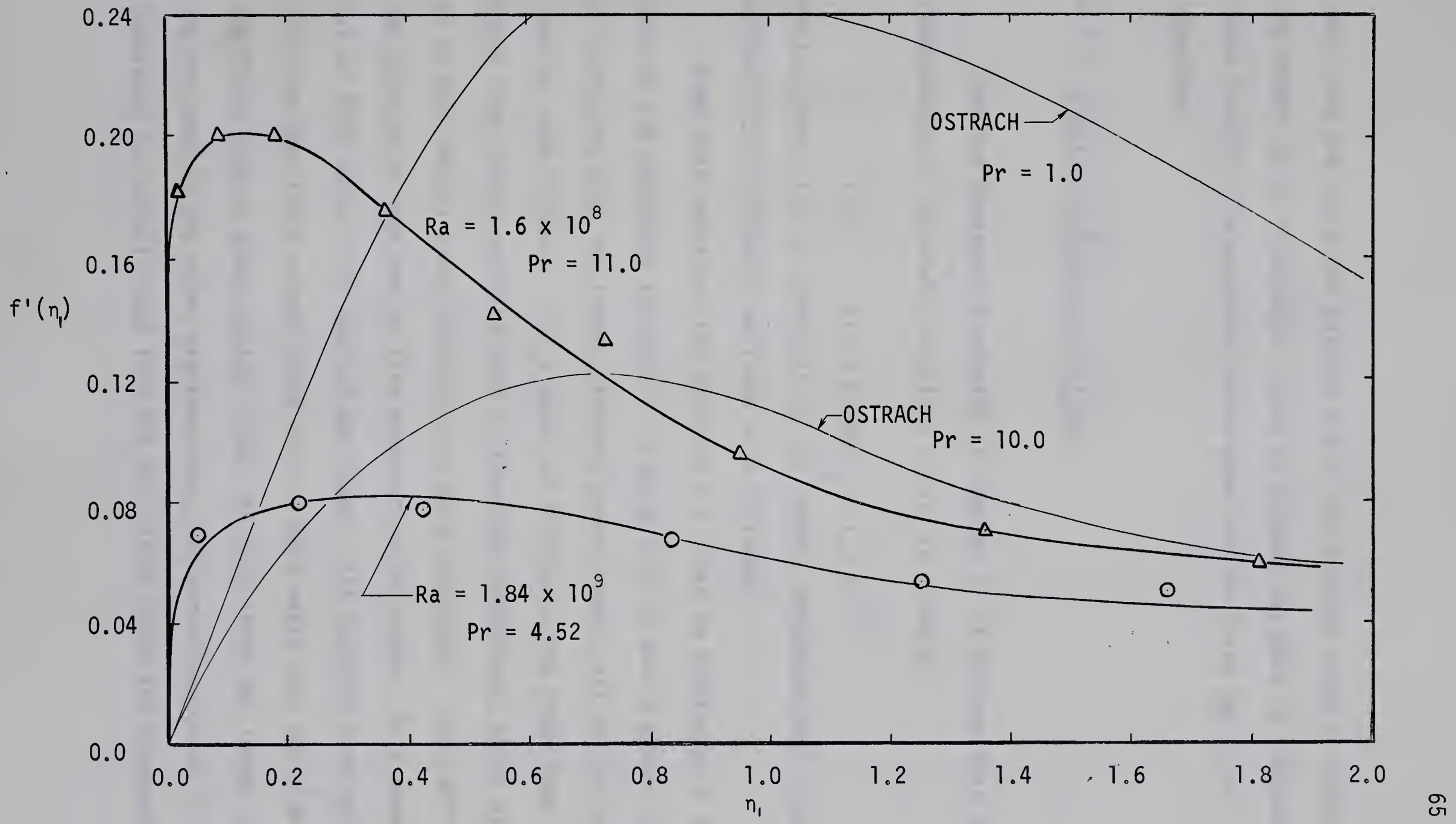

FIG. 4.15 VELOCITY DISTRIBUTION IN A LAMINAR BOUNDARY LAYER

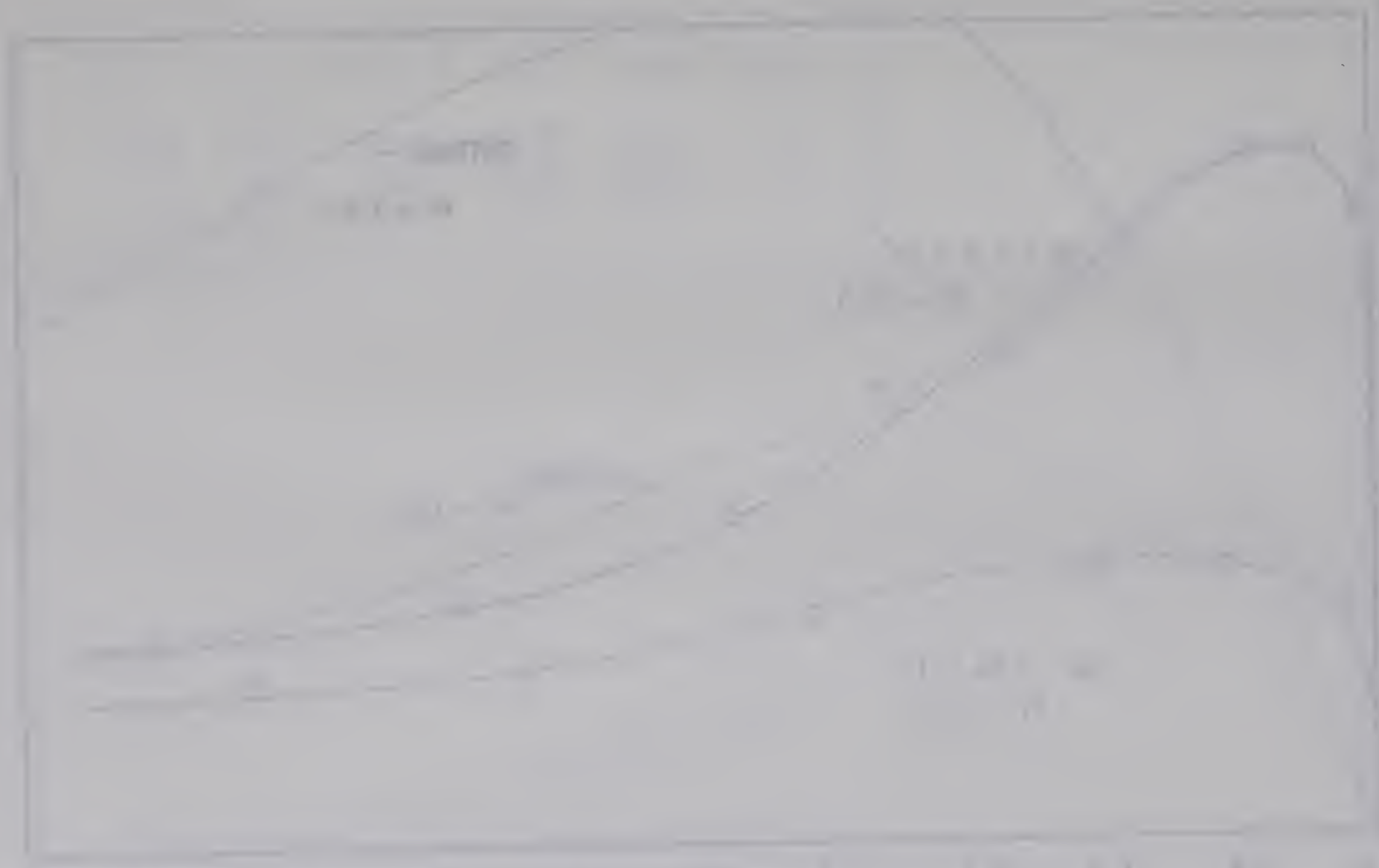

Away from the plate the results are of the correct order of magnitude and appear to be acceptable. When an attempt was made to reproduce these results, the apparatus broke down and the tests had to be abandoned.

4.3-2 Similarity Velocity Profiles

From the treatment presented in Chapter II it follows that the nondimensional turbulent velocity, $f'(\eta)$, is given by

$$f'(\eta) = 1/2\ u\ [\ xg\beta(T_w - T_\infty)\ ]^{-1/2}$$

Notice that $f'(\eta)$ is identical to the laminar nondimensional velocity although the similarity variable η is different.

From this relation, the velocity $f'(\eta)$ can be plotted as a function of the turbulent variable η. Figure 4.16 is such a graph, composed of turbulent data for three different power inputs, all at the same leading edge distance. For a power of 7120 watts the graph data were taken from eleven velocity runs at identical conditions, while at a power of 6000 watts, seven velocity runs were considered. Each point is the average of from one to five readings as indicated. At a power input of 4000 watts, only one run was taken. All readings were obtained with the same fibre except those for the 4000 watts run, which employed the fibre used to study laminar flow. As this fibre was longer than the one used in the other eighteen runs, the percentage error in determining the velocity was less and the values shown are comparable

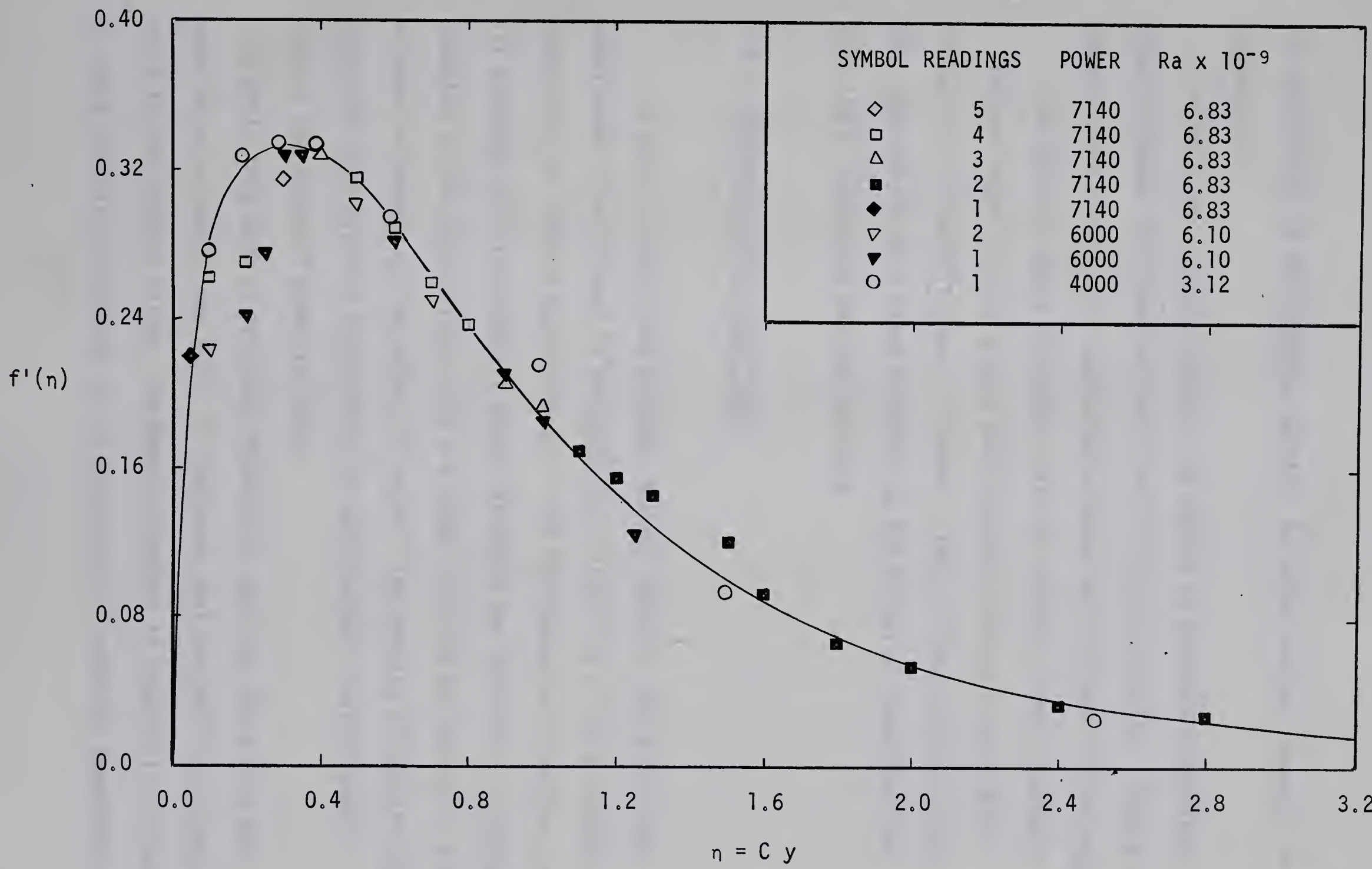

FIG. 4.16 VELOCITY DISTRIBUTION IN THE TURBULENT BOUNDARY LAYER

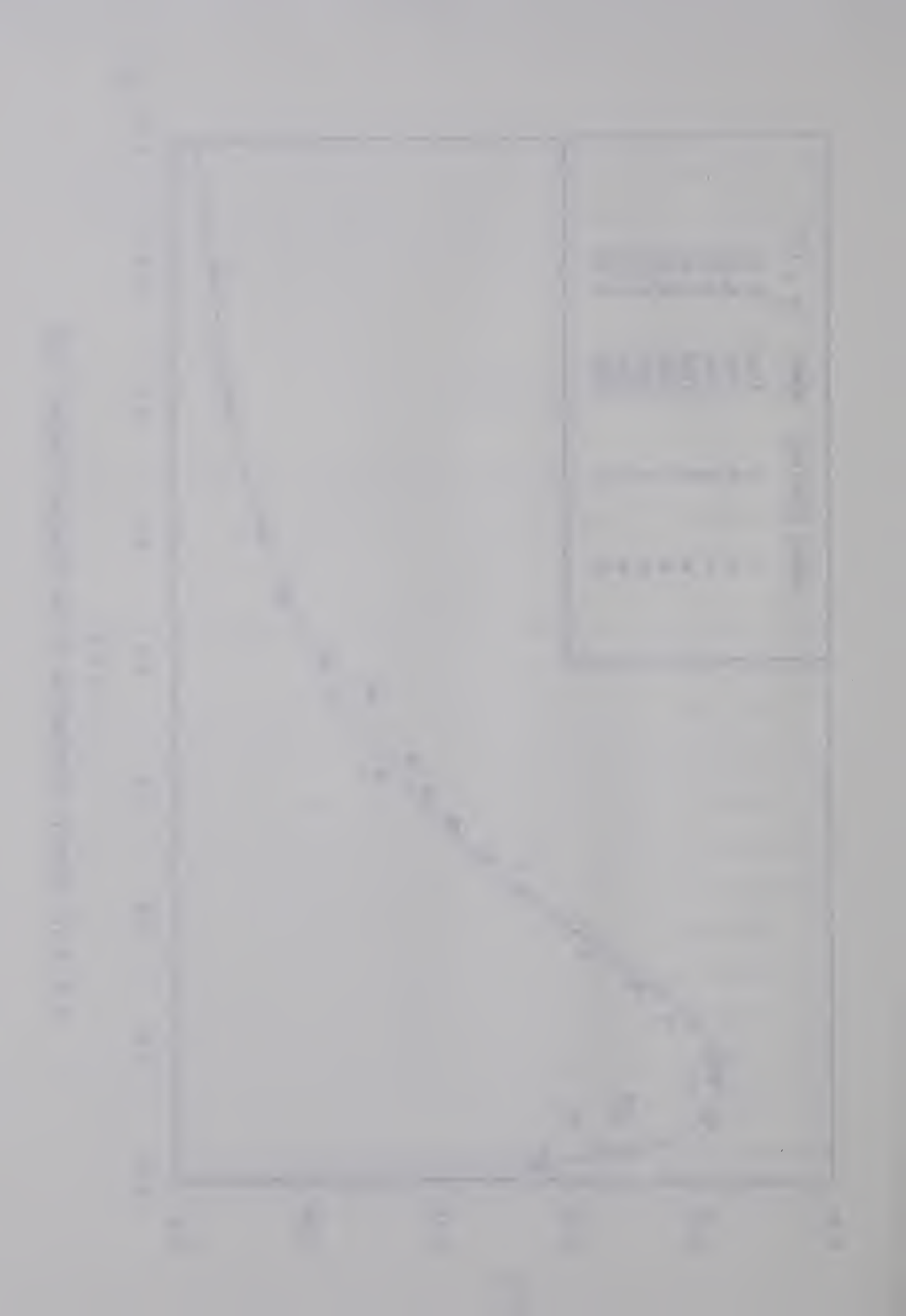

in reliability to the averaged points. An error analysis appears in Appendix F.

As with the laminar results, the region of greatest uncertainty occurs between the plate and the point of maximum velocity. Figure 4.16 demonstrates that only an approximate shape can be drawn in this region.

The equation above indicates that the velocity along a constant η line was found to depend upon the distance from the leading edge raised to the one-half power. However, since all the turbulent tests were carried out at a fixed distance up the plate, an investigation into the x dependency was not possible.

4.3-3 Comparison with Other Work

The work of Eckert and Jackson, Bayley, Waibler, and Fujii was considered in an attempt to evaluate the reliability of this velocity dependency on leading edge distance. With the exception of Bayley, they all proposed that the one-half power variation was applicable. Bayley accepted it for mercury, but felt the power of 0.305 was better in air. He made no comment on the value for water. The results of Waibler, who conducted some velocity experiments in water using a "mirror gage", support the one-half power variation.

While this work of previous researchers does not prove that the power of x is exactly one half, it indicates that one half is at least close to the correct value. The model presented in Chapter II is then at least partially supported in its conclusion on velocity dependency.

4.3-4 The Laminar Sublayer

The existence of a region of laminar flow near a wall is hypothesized by Eckert and Jackson, Bayley, Waibler, and Fujii in their treatment of the problem. From the work of Bayley and the turbulent velocity results given in section 4.3-1, the laminar sublayer should be from 7 to 30 per cent of the boundary layer width. For a boundary layer 0.32 inches wide the sublayer would be at least 0.0224 inches thick. As the diameter of the probe thermocouple is only 0.010 inches, and a fluctuating signal is obtained even when the probe touches the plat plate (see fig. 4.9e), the existence of a laminar sublayer becomes questionable. In addition the fibre (which had a diameter of 0.0019 inches) fluctuated even when in contact with the wall. As the natural frequency of the fibre was very large compared to any random frequency that may have occurred it is only possible to conclude that the fibre was still in a flow area at least partially turbulent. Thus the laminar sublayer hypothesis is very questionable. If such a sublayer does exist, then its width is less than the diameter of the fibre. That is, it is less than one per cent of the boundary layer thickness. This casts considerable doubt on the practice of applying forced convection results to a free convection system.

CHAPTER V

SUGGESTIONS AND CONCLUSIONS

5.1 DESIGN SUGGESTIONS AND IMPROVEMENTS

5.1-1 Apparatus

The apparatus was originally designed for pressurized tests in which the Prandtl number would be unity. Thus the tank was exceptionally sturdy, with a minimum of observation windows. Also the plate was only fourteen inches high since this was adequate to obtain "fully developed" turbulence at a high temperature and pressure.

Unfortunately the unit Prandtl number tests failed and the experiments had to be performed at atmospheric conditions. Apart from any Prandtl number effect this may have introduced, the arrangement had the disadvantage that the flow was laminar over a considerable length of the plate.

To realize a high plate temperature, using resistance heating, it was necessary to use an alternating current power supply. This unfortunately produced extraneous signals in the thermocouple output. Any further tests should avoid heating the plate with an alternating current.

If future water tests are run at atmospheric conditions under the influence of the earth's gravitational field only, it would be advisable to use a heated plate at least four feet in length. This would permit air tests to be run also. In addition, large windows should be fitted to three sides of the tank so that Schlieren and Interferometric

studies could be made. The lack of windows in the existing tank made such studies impossible. It is further recommended that the plate, electrical connections, thermocouples and probe positioning equipment all form one unit which may be lifted from the tank to make adjustments. Not only would this make these parts more accessible, it would also eliminate the need to empty the tank each time adjustments were made.

If water tests are to be conducted at elevated pressures and temperatures, where a unit Prandtl number is possible, it is recommended that no windows or access ports be incorporated into the design (although this would eliminate the possibility of running velocity tests using the fibre anemometer). Instead the vessel should be a large diameter pipe, blanked at the bottom, and fitted with a flange at the top. The mating flange could then have the plate, electrical connections, thermocouples and probe positioning equipment attached to its face. This would facilitate removal of the internal equipment for easy adjustment.

In any apparatus where tests are to be run in water, it is recommended that the use of iron or mild steel be avoided to eliminate rusting. This includes not only the vessel itself but also any accessories such as bolts, screws, and thermocouple wires.

5.1-2 Fibre Anemometer

The results obtained with the fibre anemometer are not as reliable as had been expected. This is especially true in the region between the plate and the point of maximum velocity, where even the laminar

results are very questionable. However, the instrument is useful in a transparent fluid such as water away from the influence of a solid boundary. With a few refinements it could be made to yield values in which greater confidence could be placed.

The simplest and most important change necessary for the improvement of the anemometer is the substitution of a graduated grid for the cross hair on the microscope of the cathetometer. This would eliminate the large error introduced in reading the instrument's vernier and also reduce the error in determining the mean position of the fibre. With this modification, several deflection readings could be taken at a time and their average used.

The cathetometer could be further improved by lengthening the object distance of the microscope to give more flexibility in designing the equipment. At present, the object distance is about three inches.

5.2 CONCLUSIONS

This thesis has described an experimental investigation into the nature of turbulent free convection near a hot vertical wall. An attempt has been made to obtain similarity variables for the flow and to describe a turbulent model.

The experimental results, and hence the conclusions, are valid only for turbulent flow sufficiently far removed from the influence of the leading edge and the side edges. The similarity study is valid only for two dimensional turbulence far from the leading edge.

The turbulence in the free convection boundary layer was found to

be neither homogeneous nor isotropic. It is suggested that this was due to the existence of a solid boundary. The flow was only completely turbulent in the third of the boundary layer closest to the plate. From a value of unity near the plate, the intermittency factor slowly decays until it eventually reaches zero at a point so distant from the plate that the turbulent eddies can no longer penetrate to that depth. This point is well outside the mean boundary layer edge.

The fluctuations in temperature are found to be of the same order of magnitude as $T - T_\infty$, for turbulent flow. The velocity fluctuations could not be recorded but they also appear to be of the same order of magnitude as their mean values. In addition, the fluctuations for turbulent flow are noticeably greater than those for the transition region. Beyond the point of maximum velocity the fluctuations are actually greater than the mean values. Near the plate they are smaller than those observed around the point of maximum velocity but are not zero. In fact, fairly large fluctuations are present at positions less than one per cent of the boundary layer thickness away from the plate. These fluctuations close to the plate cast serious doubts on the validity of the accepted but untested laminar sublayer hypothesis.

A complete similarity solution can only exist if the eddy diffusivity depends upon a constant power of y across the boundary layer or if the value of D is given by

$$D = \frac{1}{2} g \beta (T_w - T_\infty)^{1/2} \cdot \qquad 5.1$$

Since the power of y is not a constant, D must equal the above value if complete similarity is to exist. Regardless of the value of D the turbulent model developed in this thesis has the following features:

a) a boundary layer of constant thickness,

b) a velocity dependent upon the leading edge distance to the one-half power,

c) an eddy diffusivity decreasing downstream, implying that the scale of turbulence decreases downstream.

d) the turbulent shearing stress described by the extension of Prandtl's mixing length theory.

The first three points follow from neglecting the dissipation term in the energy equation and assuming coincident boundary conditions of constant heat flux and constant wall temperature. Unfortunately the experimental results were neither sufficient in number nor precise enough to support the model completely. However, points (a) and (d) were at least partially supported by the experiments and none of the above points were ever contradicted. If complete similarity exists with D given by equation 5.1 then the similarity variable η does not depend on the fluid properties. This lack of property dependency was supported fairly well and thus it is believed that the turbulent model will reasonably predict the gross characteristics of a turbulent boundary layer.

REFERENCES

1. GRIFFITHS, E. and DAVIS, A. H., "The Transmission of Heat by Radiation and Convection", Dept. of Scientific and Industrial Research Food Investigation S.R. 9, His Majesty's Stationery Office, 1922.

2. CHEESEWRIGHT, R., "Turbulent Natural Convection From a Vertical Plane Surface", Transactions of the ASME, Paper No. 67-HT-17,1967.

3. SAUNDERS, O.A., "Natural Convection in Liquids", Proceedings of the Royal Society A, Vol. 172, pp. 55-71, 1939.

4. ECKERT, E. R. G. and JACKSON, T. W., "Analysis of Turbulent Free-Convection Boundary Layer on Flat Plate", NACA TR 1015, 1951.

5. SCHMIDT, E. and BECKMANN, W., "Das Temperatur- und Geschwindigkeitfeld von einer Wärme abgebenden senkrechten Platte bei natürlicher Konvektion", Tech. Mech. u. Thermodynamik, Bd. 1, No. 10, pp. 341-349; cont. Bd. 1, No. 2, pp. 391-406, 1930.

6. SCHLICHTING, H., "Boundary Layer Theory" (translated by J. Kestin), McGraw-Hill Book Company, Inc., p. 466, 1960.

7. Ibid., p. 16.

8. EITEL, W., "The Physical Chemistry Of the Silicates", University of Chicago Press, Chicago, Illinois, p. 612, 1954.

9. BOYS, C. V., Roy. Soc. Phil. Trans., 143, 159, 1889; as quoted in Strong, "Procedures in Experimental Physics", Prentice-Hall, Inc., New York, p. 191, 1941.

10. LOCK, G. S. H., GORT, C. and POND, G.R., "A Study Of Instability in Free Convection from an Inclined Plate", Appl. Sci. Res., Vol 18, pp. , 1967.

11. SZEWCZYK, A. A., "Stability and Transition of the Free Convection Layer Along a Vertical Flat Plate", Int. Jour. of Heat and Mass Transfer, Vol. 5, pp.903-914, 1962.

12. NACHTSHEIM, P. R., "Stability of Free-Convection Boundary Layer Flows", NASA, TN D-2089, 1963.

13. WAIBLER, P. J., "Natural Convection Heat Transfer with Water at High Grashof Numbers", Ph.D. Thesis, University of Illinois, 1958.

14. FUJII, T., "An Analysis of Turbulent Free Convection Heat Transfer from a Vertical Surface", Bull. Japan Soc. Mech. Engrs. 2, No. 8, pp. 559-563, 1959.

15. VAN DYKE, M.S., "Boundary Layer Temperature in Natural Convection Flow of Water", M.S. Thesis, University of Washington, 1960.

16. BAYLEY, F.J., "An Analysis of Turbulent Free-Convection Heat-Transfer", Proc. Inst. Mech. Engrs., London, Vol. 169, No. 20, pp. 361-368, 1955.

17. LAMB, H., "Hydrodynamics", Cambridge University Press, London, p. 614, 1959.

18. OSTRACH, S. "An Analysis of Laminar Free-Convection Flow and Heat Transfer About a Flat Plate Parallel to the Direction of the Generating Body Force", NACA Report 1111, 1953.

ADDITIONAL REFERENCE

TRITTON, D.J., "The Use of a Fibre Anemometer in Turbulent Flows", J. Fluid Mech., Vol. 16, Part 3, p. 417, 1963.

APPENDIX A

SCHLIEREN INVESTIGATION

The initial leading edge attachment is illustrated in figure A.1. Since during preliminary velocity tests it was found to be impossible to determine the position and condition of the boundary layer edge with any degree of accuracy, a Schlieren investigation of the leading edge was made. This investigation was conducted in air. The brass jaw was found to be heating the fluid from beneath, producing a second boundary layer (a turbulent buoyant jet) which flowed externally to the first. This system existed on both sides of the plate.

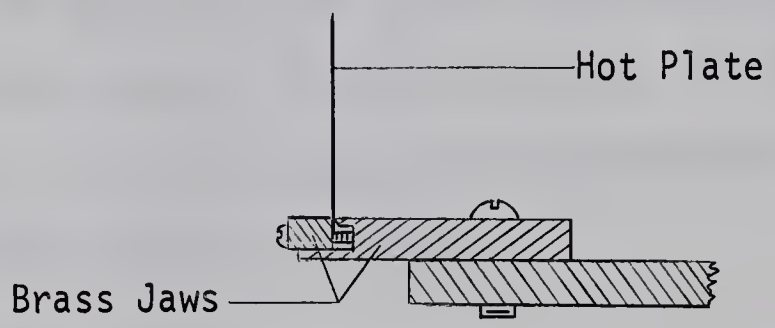

FIG. A.1 INITIAL LEADING EDGE ATTACHMENT

The final arrangement for the leading edge attachment, shown in figure 3.2 and reproduced in figure A.2, proved satisfactory. As before, the jaw was heated (and set up buoyant jet effects) but since the effects were limited to one side of the plate it was possible to obtain reasonable velocity and temperature curves on the other side.

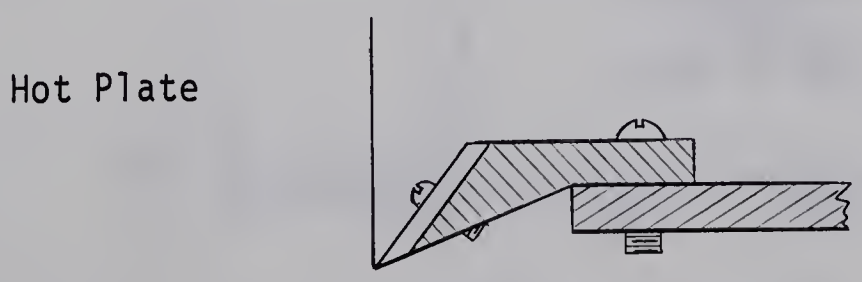

FIG. A.2 IMPROVED LEADING EDGE ATTACHMENT

APPENDIX B

RESPONSE TIME OF PROBE THERMOCOUPLE

To estimate the response time of the probe thermocouple the following experiment was performed. Two constant temperature baths were prepared: one a mixture of ice and water at 32°F and the other simply boiling water at 208°F. The thermocouple was held in the cold bath with its output fed to an oscilloscope. It was then quickly transferred to the boiling water at the same instant as a photograph was taken of the oscilloscope screen. Figure B.1 is a reproduction of such a photograph. It is evident that it took the thermocouple about 100 milliseconds to reach the temperature of the boiling water. For about one-half of this time the thermocouple was reading temperature very close to the boiling point. If the value of 100 milliseconds is used, in a similar system the thermocouple's response rate would be 1760 Fahrenheit degrees per second.

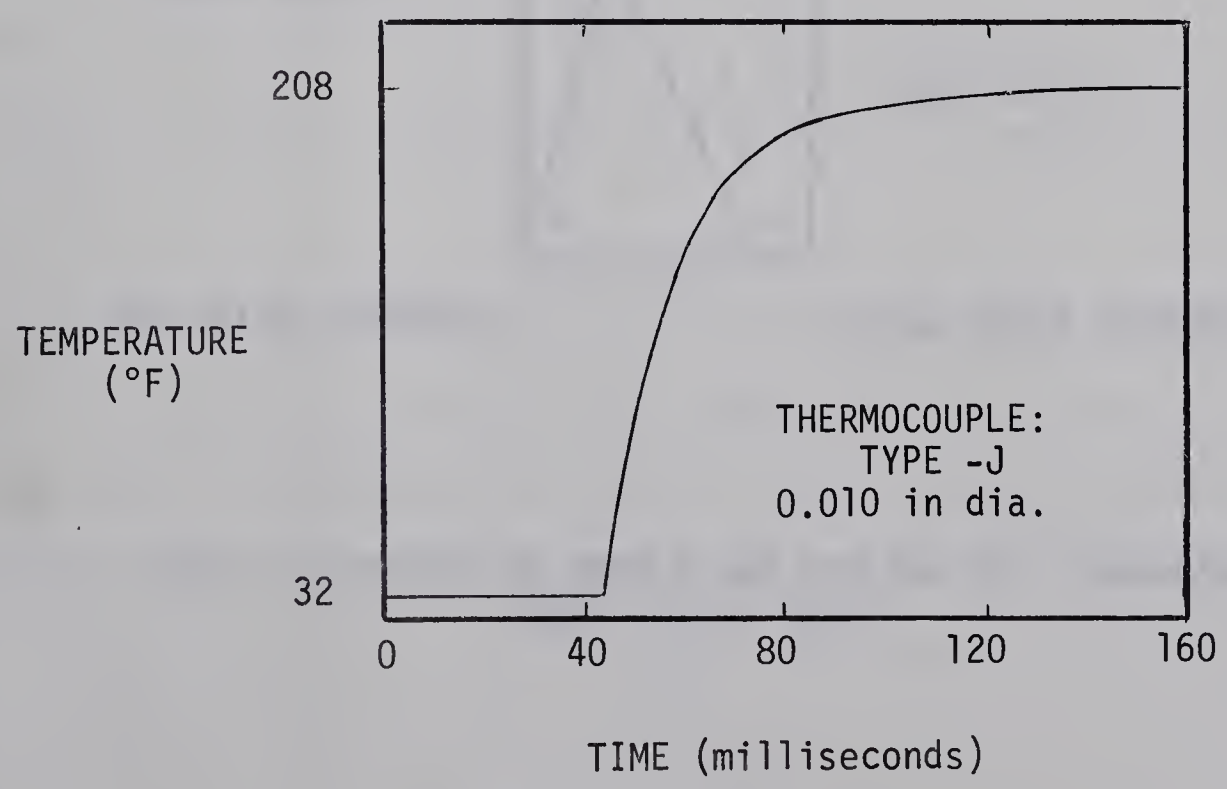

FIG. B.1 RESPONSE TIME OF THE PROBE THERMOCOUPLE

APPENDIX C

BAFFLE AND COOLING COIL ARRANGEMENT

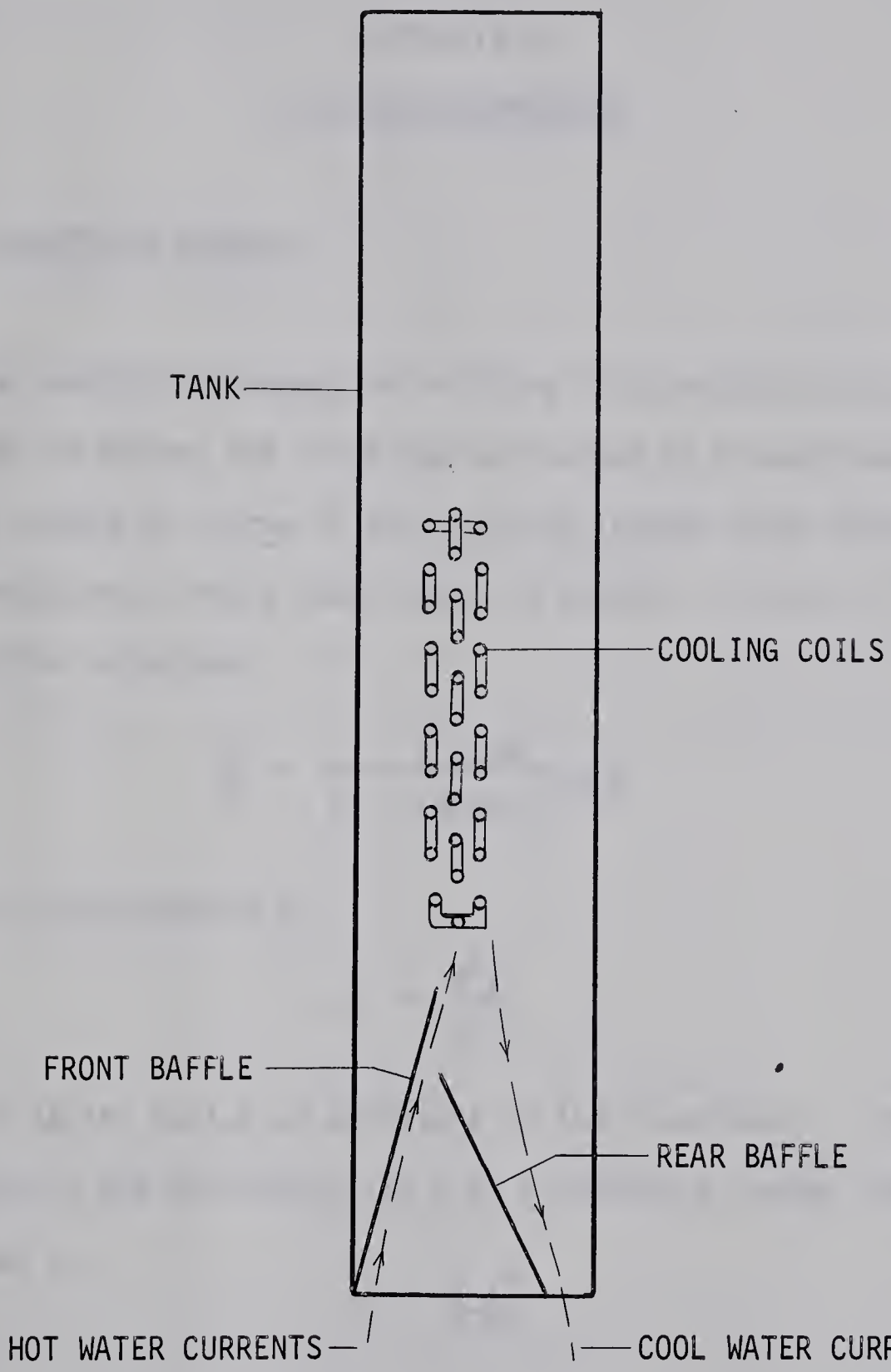

FIG. C.1 SKETCH OF BAFFLE AND COOLING COIL ARRANGEMENT NEAR TOP OF TANK

APPENDIX D

THE FIBRE ANEMOMETER

D.1 DEFLECTION FORMULA

To develop an expression relating fluid velocity to the deflection of the fibre, the fibre may be treated as a cantilever beam, uniformly loaded by virtue of the velocity-induced drag force. To obtain the deflection, simple beam theory is assumed. That is, for small slopes the curvature,

$$\frac{1}{R} = \frac{d^2y/dx^2}{[1 + (dy/dx)^2]^{3/2}}$$

reduces approximately to

$$\frac{1}{R} = \frac{d^2y}{dx^2}$$

where R is the radius of curvature of the fibre beam. With this assumption, the end deflection δ of a uniformly loaded cantilever beam is given by

$$\delta = \frac{w\, l^4}{8\, EI} \qquad \text{D-1}$$

where w is the drag load per unit length, E is the modulus of elasticity, and I is the moment of inertia. For a circular cross-section of diameter d the moment of inertia is

$$I = \frac{\pi d^4}{64}$$

and equation D-1 becomes

$$\delta = \frac{8\, w\, l^4}{E\, d^4} . \qquad \text{D-2}$$

If the Reynolds number does not exceed 0.5, the inertia terms in the Navier-Stokes equations may be neglected and creeping flow theory assumed. With this assumption, Lamb [17] has shown that the resistance per unit length, w, on an unyawed circular cylinder is given by

$$w = \frac{4\pi\, \mu\, U}{1/2 - \gamma - \ln(Ud/8\nu)} \qquad \text{D-3}$$

where U is the uniform free stream velocity: μ, the absolute viscosity; ν, the kinematic viscosity; and γ, Euler's constant with the value

$$\gamma = 0.577216.$$

Combining equations D-2 and D-3 yields

$$\delta = \frac{32\, \mu\, U\, l^4}{Ed^4[1/2 - \gamma - \ln(1/8\ Re)]}$$

where

$$Re = \frac{Ud}{\nu} .$$

Generally, the resistance per unit length of a body is given by

$$w = 1/2\ C_D\ \rho_\infty\ U^2 A$$

where ρ_∞ is the free stream density, C_D is the drag coefficient, and A is the projected area of the body. Combining this equation with equation D-2 yields

$$\delta = \frac{4 l^4 \rho_\infty U^2 C_D}{\pi\, E\, d^3} \qquad \text{3-1}$$

as the deflection of an unyawed circular cylinder in a forced flow. It is assumed that this expression is valid also for the deflection of a fibre in a free flow where ρ_∞ and U are replaced by their local mean values ρ and u.

D.2 DIAMETER MEASUREMENTS

As the value of 50 microns as a fibre diameter was only a nominal value, an attempt was made to obtain this dimension more accurately. Because of the very small diameters involved, a micrometer was useless. A toolmaker's microscope and shadowgraph were also of little value because of the cylindrical shape of the probe and its small dimension.

The most precise dimensions obtained were measured by interferometric techniques. This involved illuminating a thin wedge of air with a monochromatic helium light source. The fibre was placed on gauge blocks separated by about two inches and the number of interference bands was counted. Although the precision of this method was good ($\pm$ 2 x 10^{-6} inches) the accuracy was unreliable. The lack of accuracy can be attributed to two sources. The first is the difficulty in determining the exact number of interference bands. The second is that the gauge blocks were inexplicably out of square when wrung to the optical flat. If these two difficulties could be overcome, this method should prove most satisfactory. A sketch of the arrangement is presented in figure D.1.

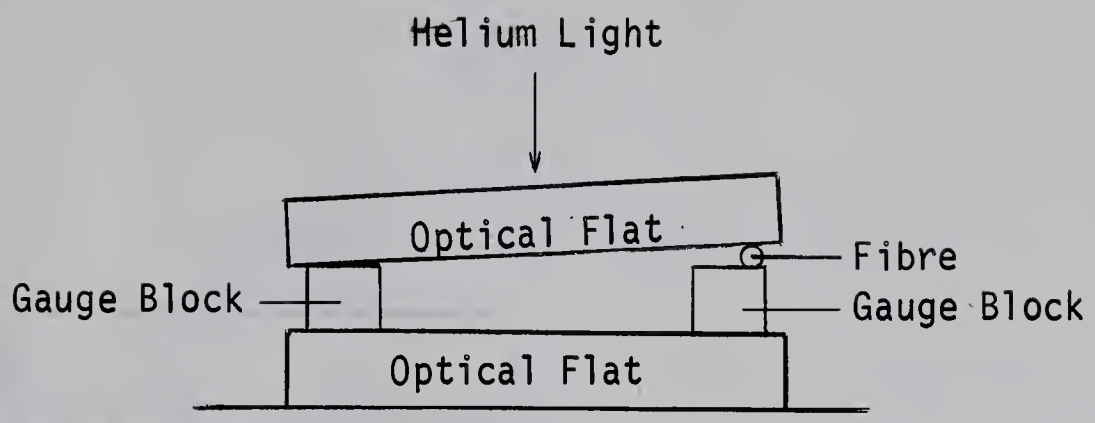

FIG. D.1 FIBRE DIAMETER USING INTERFEROMETER TECHNIQUES

The most reliable measurements were obtained with the Pitter Gauge and Tool Company Limited Diameter Measuring Machine represented in figure D.2. This tool consists, basically, of two parts. The first is a micrometer unit with a nonrotating spindle. This unit has a vernier scale that can be read to 0.00001 inches (0.00025 mm.). The second part is a Fiducial Indicator which ensures that a constant force is applied to the specimen for all readings. This indicator enables repeat readings to be taken from the micrometer with an accuracy of 0.00002 inches (0.0005 mm.). The machine found the diameter of one fibre, 10 centimetres in length, to vary between 0.00190 and 0.00200 inches, with the average of eight readings being 0.00197 inches, or 50.04 microns. This fibre was the one used in the velocity measurement tests.

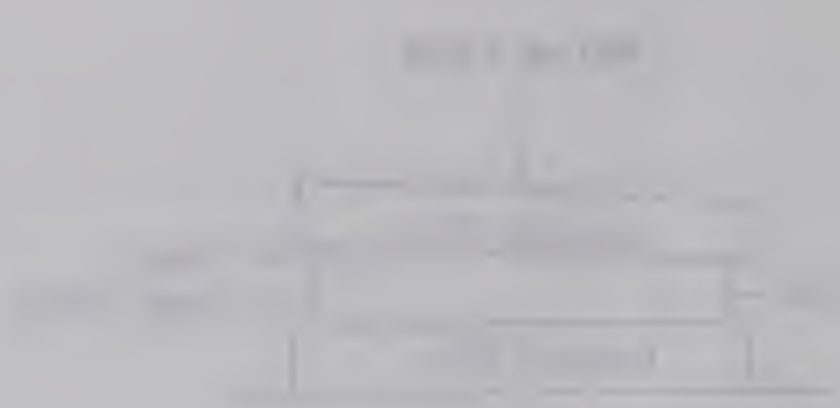

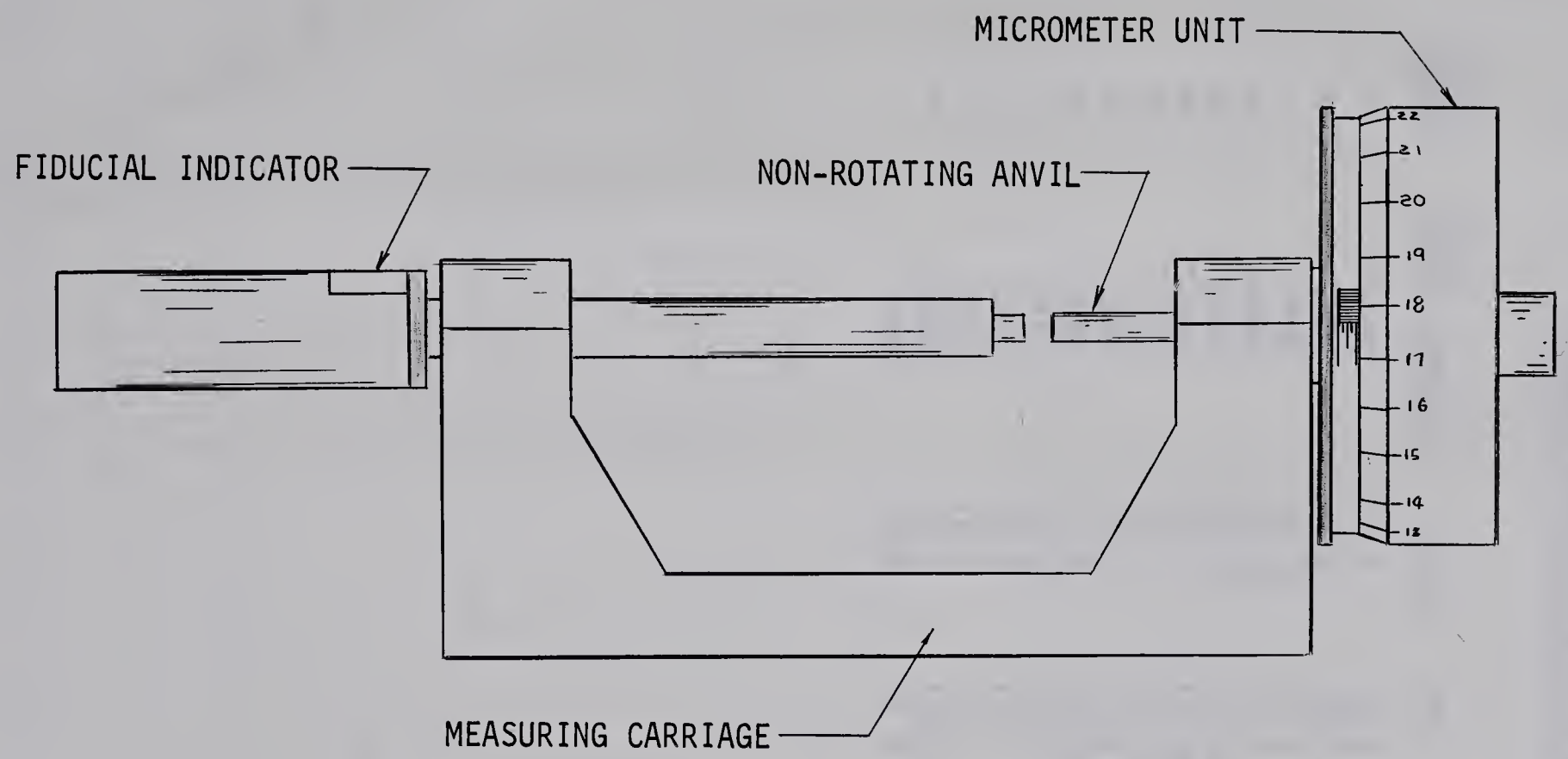

FIG. D.2 SKETCH OF CARRIAGE OF DIAMETER MEASURING MACHINE

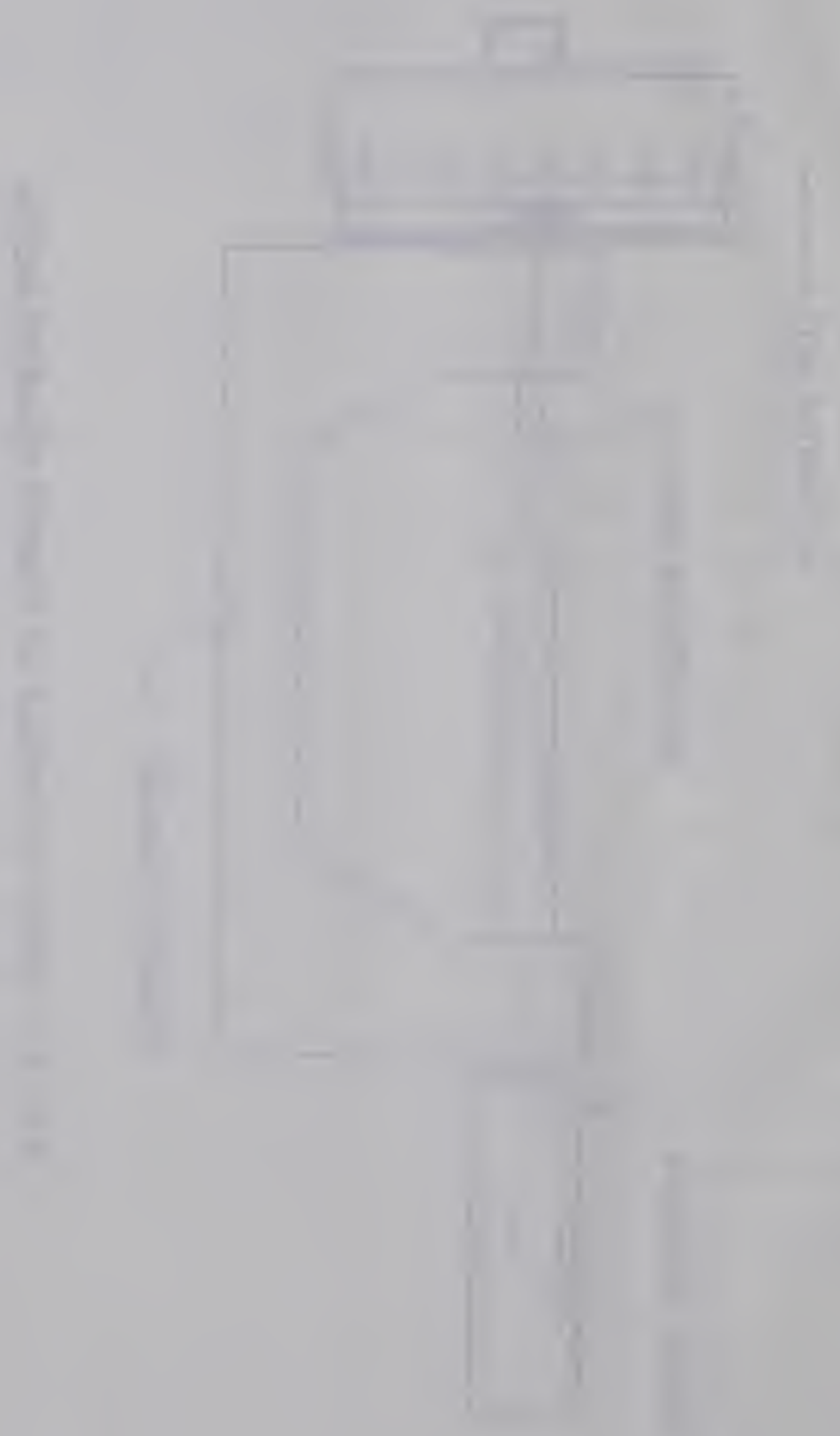

APPENDIX E

TABLE II

SYMBOLS FOR FIG. 4.3, 4.6, and 4.7

SYMBOL	POWER (watts)	x (in)	Pr	Gr x 10^{-8}	Ra x 10^{-9}
+	6080	11.0	10.6	5.41	5.74
X	6920	11.0	9.8	8.4	8.23
Y	7400	10.02	11.4	2.66	3.03
⅄	6600	10.02	11.6	1.9	2.20
O	6640	10.02	11.85	1.44	1.71
△	7200	12.1	10.45	8.0	8.36
▽	7150	12.1	10.45	7.56	7.91
□	7240	12.1	11.0	5.95	6.55
●	7080	12.1	10.45	8.0	8.36
◇	7420	12.1	10.8	6.74	7.27
T	6800	12.1	11.1	5.48	6.06
A	6720	12.1	10.6	7.53	8.00
N	6800	12.1	10.45	7.94	8.30
⊥	7040	9.5	11.0	2.98	3.28

APPENDIX F

ERRORS

F.1 VELOCITY

For a particular deflection δ of the fibre, the velocity of the fluid is given by

$$V = \left[\frac{P\ 327\ l_1^{\,3}\ \delta}{\delta_1 C_D\ \rho\ d\ l^4}\right]^{1/2} \qquad 3\text{-}1a$$

For the fibre of length 2.196 centimetres, the errors involved are given in Table III

TABLE III

Quantity	Value	Error	% Error	Total	% Error
l_1	2.572	0.003	0.167		0.5
l	2.196	0.003	0.137		0.6
d	188	5	2.7		2.7
P/δ_1	6.44	.18	2.8		2.8
C_D					3.5
				Total	10.1

Therefore the percentage error of the velocity is given by

$$\%\ \text{error of velocity} = 5.1 + 1/2(\%\ \text{error of}\ \delta). \qquad F.1$$

Similarly, for the fibre of length 1.444 centimetres, the percentage error is

$$\%\ \text{error of velocity} = 5.2 + 1/2(\%\ \text{error of}\ \delta). \qquad F.2$$

Figure F.1 is a graph of equation F.1 and figure F.2 is a graph of equation F.2. The latter graph shows the estimated percentage error both when a single reading is taken and when the average of four readings is calculated.

These curves are completely valid from the point of maximum velocity y_m to the edge of the mean boundary layer. Near y_m the maximum deviation from the mean curves is about six per cent, as seen in figure 4.14, which is much less than the maximum predicted by figures F.1 and F.2. It is possible that the "correct" curves are different from those obtained but at least the scatter is within the expected limits.

Between the wall and the point of maximum velocity, a region where high velocity gradients exist, an error well in excess of that predicted could result if the assumption that steady uniform field results can be applied to an unsteady non-uniform system is invalid. Figure 4.15 suggests that this assumption is not strictly valid in the region close to the plate and that a large error exists, even though the maximum scatter (eight per cent) is still within the predicted limits.

F.2 TEMPERATURE

Unfortunately, the boundary layer thermocouple was receiving an unknown alternating current signal from the plate when the power was on. An attempt was made to measure this signal using the Varian recorder. This pick-up tended to reduce the temperatures recorded from about 0.5

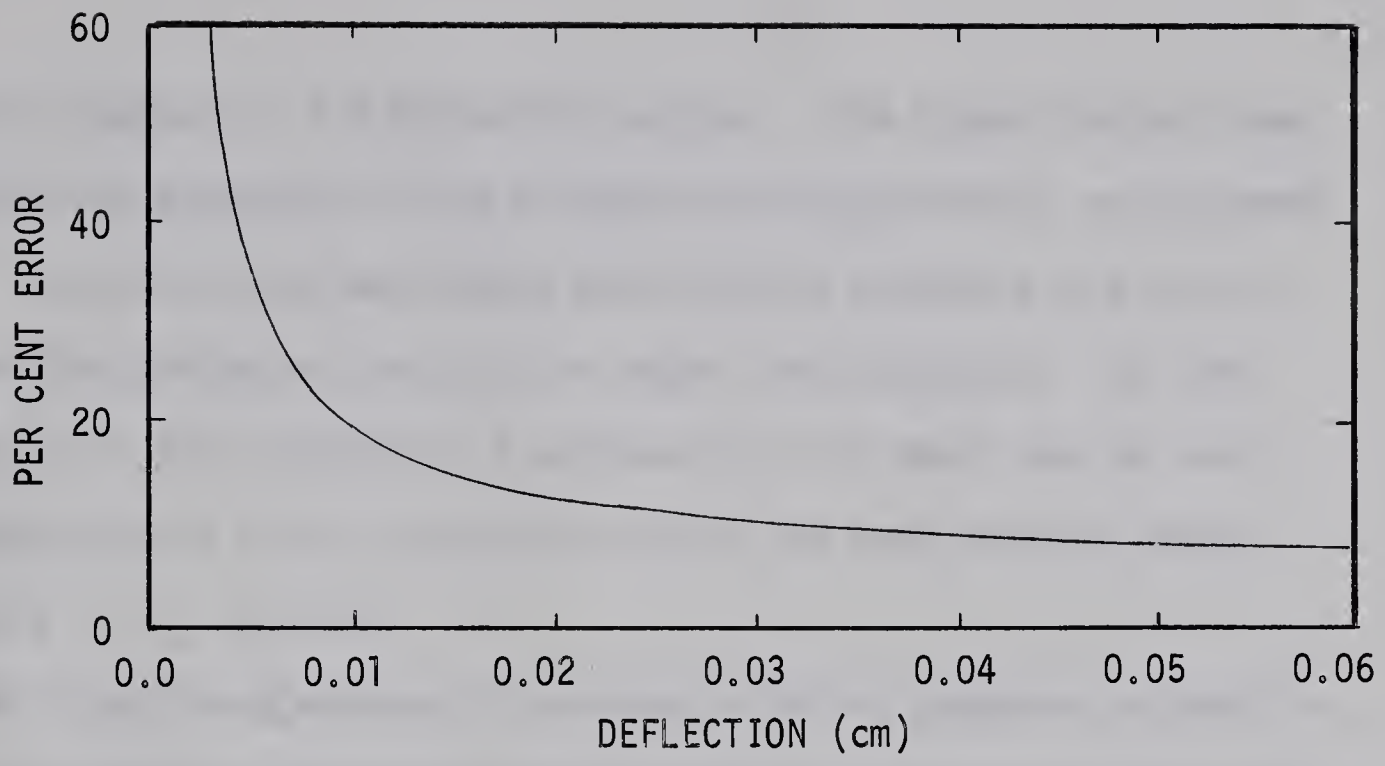

FIG. F.1 ESTIMATED ERROR IN VELOCITY
(l = 2.196 cm)

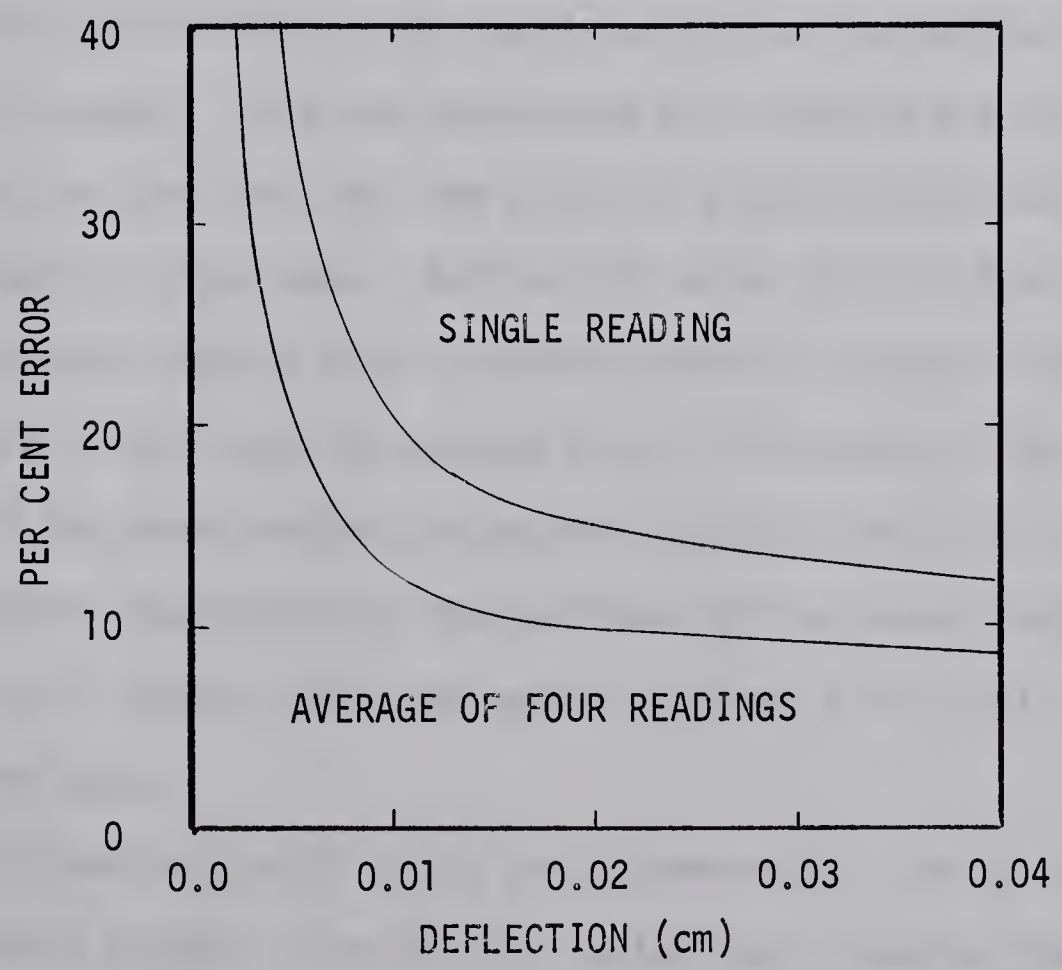

FIG. F.2 ESTIMATED ERROR IN VELOCITY
(l = 1.444cm)

Fahrenheit degrees to 3.0 Fahrenheit degrees. The signal did not seem to be strongly dependent on the distance from the plate or on the power input. Since the value was almost constant and therefore did not affect the fluctuating recordings, the signal was neglected. For the turbulent runs this introduced a maximum error of about two per cent near the plate and a much larger error near the mean boundary layer edge where $T - T_\infty$ is small.

When using the Speedomax G recorder to obtain temperature profiles, twenty readings were averaged to give each point. The mean values thus obtained were in error if the recorder happened to punch at the peak temperatures (during fluctuations) a disproportionate number of times. Visual assessment of the mean position of the temperature indicator showed that the calculated mean value could be in error as much as $\pm$ 3.0 Fahrenheit degrees. Thus the percentage error due to averaging varied from about two per cent near the plate to a much larger value near the mean boundary layer edge. Adding this error to that due to the alternating signal gives a total possible error of four per cent near the plate and a very large percentage error in the outer region. However, since in the outer region the maximum possible variation is only $\pm$ 6.0 Fahrenheit degrees, only the position of the curve, rather than its shape, is in doubt. All mean values obtained fell within the expected error band.

The error in reading the millivolt potentiometer for laminar flow was $\pm$ 0.1 Fahrenheit degrees. The error in obtaining a reading from the chart of the Speedomax G recorder was $\pm$ 0.3 Fahrenheit degrees.

If the Varian recorder was set at 10 millivolts full scale deflection the graph could be read to ± 0.6 Fahrenheit degrees. The resolution improved to ± 0.06 Fahrenheit degrees if the instrument was set at a full scale deflection of one millivolt.

F.3 POSITION

Although changes in the probe thermocouple's position could be read to ± 0.0002 inches, using a dial gauge, the position relative to the plate could be judged only to ± 0.005 inches, or one half of its diameter. This led to a large percentage error near the plate and a maximum possible error at the boundary layer edge of two per cent. The mean temperature curves pass through all of the error ellipses formed by combining the position and temperature uncertainties.

The uncertainty in locating the fibre was about ± 0.001 inches. This error source was also very large near the plate, but was only about one third of one per cent at the boundary layer edge. The mean velocity curves pass through all the ellipses formed by combining the position and velocity uncertainties. In the region near the plate, however, the major axis of each ellipse is extended by the velocity errors discussed in section F.1.